Mission-Oriented Seismic
Research Program

Annual Report

2011

M-OSRP

University of Houston

Sponsors and Advisory Board representatives

May 25, 2012

Corporate Sponsors

Anadarko ..... Roger Reagan
BHP ..... Corey Morgan
BP ..... Jingfeng Zhang
Chevron ..... Debbie Bones
ConocoPhillips ..... Haiyan Zhang, Robert Stolt
Devon Energy ..... Kenneth Beeney, Richard Brietzke
Encana ..... David Mackidd
ENI-Agip ..... Nicola Bienati
ExxonMobil ..... Peter Traynin
GX Technology ..... Nick Bernitsas, Robert Bloor
Hess ..... Scott Morton
IBM ..... Tom McClure
Landmark ..... Dave Diller
Petrobras ..... Neiva Zago
Petrochina Company Limited ..... Jixiang Xu
PGS ..... Nizar Chemingui, Sverre Brandsberg-Dahl
Repsol ..... Gladys Gonzalez, Francisco Ortigosa
Saudi Aramco ..... Yi Luo
Shell ..... Jonathan Sheiman
Statoil ..... Marianne Houbiers, Lasse Amundsen
Total ..... Wafik Beydoun
WesternGeco ..... Richard Coates

Federal Support

DOE Basic Sciences award DE-FG02-05ER15697 ..... Nick Woodward
NSF-CMG award DMS-0327778 ..... Henry A. Warchall

M-OSRP Personnel

Faculty

Hicham Ayadi ..... Research Scholar (Physics)
Lasse Amundsen (Statoil) ..... Adjunct Professor (Physics)
Douglas J. Foster (ConocoPhillips) ..... Adjunct Professor (Physics)
Wilberth Herrera ..... PostDoc Fellow (Physics)
Kristopher A. Innanen (Associate Professor, University of Calgary) .. Adjunct Professor (Physics)
Robert G. Keys (ConocoPhillips) ..... Adjunct Professor (Physics)
Jacques Leveille (Amerada Hess) ..... Adjunct Professor (Physics)
Fang Liu ..... Research Assistant Professor (Physics)
Ken H. Matson (Shell) ..... Adjunct Associate Professor (Physics)
Bogdan Nita (Assistant Professor, Montclair State U.) ..... Adjunct Assistant Professor (Physics)
Partha Routh ..... Adjunct Professor (Physics)
Jon Sheiman (Shell) ..... Adjunct Professor (Physics)
Robert H. Stolt (ConocoPhillips) ..... Adjunct Professor (Physics)
T. Hing Tan (Shell) ..... Adjunct Professor (Physics)
Arthur B. Weglein ..... Cullen Professor (Physics)
Daniel Whitmore (PGS) ..... Adjunct Professor (Physics)

Graduate Students

Di Chang ..... Physics
Hong Liang ..... Physics
Chao Ma ..... Physics
Jim Mayhan ..... Physics
Mozhdeh Niazmand ..... Physics
Lin Tang ..... Physics
Zhiqiang Wang ..... Physics
Jinlong Yang ..... Physics

Recent Alumni

Andre Ferreira[2] ..... Geosciences
Zhiqiang Guo ..... Geosciences
Shih-Ying Hsu ..... Physics
Xu Li ..... Physics
Jose Eduardo Lira[2] ..... Geosciences
Fang Liu ..... Physics
Francisco Miranda ..... Physics
Adriana Citlali Ramirez ..... Physics
Simon A. Shaw ..... Geosciences
Haiyan Zhang ..... Physics
Jingfeng Zhang ..... Physics

Administrative Support

Jennifer Chin-Davis ..... Associate Director, Physics Department
Andrew Fortney ..... Computer/IT Support
Chris Watts ..... Webmaster/NSM IT

[2]Petrobras, Brazil

Table of Contents

Elimination of land internal multiples based on the inverse scattering series

Yi Luo, Panos G. Kelamis, Qiang Fu, ShouDong Huo, and Ghada Sindi, Saudi Aramco
Shih-Ying Hsu and Arthur B. Weglein, University of Houston

Despite the explosion of new, innovative technologies in the area of multiple identification and subsequent attenuation, their applicability is mostly limited to marine environments especially in deep water. In land seismic data sets however, the application of such multiple-elimination methodologies is not always straightforward and in many cases poor results are obtained. The unique characteristics of land seismic data (i.e., noise, statics and coupling) are major obstacles in multiple estimation and subsequent elimination. The well-defined surface multiples present in marine data are rarely identifiable in land data. Particularly in desert terrains with a complex near surface and low-relief structures, surface multiples hardly exist. In most cases, we are dealing with so called "near-surface-related multiples." These are primarily internal multiples generated within the complex near surface.

In this paper, we employ theoretical concepts from the inverse scattering series (ISS) formulation and develop computer algorithms for land internal multiple elimination. The key characteristic of the ISS-based methods is that they do not require any information about the subsurface: i.e., they are fully data-driven. Internal multiples from all possible generators are computed and adaptively subtracted from the input data. These methodologies can be applied prestack and poststack and their performance is demonstrated using realistic synthetic and field data sets from the Arabian Peninsula. These are the first published field data examples of the application of the ISS-based internal multiple-attenuation technology to the daunting challenge of land internal multiples.

Introduction

Radon-based methods are commonly employed for multiple reduction in land seismic data processing. However, in land data, the lack of velocity discrimination between primaries and multiples causes unacceptable results. Thus, wave-equation-based schemes have to be introduced. The research articles of Verschuur et al. (1992), Berkhout (1997), Weglein et al. (1997), Carvalho and Weglein (1994), Dragoset and Jericevic (1998), Jakubowicz (1998), Berkhout (1999), and Verschuur and Berkhout (2001), to mention a few, offer theoretical insights to wave-equation surface and internal multiple elimination along with several applications to synthetic and marine data sets.

Kelamis et al. (2002) used concepts from the common focus point (CFP) technology and developed algorithms for internal multiple elimination applicable in land. Luo et al. (2007) and Kelamis et al. (2008) have also presented successful applications of land internal multiple suppression. They employed the layer/boundary approaches introduced by Verschuur and Berkhout (2001). In these schemes, the user has to define phantom layers/boundaries which correspond to the main internal multiple generators. Thus, some advanced knowledge of the main multiple generators is required. On land, as shown by Kelamis et al. (2006), the majority of internal multiples are generated by a series of complex, thin layers encountered in the near surface. Thus, the applicability of the CFP-based layer/boundary approach is not always straightforward because it requires the definition of many phantom layers. In contrast, the ISS theory does not require the introduction of phantom layers/boundaries. Instead, it computes all possible internal multiples produced by all potential multiple generators. Therefore, fully automated internal multiple-elimination algorithms can be developed in the prestack and poststack domains.

Basic principles of ISS technology

The ISS-based formulation for internal multiple attenuation (Araújo et al., 1994; Weglein et al., 1997) is a data-driven algorithm. It does not require any information about the reflectors that generate the internal multiples or the medium through which the multiples propagate and, in principle, it does not require moveout differences or interpretive intervention. The algorithm predicts internal multiples for all horizons at once.

$$b_{3IM}(k_g,k_s,q_g+q_s)=\frac{1}{(2\pi)^2}\int_{-\infty}^{\infty}dk_1e^{-iq_1(z_g-z_s)}\int_{-\infty}^{\infty}dk_2e^{iq_2(z_g-z_s)}$$
$$\times\int_{-\infty}^{\infty}dz_1'b_1(k_g,k_1,z_1')e^{i(q_g+q_1)z_1'}$$
$$\times\int_{-\infty}^{z_1'-\epsilon}dz_2'b_1(k_1,k_2,z_2')e^{-i(q_1+q_2)z_2'}$$
$$\times\int_{z_2'+\epsilon}^{\infty}dz_3'b_1(k_2,k_s,z_3')e^{i(q_2+q_s)z_3'}$$

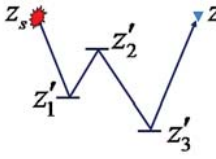

$\epsilon > 0$ ensures $z_1' > z_2'$ and $z_3' > z_2'$

Figure 1. *ISS internal multiple prediction formulation.*

This ISS internal multiple-attenuation scheme is basically the first term in a subseries of the ISS that predicts the exact time and amplitude of all internal multiples without subsurface information. The ISS attenuation algorithm predicts the correct traveltimes and approximate amplitudes of all the internal multiples in the data, including converted-wave internal multiples (Coates and Weglein, 1996). Carvalho et al. (1992) pioneered the free-surface ISS method and applied it to field data. Matson et al. (1999) were the first to apply the ISS internal multiple algorithm to marine towed-streamer field data, and Ramírez and Weglein (2005) extended the theory from attenuation toward elimination by including more terms in the subseries, thereby improving the amplitude prediction.

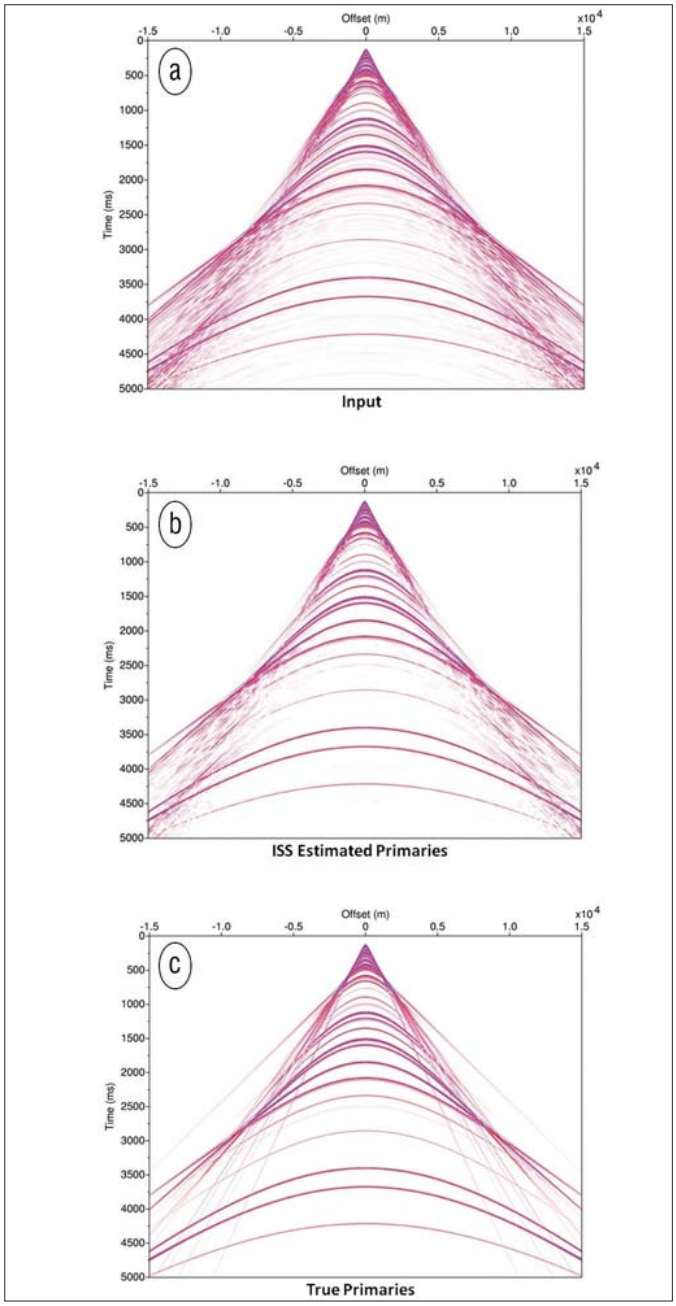

Figure 2. *(a) Synthetic CMP gather from 18-layer velocity model. (b) ISS-estimated primaries. (c) True primaries.*

Matson (1997) and Weglein et al. (1997) extended the ISS methods for removing free-surface and internal multiples from ocean-bottom and land data.

The ISS internal multiple-attenuation algorithm in 2D starts with the input data, $D(k_g, k_s, \omega)$ that are deghosted and have all free-surface multiples eliminated. The parameters, k_g, k_s, and ω represent the Fourier conjugates to receiver, source, and time, respectively. The ISS internal multiple-attenuation algorithm for first-order internal multiple prediction in a 2D Earth is given by Araújo (1994) and Weglein et al. (1997). Figure 1 depicts the mathematical formulation along with a pictorial construction of a first-order multiple. The quantity $b_1(k_g, k_s, z)$ corresponds to an uncollapsed migration (Weglein et al., 1997) of an effective incident plane-wave data which is

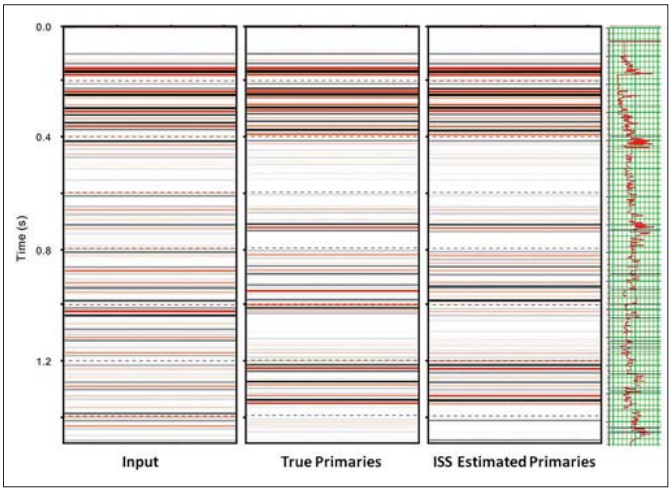

Figure 3. *(left) 1D synthetic with primaries and internal multiples modeled from the field sonic log (right). (center left) True primaries. (center right) ISS-estimated primaries.*

given by $-2iq_sD(k_g, k_s, \omega)$ The vertical wavenumbers for receiver and source, q_g and q_s, and are given by

$$q_i = sqn(\omega)\sqrt{\frac{\omega^2}{c_0^2} - k_i^2} \quad \text{for } i = (g,s);$$

c_0 is the constant reference velocity; z_s and z_g are source and receiver depths; and z_i (i = 1,2,3) represents pseudodepth. Note that the obliquity factor, $-2iq_s$, is used to transform an incident wave into a plane wave in the Fourier domain (Weglein et al., 2003).

The first-order internal multiple is composed of three events that satisfy $z'_2 < z'_1$ and $z'_2 < z'_3$. The traveltime of the internal multiple is the sum of the traveltimes of the two deeper events minus the traveltime of the shallower one. The parameter ε is introduced in the equation of Figure 1 to preclude $z'_2 < z'_1$ and $z'_2 < z'_3$ in the integrals. For band-limited data, ε is related to the width of the wavelet. The output of the equation, b_{3IM}, is divided by the obliquity factor and transformed back to the space-time domain. When we subtract the estimated internal multiples from the original input data, all first-order internal multiples are suppressed and higher-order internal multiples are altered.

Synthetic and field data

Figure 2 shows a synthetic CMP gather obtained from an 18-layer velocity model. The data contain only primary reflections and internal multiples (Figure 2a). The results of our 1.5D ISS-based algorithm are shown in Figure 2b and compared with the true-primaries-only gather (Figure 2c). Note that almost all internal multiples are attenuated considerably. There is some degradation of the primaries which is due to the adaptive least-squares subtraction. The results of Figure 2 are obtained without any user intervention (i.e., are fully automatic) and are encouraging. More full prestack tests are currently underway in both the shot and CMP domains.

Next the application of ISS-based internal multiple attenuation is shown on poststack data. One of our goals is to study

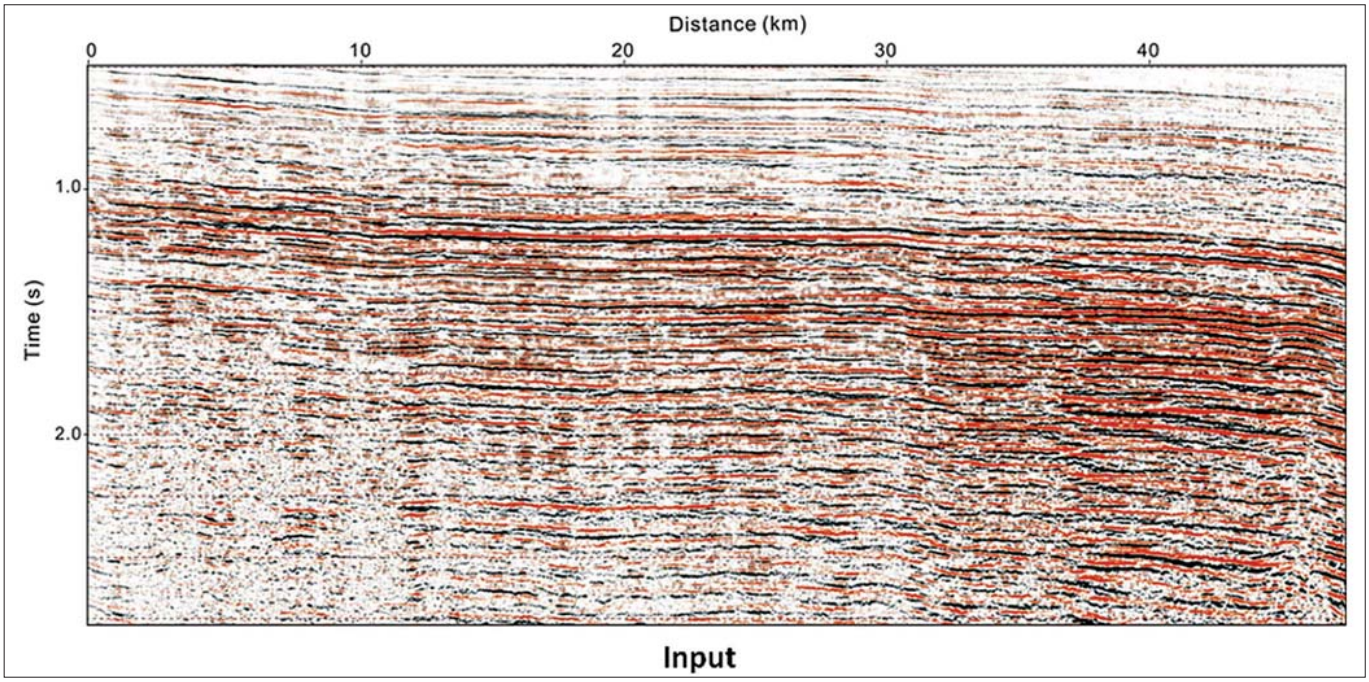

Figure 4. *Stacked section from a land data set from Saudi Arabia. The presence of internal multiples is obvious.*

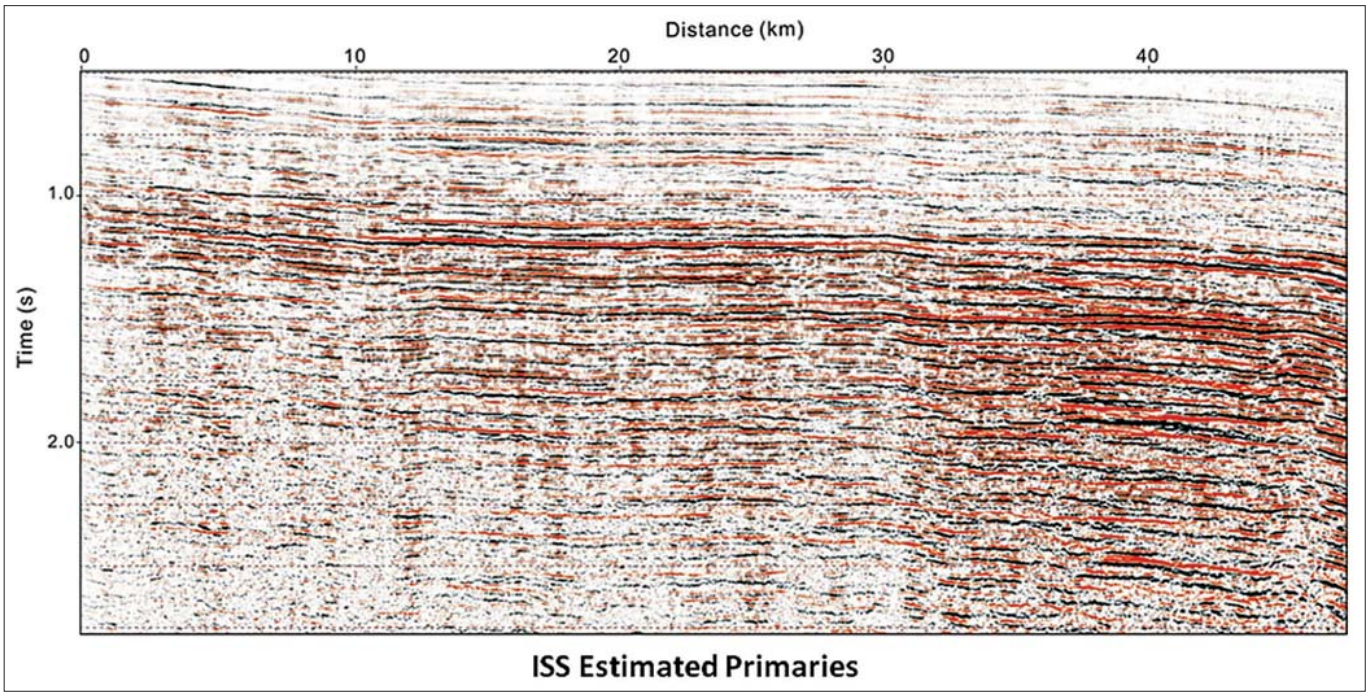

Figure 5. *Same data as in Figure 4 after ISS internal multiple elimination.*

if ISS can successfully predict internal multiples generated by thin layers. Figure 3 depicts the ISS performance on a realistic zero-offset synthetic data set. The model is composed of a large number of layers with thickness of 1 ft and is obtained from a field sonic log shown on the extreme right. The data (primaries and internal multiples) are modeled using the acoustic wave equation. The 1D ISS internal multiple-elimination result is shown on the right, while the primaries-only traces are also depicted in the middle panel. The performance of the 1D ISS-based algorithm is very good. Despite the poststack application, note the complete internal multiple elimination obtained in the zone of interest between 1.0 and 1.4 s. At the same time, the main primary events are preserved with a minimum degradation.

Figure 4 shows a stacked section of land seismic data from Saudi Arabia. The presence of internal multiples is evident in this data set. Moreover, note the spatial variability of these multiples that follows the complex near surface. It's a clear indication that they are all generated within the complex, thin layers of the near surface. Figure 5 exhibits the data after 1D

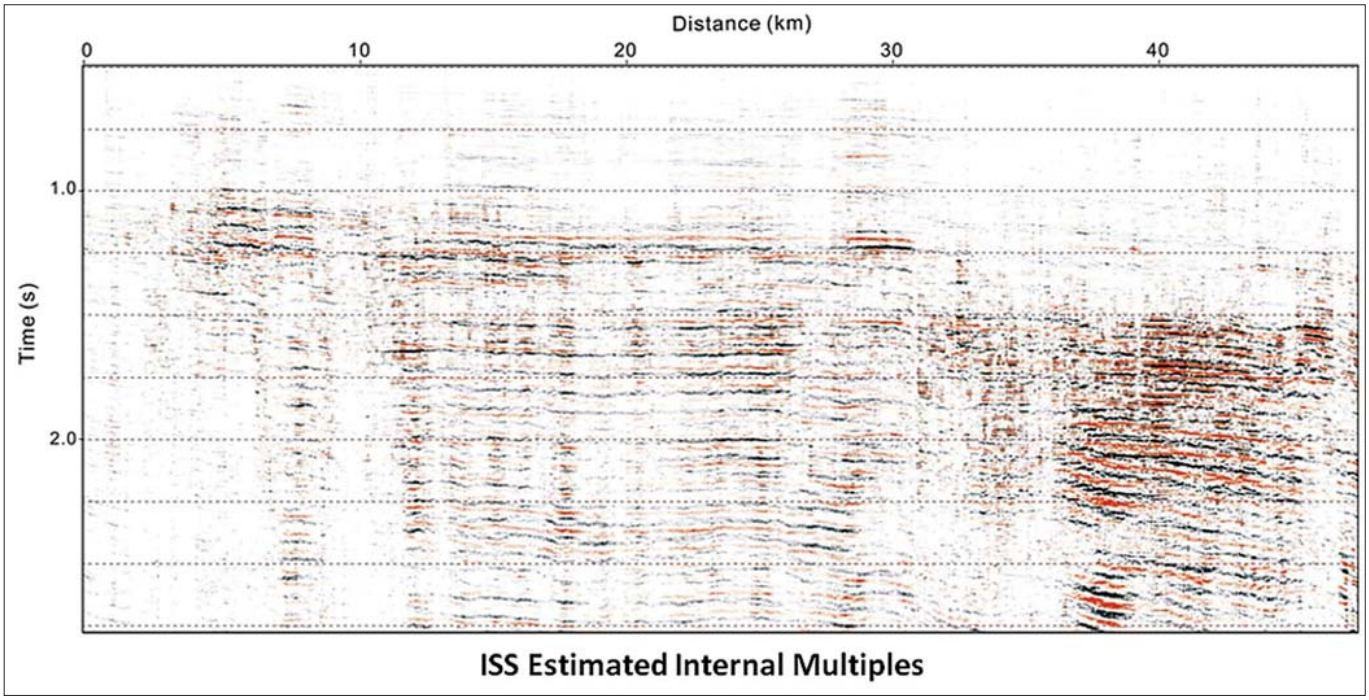

Figure 6. *Difference between Figure 4 and Figure 5 (i.e., the internal multiples).*

ISS internal multiple elimination, and Figure 6 shows the difference (i.e., the estimated internal multiples). The results are encouraging. Note the overall reduction of internal multiples. Especially, at the zone of interest between 1.4 and 2.0 s, the ISS internal multiple elimination has resulted in an improved definition of the primaries and thus increased the interpretability of the data. It is also interesting to examine the difference section where the estimated internal multiples are shown (Figure 6). The spatial variability of the internal multiples is quite obvious along with the "dull" character-free ringing appearance that represents no real geology.

Conclusions

We have developed and employed algorithms from the inverse scattering series theory for the estimation of internal multiples. They can be applied prestack (1.5D) in the CMP domain and in zero-offset (1D) data. Their performance was demonstrated with complex synthetic and challenging land field data sets with encouraging results; other internal multiple-suppression methods were unable to demonstrate similar effectiveness. This paper presents the first series of onshore field data tests of the ISS-based internal multiple-attenuation technology. ISS technology requires no velocity information for the subsurface or any advanced knowledge of the multiple generators. The main idea is to remove multiples without damaging primaries. In practice, a method like ISS can be used for high-end prediction, and then some form of adaptive subtraction is called upon to address issues omitted in the prediction. The improved multiple prediction offered by ISS is crucial in land seismic data where close interference between primaries and internal multiples occurs. The examples of this paper point to the pressing need to improve the prediction and reduce the reliance on adaptive steps, because the latter can fail precisely when you have interfering events. We will continue our research efforts for more accurate and complete prediction algorithms in order to produce effective, practical and automated internal multiple-attenuation methodologies applicable for land seismic data. TLE

References

Araújo, F. V., 1994, Linear and nonlinear methods derived from scattering theory: backscattered tomography and internal multiple attenuation: Ph.D. Thesis, Universidad Federal de Bahia (in Portuguese).

Araújo, F. V., A. B. Weglein, P. M. Carvalho, and R. H. Stolt, 1994, Inverse scattering series for multiple attenuation: An example with surface and internal multiples: 64th Annual International Meeting, SEG, Expanded Abstracts, 1039–1041.

Berkhout, A. J., 1997, Pushing the limits of seismic imaging, Part I: Prestack migration in terms of double dynamic focusing: Geophysics, **62**, no. 3, 937–953, doi:10.1190/1.1444201.

Berkhout, A. J., 1999, Multiple removal based on the feedback model: The Leading Edge, **18**, no. 1, 127–131, doi:10.1190/1.1438140.

Carvalho, P. M., A. B. Weglein, and R. H. Stolt, 1992, Nonlinear inverse scattering for multiple suppression: Application to real data. Part I: 62nd Annual International Meeting, SEG, Expanded Abstracts, 1093–1095.

Carvalho, P. M. and A. B. Weglein, 1994, Wavelet estimation for surface multiple attenuation using a simulated annealing algorithm: 64th Annual International Meeting, SEG, Expanded Abstracts, 1481–1484.

Coates, R. T. and A. B. Weglein, 1996, Internal multiple attenuation using inverse scattering: Results from prestack 1 and 2D acoustic and elastic synthetics: 66th Annual International Meeting, SEG, Expanded Abstracts, 1522–1525.

Dragoset, W. H. and Z. Jericevic, 1998, Some remarks on sur-

face multiple attenuation: Geophysics, **63**, no. 2, 772–789, doi:10.1190/1.1444377.
Jakubowicz, H., 1998, Wave equation prediction and removal of interbed multiples: 68th Annual International Meeting, SEG, Expanded Abstracts, 1527–1530.
Kelamis, P. G., E. Verschuur, K. E. Erickson, R. L. Clark, and R. M. Burnstad, 2002, Data-driven internal multiple-attenuation applications and issues on land data: 72nd Annual International Meeting, SEG, Expanded Abstracts, 2035–2038.
Kelamis, P. G., W. Zhu, K. O. Rufaii, and Y. Luo, 2006, Land multiple attenuation-The future is bright: 76th Annual International Meeting, SEG, Expanded Abstracts, 2699–2703.
Kelamis, P. G., Y. Luo, W. Zhu, and K. O. Al-Rufaii, 2008, Two pragmatic approaches for attenuation of land multiples: 70th EAGE Conference & Exhibition.
Luo, Y., W. Zhu, and P. G. Kelamis, 2007, Internal multiple reduction in inverse-data domain: 77th Annual International Meeting, SEG, Expanded Abstracts, 2485–2489.
Matson, K., 1997, An inverse scattering series method for attenuating elastic multiples from multi-component land and ocean bottom seismic data: Ph. D. thesis, The University of British Columbia.
Matson, K., D. Corrigan, A. B. Weglein, C. Y. Young, and P. Carvalho, 1999, Inverse scattering internal multiple attenuation: Results from complex synthetic and field data examples: 69th Annual International Meeting, SEG, Expanded Abstracts, 1060–1063.
Ramírez, A. C. and A. B. Weglein, 2005, An inverse scattering internal multiple-elimination method: beyond attenuation, a new algorithm and initial tests: 75th Annual International Meeting, SEG, Expanded Abstracts, 2115–2118.
Verschuur, D. J., A. J. Berkhout, and C. P. A. Wapenaar, 1992, Adaptive surface-related multiple elimination: Geophysics, **57**, no. 9, 1166–1177, doi:10.1190/1.1443330.
Verschuur, D. J. and A. J. Berkhout, 2001, CFP-based internal multiple removal, the layer-related case: 71st Annual International Meeting, SEG, Expanded Abstracts, 1997–2000.
Weglein, A. B., F. A. Gasparotto, P. M. Carvalho, and R. H. Stolt, 1997, An inverse scattering series method for attenuating multiples in seismic reflection data: Geophysics, **62**, no. 6, 1975–1989, doi:10.1190/1.1444298.
Weglein, A. B., F. Araújo, P. Carvalho, R. Stolt, K. Matson, R. Coates, D. Corrigan, D. Foster, S. Shaw, and H. Zhang, 2003, TOPICAL REVIEW: Inverse scattering series and seismic exploration: Inverse Problems, **19**, no. 6, 27, doi:10.1088/0266-5611/19/6/R01.

Acknowledgments: We thank the Saudi Arabian Oil Company (Saudi Aramco) for support and permission to present this paper. We also thank Kevin Erickson for providing the synthetic data sets and Roy Burnstad for many discussions related to the processing of field data. Arthur B. Weglein and Shih-Ying Hsu thank Saudi Aramco for Shih-Ying's internship with Geophysics Technology of EXPEC Advanced Research Center. They also thank all M-OSRP sponsors for their support.

Corresponding author: panos.kelamis@aramco.com

Exemplifying the specific properties of the inverse scattering series internal-multiple attenuation method that reside behind its capability for complex onshore and marine multiples

PAOLO TERENGHI, SHIH-YING HSU, ARTHUR B. WEGLEIN, and XU LI, University of Houston

The world of petroleum exploration constantly demands higher efficacy at every link in the data processing chain, from preconditioning to imaging and inversion. Within that chain, the removal of internal multiples constitutes a particularly resilient problem, whose resolution has only partially benefited from the advent of the data-driven technologies which have transformed the practice of free-surface multiple elimination.

Historically, internal multiples have received less attention than free-surface multiples. In offshore surveys, for example, their relative importance is often outweighed by dominant water-column multiples. However, as the demand for accuracy increases driven by improvements in imaging capability and removal of free-surface multiples, the interest in removing troublesome internal multiples rises in priority. Internal multiples can cause uncertainty in the interpretation process and can obscure both onshore and offshore exploration targets.

In all scenarios, the key to addressing the internal multiple problem consists of responding to a combination of several challenges, and exemplified in Weglein et al. in this special section of *TLE*. We seek a method that can accommodate an Earth with strong lateral variations and the wavefield phenomena it creates (such as multipathing, diffracted internal multiples). That capability is likely to be critical in offshore areas with a highly rugose (diffractive) water bottom and for internal multiples generated within salt bodies.

Other desirable characteristics are the ability to (1) operate independently of a priori information and (2) accommodate the broadest set of multiples without the user being required to identify the portion of the Earth responsible for the multiple's subevents. In a variety of situations, internal multiples are generated within alternating sequences of rocks and sediments with contrasting seismic properties. In certain geologic settings, those sequences can exist for several hundred or thousand meters and choosing one or more significant multiple generators represents a challenge by itself, which can only be confidently addressed using information from nearby well logs.

A further interest is in producing a simultaneous prediction of all internal multiples with equal accuracy at all offsets, because an accurate match between predicted and actual multiples (amplitude, phase, number of events) alleviates the burden on adaptive subtraction.

Currently available methods for internal multiple attenuation/removal can be divided into two groups. The first group of methods requires the user to identify the primaries as internal multiple subevents or the portion of the Earth responsible for the internal multiple's downward reflection. Typically, the interpretation consists in picking the traveltime of the event corresponding to a chosen downward reflector, often referred to as the internal multiple generator. The interpretation can be used directly to isolate the chosen generator from other events corresponding to deeper reflectors (pioneered by Key-

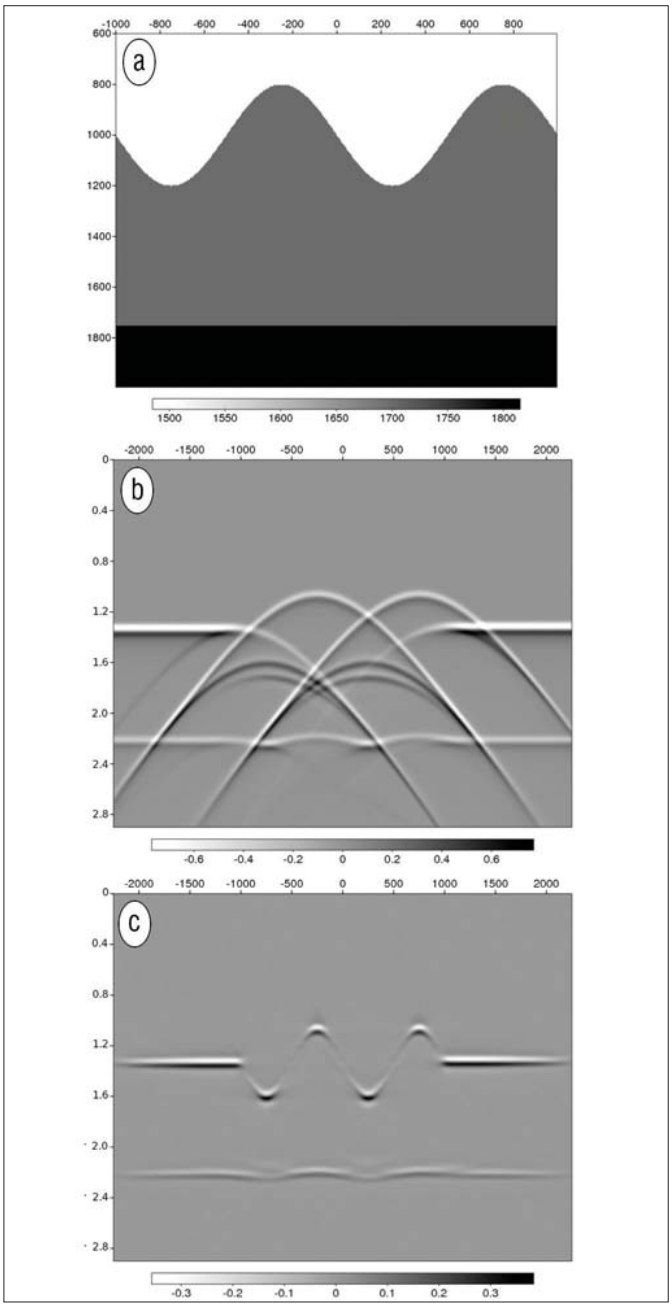

Figure 1. *(a) Velocity model; (b) zero-offset section of the input data; (c) zero-offset section of the water-speed* f-k *migration, first-order term in the ISS internal-multiple algorithm.*

dar et al., 1997, promulgated by Jakubowicz, 1998) or used to downward continue the wavefield (through common-focus-point operators) toward the generator (feedback methods, boundary approach) or toward a chosen reference level, i.e., layer approach (Berkhout and Verschuur, 2005; Verschuur and Berkhout, 2005). The reference level is chosen to separate the regions of the Earth that contain downward reflectors from those that contain upward reflectors in the construction of internal multiples. The second group of internal multiple attenuation/removal methods does not require generator identification and the internal multiples are constructed by combining three events that satisfy an automated constraint. In the method based on the inverse scattering series (ISS), the constraint is a deeper-shallower-deeper relationship in pseudodepth or vertical travel time (Araújo, 1994; Weglein et al., 1997; Weglein et al., 2003, Nita and Weglein, 2007). Ten Kroode (2002) proposed an asymptotic derivation of the results in Weglein et al. (1997), where the constraint is a longer-shorter-longer relationship between total traveltimes under the assumption of traveltime monotonicity (deeper events yield longer traveltime). The automated constraint enables the algorithms in the second group to predict internal multiples for all possible generators in one step and can be considered truly independent of subsurface information.

Through a set of examples, the analysis in this paper provides insights into the inner workings of the ISS algorithm, and an explanation for the success recently reported in a field data application on data from Saudi Arabia (Fu et al., 2010; and Luo et al. in this special section). The first example illustrates the case of internal multiples generated at a highly curved interface and demonstrates the advantage of the ISS internal multiple algorithm using vertical traveltime in contrast to total traveltime based algorithms. In the second numerical example, we illustrate the ability of the ISS internal multiple-attenuation algorithm to address all existing internal multiples generated by all downward reflectors in a single step. That ability is in contrast to the methods of the first group above, which are unable to match that removal efficacy.

Internal multiple attenuation using the inverse scattering series

The removal of internal multiples can be regarded as a particular task within the general inversion machinery of the ISS (Weglein et al., 2003). Within that framework, it is possible to identify a subset of ISS terms to suppress internal multiples starting from an input wavefield with all free-surface effects (source- and receiver-side ghosts and free-surface multiples) removed (Araújo et al., 1994; Weglein et al., 1997). ISS and all tasks within ISS (e.g., free-surface and the internal multiple-attenuation algorithms) are entirely data-driven tools which do not require information about the medium through which the multiples propagate, nor do they require moveout discrimination between primaries and multiples, nor interpretive intervention. The ISS internal multiple-attenuation algorithm predicts internal multiples for all horizons at once without needing or using information about the reflectors involved in generating them. Its leading-order term

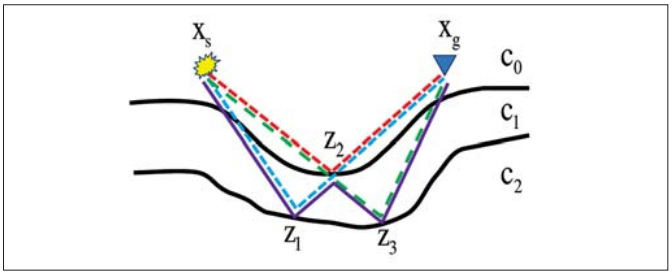

Figure 2. *An internal multiple (solid blue) satisfying monotonicity in vertical time but not in total traveltime. If wave speed c_1 is much greater than c_0, the (dashed blue) and (dashed green) primaries arrive at the surface earlier than the (dashed red) primary. The multiple is removed by the ISS method, but not by methods based on total traveltime monotonicity.*

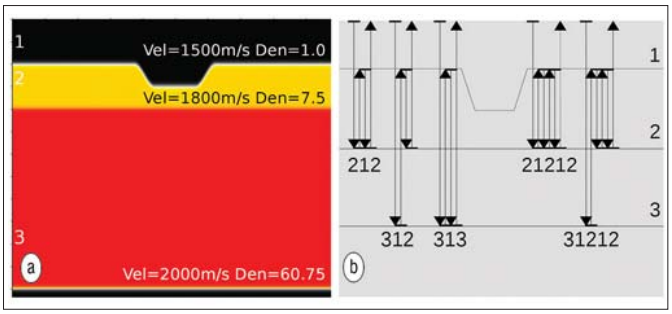

Figure 3. *(a) Earth model and (b) event labeling. Densities are chosen to yield a vertical-incidence reflection coefficient of 0.8 at all layer boundaries.*

predicts the correct traveltimes and approximate amplitudes of all the internal multiples in the data. Ramírez and Weglein (2005) extended the theory from attenuation toward elimination by including more terms in the elimination subseries, thereby improving the amplitude prediction. Although the ISS free surface and internal-multiple algorithms were initially designed for a marine towed streamer experiment (had an acoustic reference medium of water), Coates and Weglein (1996) showed that all free surface and internal multiples with converted waves in their history were also predicted. The latter free-surface and internal multiple cases are using a reference medium for which S-waves don't even exist. This is not model matching, indirect inversion or modeling run backward! Matson (1997) extended ISS multiple removal to ocean-bottom and land data. Matson et al. (1999) and Weglein et al. (2003) were the first to apply the ISS free-surface and internal multiple algorithms to marine towed-streamer field data, while Fu et al. (2010) contains the first ISS internal multiple application on land data.

Properties of the first-order term in the ISS internal multiple-attenuation algorithm—uncollapsed *f-k* migration

The algorithm starts with source- and receiver-side deghosted data absent of free-surface effects. Using only reference velocity, an uncollapsed migration (Stolt, 1978; Stolt and Weglein, 1985) maps the input data from time to pseudodepth (i.e., depth identified by imaging using a reference velocity). The concept of pseudodepth is similar to that of traveltime at vertical incidence. The pseudodepth is achieved in the fre-

quency domain, where the temporal frequency (ω) observed in the surface recordings can be related to the vertical wavenumber ($k_z = q_g + q_s$)of a constant-velocity image, through the relationship

$$q_i = \mathrm{sgn}(\omega)\sqrt{(\omega / c_0)^2 - k_i^2}$$

for i=(g,s), where, c_0 is the chosen reference velocity k_i the horizontal wavenumber and the subscripts g and s characterize the Fourier domain variables on the receiver and source side, respectively (Clayton and Stolt, 1981).

Within constant velocity migration assumptions, the *f-k* Stolt migration correctly images the reflected wavefield generated by interfaces of any arbitrary shape, including diffractions and multipathing. One example of such phenomena is the bow-tie pattern generated by reflections over a sufficiently curved boundary. These effects are common in seismic exploration data and can occur in a variety of geologic features, including salt domes, faults, layer terminations, pinch-outs, fractured and/or irregular volcanic layers and for a rough sea bottom. As we mentioned, several internal multiple-removal algorithms require picking events and traveltimes. In some of those methods (Keydar et al., 1997), the picked traveltimes are directly used to mute the wavefield at earlier or later times with respect to the generator, and internal multiples are predicted using auto- and cross-correlation operations between traces from the resulting fields. In others (e.g., the feedback methods), the traveltimes are used to determine approximate redatuming operators. However, all these approaches are based on the implicit assumption that a one-to-one relationship exists between seismic events (their traveltime) and the Earth features that create them (such as layer boundaries). In the presence of diffractions and/or multipathing, a one-to-one relationship does not exist, as, e.g., a single curved interface can produce several seismic arrivals in a single seismic trace. Picking events, traveltimes, and generators may not be viable even in a normal-incidence experiment in a 1D Earth, since destructively interfering primary and multiple events are possible and often prevalent in land field data (Kelamis et al., 2006; Fu et al., 2010).

We present an example based on a simple three-layer Earth model where the shallowest interface is sine-shaped. The model in Figure 1a produces the data in Figure 1b where all seismic events except the second primary at 2.2 s originate at the shallow reflector. Clearly, it is an issue to pick a unique traveltime to represent the curved reflector, as many events are generated which interfere among themselves and even with the second primary. The ISS method provides a natural solution by using as input the uncollapsed prestack water-speed migration (Figure 1c) where the spatial (pseudodepth) relationship between seismic arrivals matches the spatial relationship of the reflectors in the actual Earth (Nita and Weglein, 2007). The sketch in Figure 2 describes another example of an internal multiple which would not be predicted if total traveltimes were the basis of the method. The multiple can be traced back to an Earth feature where the relationship between total traveltimes and vertical traveltimes (pseudodepth) is inverted due to the presence of a high-velocity layer at depth. Vertical travel times have a closer relationship to actual depth than total time, and hence represent a more effective way to approach the removal of actual internal multiples (see, e.g., Hsu, 2011). The latter vertical traveltime is the tool used in ISS internal multiple attenuation algorithms.

Properties of the leading (third) order term ISS internal multiple attenuation algorithm

Let z_1, z_2, and z_3 be the pseudodepths of three generic points in the data produced by the first-order term in the internal multiples series. The leading-order internal multiple prediction is composed of three events that satisfy a deeper-shallower-deeper condition in pseudodepth. As those points span the entire data volume, the leading-order attenuation algorithm (which is third-order in the imaged data) allows any combination such that z_1 is greater than z_2 and z_3 is greater than z_2 to contribute to the prediction (see equation on next page), where $b_1(k_g, k_s, z)$ corresponds to effective incident plane-wave data in the pseudodepth domain.

$$b_{3IM}(k_g,k_s,\omega) = \frac{1}{(2\pi)^2}\int_{-\infty}^{\infty} dk_1 e^{iq_2(z_g-z_s)} \int_{-\infty}^{\infty} dz_1 b_1(k_g,k_1,z_1) e^{i(q_g+q_1)z_1} \times \int_{-\infty}^{\infty} dk_2 e^{iq_1(z_g-z_s)} \int_{-\infty}^{z_1-\varepsilon} dz_2 b_1(k_1,k_2,z_2) e^{-i(q_1+q_2)z_2} \int_{z_2+\varepsilon}^{\infty} dz_3 b_1(k_2,k_s,z_3) e^{i(q_2+q_s)z_3}$$

In contrast with the methods based on the convolution and correlation of wavefields, where the definition of the generator is static, the ISS algorithm's deeper-shallower-deeper constraint does not refer to any particular interface or event in the data. On the contrary, it applies to all of their water-speed images, allowing the simultaneous prediction of all first-order internal multiples from any depth without interpretation and traveltime picking of the data or knowledge of the medium.

In our second example, we demonstrate the properties of the ISS internal multiple-prediction algorithm using a set of acoustic finite-difference data. The model shown in Figure 3a consists of three interfaces, the first of which features a trench approximately 1.5 km long and 100 m deep. In Figure 3b, the travel paths of some internal multiples are drawn schematically using upgoing and downgoing arrows to represent wave propagation. In a zero-offset section of the data (Figure 4a), a first train of closely spaced internal multiples (characterized by the pattern 2[12]n) can be shown to originate from the energy reflected between the two shallow reflectors (1) and (2).

A deeper reflector (3) causes the entire train to begin again at around 1.4 s (3[12]n train) and once more at 2.1 s (313[12]n and 323[12]n trains). In general, even in a simple three-interface Earth model, the number of reverberations

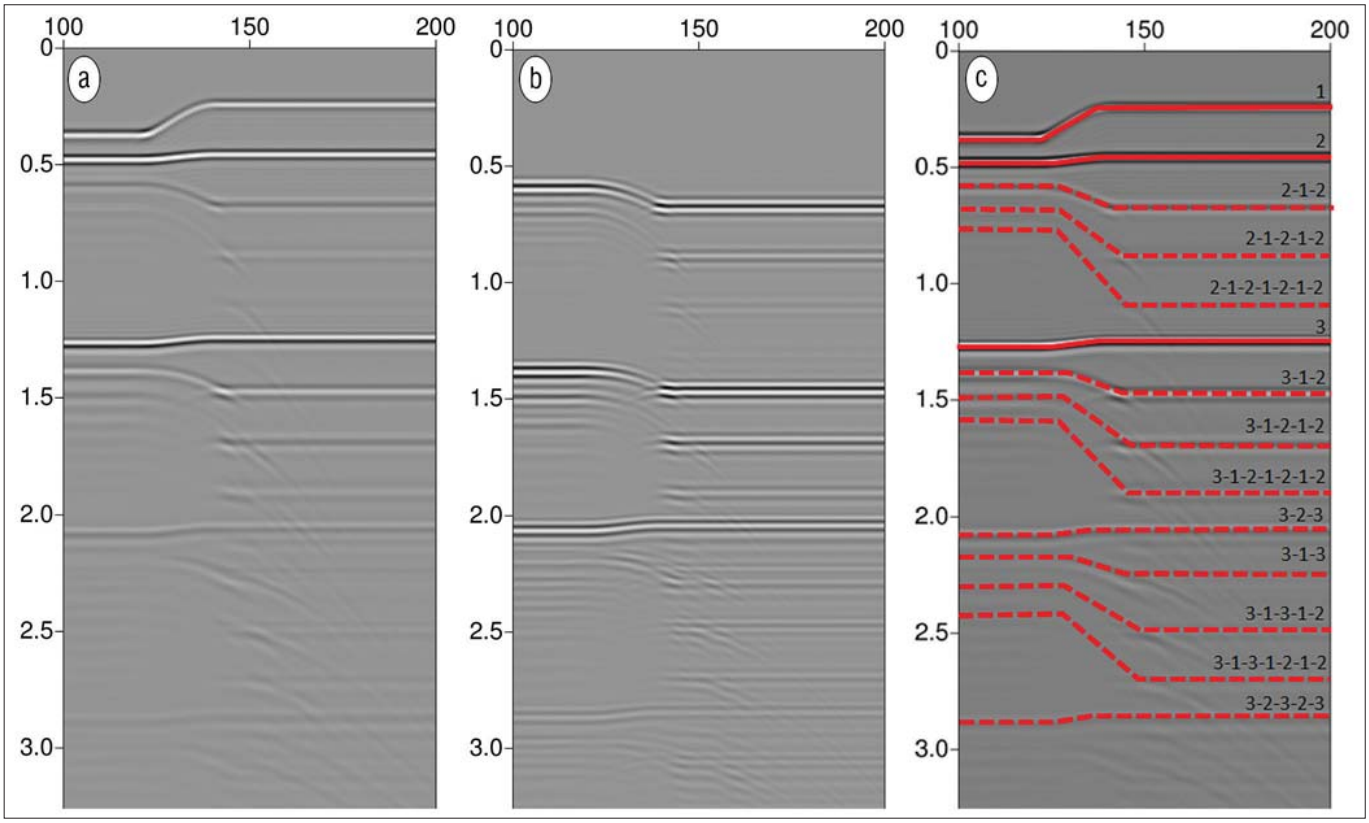

Figure 4. *Zero-offset sections: (a) input data, (b) predicted multiples, and (c) labeling of events.*

recorded at the surface is extremely large as a result of the various ways three reflectors can be combined to form internal multiples. The ISS internal multiple algorithm predicts all of them at once, without any interpretation required on the data, as shown in Figure 4b and Figure 4c.

Discussion

We observe that the layer-related approach (Berkhout and Vershuur, 2005; Vershuur and Berkhout, 2005) would not achieve the same result. Figure 5a shows the four types of first-order internal multiples generated within a three-reflector Earth. If the reference level (the lower boundary of the layer) that separates an internal multiple's upward and downward reflections were chosen between the first and the second reflectors, the layer-related method would predict the three types of first-order internal multiples shown in Figure 5b. If that strategy were applied in the example shown in Figure 4, all multiples characterized by type 3[23]n would be absent in the prediction. Figure 5c shows a different prediction produced by selecting the reference level between the second and third reflector. Similarly, in the example in Figure 4, if the downward-reflecting level were chosen between events (2) and (3), the 2[12]n event type would not be predicted. Notice that once the reference level is chosen, the events above this level can act only as downward reflectors; similarly, the events below this level can contribute only as upward reflectors. In Figure 5a, however, the second reflector contributes both as an upward reflector (for the two internal multiples in the middle) and as a downward reflector (for the rightmost internal multiple). Therefore, for any choice of downward-reflecting layer, there is at least one type of first-order internal multiple which cannot be predicted.

Conclusions

The inverse scattering series provides an approach to internal multiple attenuation with the potential to address the challenges of modern seismic exploration on land and in complex marine settings. That capability has recently been further delineated and demonstrated by complex synthetic and land field data tests (Fu et al.; Luo et al.). Through the analysis and the examples in this paper, we illustrate its inner workings and emphasize the key concepts at the base of its capability to provide (1) a comprehensive and accurate prediction of all internal multiples (2) in a purely data-driven manner, and (3) in an Earth with strong lateral variations. TLE

References

Araújo, F., 1994, Linear and non-linear methods derived from scattering theory: backscattered tomography and internal multiple attenuation: Ph.D. thesis, Universidade Federal da Bahia.

Araújo, F., A. Weglein, P. Carvalho, and R. Stolt, 1994, Inverse scattering series for multiple attenuation: An example with surface and internal multiples: 64th Annual International Meeting, SEG, Expanded Abstracts, 1039–1041.

Berkhout, A. J. and D. J. Verschuur, 2005, Removal of internal multiples with the common-focus-point (CFP) approach: Part 1—Explanation of the theory: Geophysics, **70**, no. 3, V45–V60, doi:10.1190/1.1925753.

Coates, R. and A. Weglein, 1996, Internal multiple attenuation using inverse scattering: Results from prestack 1 & 2D acoustic and

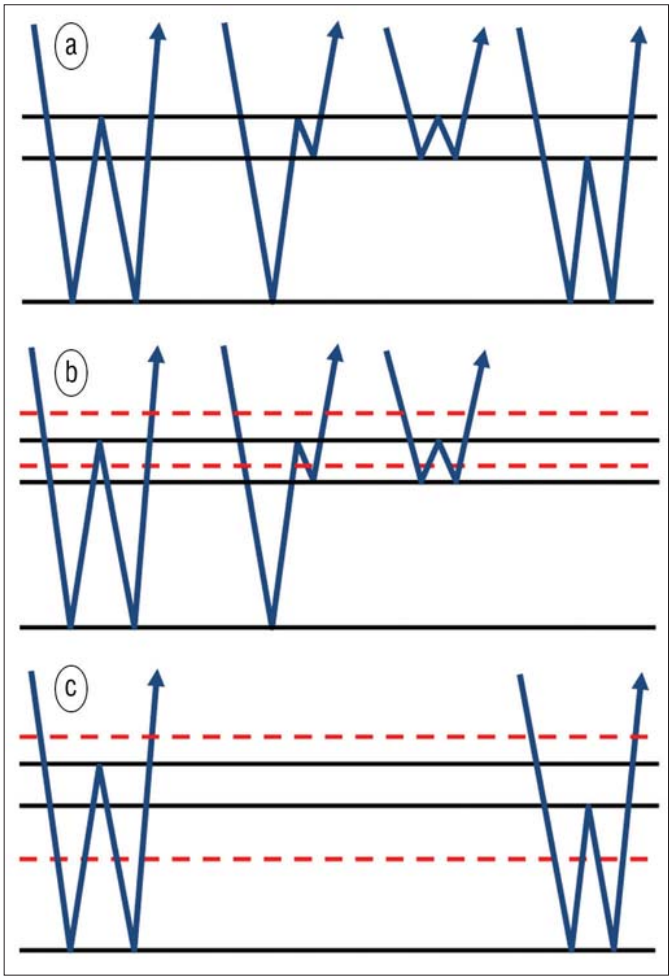

Figure 5. *(a) Four types of first-order internal multiples are generated by three reflectors; (b) and (c) the first-order internal multiples predicted by the feedback layer method using different definitions of the downward generator layer (red dashed lines).*

elastic synthetics: 66th Annual International Meeting, SEG, Expanded Abstracts 1522–1525.

Clayton, R. W., and Stolt, R. H., 1981, A Born-WKBJ inversion method for acoustic reflection data: Geophysics, **46**, 1559–1660, 10.1190/1.1441162.

Fu, Q., Y. Luo, P. Kelamis, S.-D. Huo, G. Sindi, S.-Y. Hsu, and A. Weglein, 2010, The inverse scattering series approach towards the elimination of land internal multiples: 80th Annual International Meeting, SEG, Expanded Abstracts, 3456–3461.

Hsu, S.-Y., 2011, Efficacy determination and efficiency advances for the inverse scattering series internal multiple attenuation: Complex synthetic and land field data testing, and the impact of reference velocity sensitivity: PhD thesis, University of Houston

Jakubowicz, H., 1998, Wave equation prediction and removal of interbed multiples: EAGE Extended Abstracts.

Keydar, S., E. Landa, B. Gurevich, and B. Gelchinsky, 1997, Multiple prediction using wavefront characteristics of primary reflections: EAGE Extended Abstracts.

Matson, K. H., 1997, An inverse-scattering series method for attenuating elastic multiples from multicomponent land and ocean bottom seismic data: Ph.D. thesis, University of British Columbia.

Matson, K., D. Corrigan, A. Weglein, C. Y. Young, and P. Carvalho, 1999, Inverse scattering internal multiple attenuation: Results from complex synthetic and field data examples, 69th Annual International Meeting, SEG, Expanded Abstracts, 1060–1063.

Nita, B. G. and A. Weglein, 2007, Inverse-scattering internal multiple-attenuation algorithm: An analysis of the pseudodepth and time-monotonicity requirements: 77th Annual International Meeting, SEG, Expanded Abstracts, 2461–2465.

Ramírez, A. C. and A. Weglein, 2005, An inverse scattering internal multiple elimination method: Beyond attenuation, a new algorithm and initial tests: 75th Annual International Meeting, SEG, Expanded Abstracts, 2115–2118.

Stolt, R., 1978, Migration by Fourier transform: Geophysics, **43**, no. 1, 23–48, doi:10.1190/1.1440826.

Stolt, R. H. and A. B. Weglein, 1985, Migration and inversion of seismic data, Geophysics, **50**, 2458–2464, doi: 10.1190/1.1441877.

ten Kroode, F., 2002, Prediction of internal multiples: Wave Motion, 35, no. 4, 315–3385, doi:10.1016/S0165-2125(01)00109-3.

Verschuur, D. J. and A. J. Berkhout, 2005, Removal of internal multiples with the common-focus-point (CFP) approach: Part 2—Application strategies and data examples: Geophysics, **70**, no. 3, V61–V72, doi:10.1190/1.1925754.

Weglein, A., F. Araújo, P. Carvalho, and R. Stolt, 1997, An inverse-scattering series method for attenuating multiples in seismic reflection data: Geophysics, **62**, no. 6, 1975–1989, doi:10.1190/1.1444298.

Weglein, A., F. Araújo, P. Carvalho, R. Stolt, K. Matson, R. Coates, D. Corrigan, D. Foster, S. Shaw, and H. Zhang, 2003, Inverse scattering series and seismic exploration: Inverse Problems, **19**, no. 6, R27–R83, doi:10.1088/0266-5611/19/6/R01.

Acknowledgments: The authors thank Bill Dragoset of WesternGeco (Houston) for providing the data shown in the second example, and for permission to publish the results. We thank all M-OSRP sponsors for constant support and encouragement.

Corresponding author: pterenghi2@uh.edu

Multiple attenuation: Recent advances and the road ahead (2011)

ARTHUR B. WEGLEIN, SHIH-YING HSU, PAOLO TERENGHI, and XU LI, University of Houston
ROBERT H. STOLT, ConocoPhillips

Multiple removal is a longstanding problem in exploration seismology. Although methods for removing multiples have advanced and have become more effective, the concomitant industry trend toward more complex exploration areas and difficult plays has often outpaced advances in multiple-attenuation technology. The topic of multiples, and developing ever more effective methods for their removal, remains high in terms of industry interest, priority and research investment. The question as to whether today, in 2011, multiples or multiple removal is winning is a way of describing what we are about to discuss. This paper focuses on recent advances, progress and strengths and limitations of current capability and a prioritized list of open issues that need to be addressed.

In seismic exploration it is useful to catalog events as primary- or multiple-based on whether the wave arriving at the receiver has experienced one or more upward reflection(s), respectively (Figure 1). Multiples are further subdivided and labeled according to the location of the downward reflection between two upward reflections. If the multiple has at least one downward reflection at the free surface, it is called a free-surface multiple, and if all of its downward reflections occur below the free surface, it is called an internal multiple. These definitions and cataloging of events into primary and multiple are operative and called upon only after the reference or background wavefield and the source and receiver ghosts have all been removed (Figure 2).

Both primaries and multiples contain information about the subsurface; however, (1) unraveling the information within a multiply reflected event is a daunting task, and (2) back-propagating a wavefield containing both primaries and multiples for imaging and inversion is usually beyond our ability to provide an accurate enough discontinuous overburden (required for migration and inversion). Hence, primaries are typically considered as signal and multiples are considered a form of coherent noise to be removed prior to extracting subsurface information from primaries.

"Multiple attenuation: an overview of recent advances and the road ahead" (Weglein, 1999) provides a 1999 perspective of multiple attenuation and places wave-theory advances at that time in the context of earlier pioneering contributions. We suggest *Multiple Attenuation* (published by SEG in 2005) and the special section on multiple attenuation (*TLE* 1999) as background to comprehend and to set the stage for this update and overview of recent progress, advances, and open issues as of 2011.

Offshore and onshore multiple removal: Responding to the challenges

In offshore exploration, the industry trend to explore in deep water, with even a flat horizontal water bottom and a 1D subsurface, immediately caused many traditional and useful signal processing/statistical-based multiple-removal methods to bump up against their assumptions, break down, and fail. In addition, marine exploration plays beneath complex multi-D laterally varying media and beneath and/or at corrugated, diffractive rapid varying boundaries (for example, subsalt, sub-basalt and subkarsted sediments and fault shadow zones) cause a breakdown of many other multiple-removal methods. For example, decon, stacking, *f-k,* Radon transform, and wavefield modeling and subtraction of multiples are among methods that run into problems with the violation of any one or a combination of the following assumptions: (1) primaries are random and multiples are periodic, (2) knowledge of the velocity of primaries and assuming the Earth has no lateral variation in properties with assumptions about 1D moveout, (3) velocity discrimination between primaries and multiples, (4) interpreter intervention capable of picking and discriminating primary or multiple events, and (5) determining the generators of the experiences of the multiples, and then modeling and subtracting them. The confluence of (1) high drilling costs in deepwater plays, (2) specific deepwater and shallow subsea hazards and technical challenges, (3) the need to develop fields with fewer wells, and (4) the record of drilling dry holes drives the need for greater capability for removing marine free-surface and internal multiples, as well as improving methods of imaging.

Moving onshore, the estimation and removal of land internal multiples can make the toughest marine-multiple problem pale in comparison. The presence of proximal and

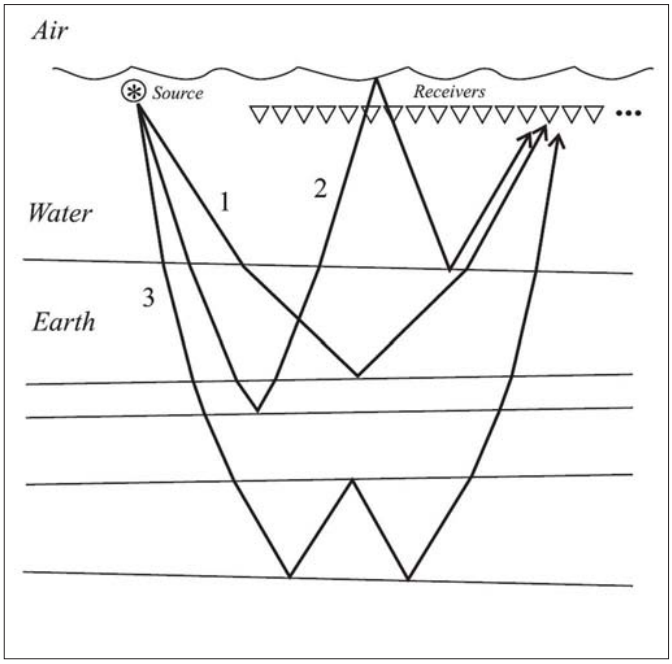

Figure 1. *Marine primaries and multiples: 1, 2 and 3 are examples of primaries, free-surface multiples, and internal multiples, respectively.*

interfering primaries and internal multiples of different orders can occur in marine situations, but their frequent occurrence for land internal multiples raises the bar of both the amplitude and phase fidelity of prediction and the priority and pressing need of developing an alternative to energy-minimizing-based adaptive subtraction techniques. For example, in Kelamis et al. (2006), Fu et al. (2010), and Luo et al. (in this special section), the basic cause of the land multiple-removal challenge in Saudi Arabia is identified as a series of complex, thin layers encountered in the near surface.

In general, strong reflectors at any depths can be identified as significant sources of internal multiples, especially where geologic bodies with different seismic properties are in contact. Typical examples are alternating sequences of sedimentary rocks and basaltic layers or coal seams, which can give rise to short-period internal multiples.

Multiples are a problem and a challenge due to violations of the assumptions and prerequisites behind methods used to remove them. There are two approaches to address those challenges: (1) remove the assumption violation (by satisfying the assumption), or (2) remove the assumption. That is, either develop a response and/or new methods that remove the violation, and arrange to satisfy the assumption, or develop fundamentally new methods that avoid the limiting or inhibiting assumption. There are cases and issues for which one or the other of these attitudes is called for and indicated. An example of seeking to satisfy a requisite is when a data acquisition is called for by a multiple-removal technique, and we seek methods of data collection and interpolation/extrapolation to remove the violation by satisfying the requirement. However, if a multiple-removal method is, for example, innately 1D in nature, then an interest in removing multiples in a multi-D Earth would call for developing a new method that did not assume a 1D Earth; i.e., it calls for developing a new multi-D method that altogether avoids the 1D assumption. The former, "remove assumption violation" approach would entail, e.g., arranging a 3D corrugated boundary subsalt play to somehow satisfy 1D layered Earth assumptions, velocity analysis, and moveout patterns, or modeling and subtraction of multiples, where seeking to satisfy those types of assumptions is not possible. The latter realization drove the search for new methods that avoid those increasingly difficult or impossible-to-satisfy criteria and prerequisites.

The list of sought-after characteristics for multiple attenuation

In response to those challenges, these new methods would therefore be required to satisfy the following criteria: (1) be fully multi-D, (2) make no assumptions about subsurface properties, (3) have no need for interpretive intervention, (4) be able to accommodate the broadest set of multiples of all orders, (5) extend to prime and composite events as introduced in Weglein and Dragoset (2005), where the definitions and meaning of primaries and multiples themselves can be extended from their original 1D Earth definitions and concepts, (6) be equally effective at all offsets, retaining effectiveness in prestack and poststack applications, and (7) last but not least, surgically remove multiples by predicting both their amplitudes and phases, and thus not harm primaries even if they are proximal and overlapping. The efficacy and choice among multiple-removal methods in response to the challenges posed in a world of complex multiple generators, in 1D Earth settings and/or in heterogeneous rapid laterally varying media and boundaries, would ultimately be evaluated, judged, and selected by how well they satisfy all of these criteria.

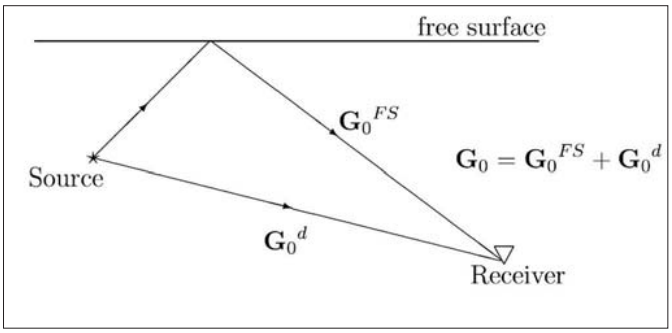

Figure 2. *The marine configuration and reference Green's function.*

The evolution and merging of methods that originally sought to either separate or wavefield-predict multiples

In Weglein (1999), multiple-removal methods were classified as: (1) separation and (2) wavefield prediction, and we refer the reader to Table 1 and Table 2 in that reference for a summary of methods within each category. Methods within the "separation" category were seeking a characteristic to separate primaries from multiples, whereas "wavefield prediction" was a way to wavefield-predict and then subtract multiples.

"Separation" methods were defined by characteristics that distinguish primaries from multiples, with, e.g., primaries considered as random and multiples as periodic, or assumptions about how primaries and multiples would separate in different transform domains. These methods earned their keep, but were ultimately hampered by their assumptions about the statistical nature of primary reflections, 1D Earth assumptions, and the assumed velocity determination for primaries.

"Wavefield-prediction" methods began with modeling and subtracting the entire history of the multiples that were targeted to be removed (e.g., Morley and Claerbout, 1983; Wiggins, 1988; Weglein and Dragoset, Chapter 4).

They moved away from 1D assumptions in principle, but were mainly confined to water-column reverberations, where they had demonstrated value, but had little hope or success in modeling and subtracting multiples with more complicated and sub-water-bottom experiences in their history.

The next step in "wavefield prediction" sought to not model the entire history of the multiple one wanted to remove, but rather to just find a wave-theory prediction to identify, isolate and separate the physical location and property that the multiple had experienced, and other events had not, and then to transform through a map of data with and without the experience as a way to "separate" events into

those that have and have not had that experience. That thinking became the cornerstone of the "free-surface and interface method" pioneered and developed by Berkhout of the DELPHI Consortium at Delft University. That DELPHI program for removing all marine multiples required a sequence of relationships between data with and without isolated and well-defined reflections, starting with downward reflections at the air-water free surface, and then through a sequence of amplitude-preserving migrations, to image and transform away all internal multiples that had their shallowest downward reflection at each successively deeper reflector/interface starting at the water bottom. Hence, it's called the free-surface and interface method. That program provided significant added-value, especially with isolated free-surface multiples, or at times for internal multiples generated at a simple and not too complex water bottom. There was considerable reliance on "adaptive subtraction" to fix omissions in the theory and limitations in data collection and prerequisites like deghosting and wavelet removal. The DELPHI approach is a wavefield-prediction method that doesn't require modeling the entire history and experience of the multiple, as earlier wavefield-prediction methods required, but required only modeling in detail the "wavefield-prediction" properties that "separated" the events experiencing a shallowest downward reflection at the free surface, and then repeating that program at the next interface or boundary in a sequence of deeper interfaces. Events are thus separated by whether they have or have not had a downward reflection at those reflecting boundaries. Hence, "wavefield prediction" and "separation" merged, with the separation requiring detail of all subsurface properties down to and including a given interface to remove all multiples having a shallowest reflection at that interface. However, that comprehensive program ran into problems of conceptual and practical issues, with the former, including: (1) how to transform away via, e.g., Green's theorem a relationship between data experiencing and not experiencing a corrugated and diffractive boundary, and, (2) the stringent requirements of determining the properties above, and down to, and at, the interface. The latter issues made the use of these interface internal multiple-removal methods difficult to be applied in practice as targets became deeper and the overburden and interfaces became rapidly varying and difficult to adequately identify.

The inverse scattering series (ISS) methods for removing free-surface and internal multiples can be viewed as representing the next step in the evolution of "separation" and "wavefield-prediction" concepts and methodology. The ISS methods are in some sense a direct response to the limitations of the DELPHI free-surface and interface approach, with (1) a more complete free-surface removal, in terms of amplitude and phase at all offsets, and (2) an internal multiple-removal method that did not require any subsurface information whatsoever. There are "wavefield-prediction" and "separation" ingredients in the ISS free-surface and internal multiple-removal methods. For free-surface multiple removal, the free-surface properties are assumed to be known, and a subseries of the inverse scattering series "separates" deghosted data with free-surface multiples from deghosted data without

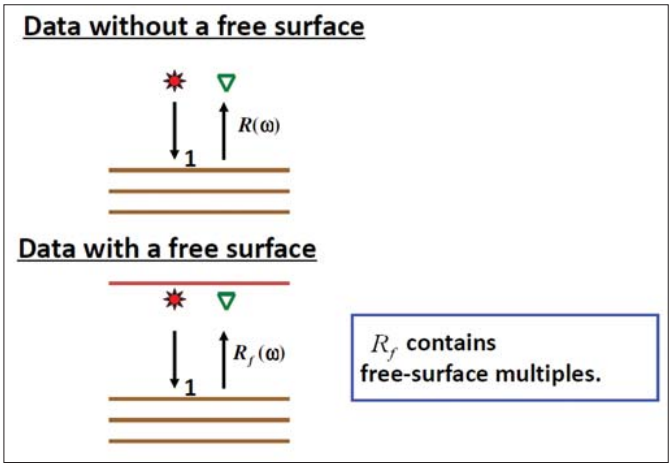

Figure 3. *Data without a free surface (top) and with a free surface (bottom).*

free-surface multiples. The ISS free-surface multiple separation is realized by the actual location and physical properties that free-surface multiples have experienced at the free surface, distinguishing themselves from data/events that have not shared that free-surface experience. For internal multiples the inverse scattering series takes on another attitude. The forward series allows the construction of primaries and internal multiples through a description entirely in terms of water speed and, through the reverse, the seismic processing or inverse scattering series, in turn, allows for the removal of internal multiples, and the depth imaging and inversion of primaries directly in terms of water speed. For internal multiple removal there is no downward continuation into the Earth, no interface identification and removal. The "separation" between primaries and internal multiples in the forward or data creation scattering series and inverse or data processing, inverse scattering series, is carried out by understanding how primaries and internal multiples differ in their forward construction, in terms of a water speed picture/construction, and then how to separate the removal of internal multiples from the imaging and inversion of primaries, also directly and only in terms of data and water speed. In contrast to the DELPHI internal multiple interface method, the ISS internal multiple-removal method never requires, determines or estimates the actual subsurface medium properties and interfaces the internal multiple experiences. The inverse scattering series multiple-removal methods are flexible, allowing (1) the separation to be in terms of distinguishing by whether or not the event has a certain well-located and well-defined experience in its history, where the actual medium properties are available and reliable, as occurs with the free surface and in ISS free-surface multiple-removal algorithm, and (2) without knowing or needing to determine anything about the actual separating experience for ISS internal multiple removal. The ISS separation of the imaging and inversion of primaries from the removal of internal multiples thus avoids all of the conceptual and practical limitations of the DELPHI free-surface and interface approach, and ultimately accounts for its current position as stand-alone for addressing the most difficult

and daunting marine and land internal multiple challenges.

The two classic multiple-removal categories separation, and wavefield prediction, have evolved and merged into the maximally flexible, accommodating and effective inverse scattering series multiple-removal methods: prediction and separation of events either with or without needing, knowing or determining the location and physical properties of the experience (e.g., a free surface or subsurface reflector, respectively) that separates events into two categories—events that have, and events that have not, experienced in their history a shallowest downward reflection at a specific reflector, and without the need for any subsurface information, event picking or interpreter intervention. The ISS allows all internal multiples to be predicted and separated from all reflectors, at all depths, at once, without knowing, needing, or determining anything about those reflectors. The inverse scattering series multiple-removal methods have incorporated the strengths of earlier separation and wavefield-prediction concepts and thinking, while avoiding the practical limitations, drawbacks and weaknesses of earlier and competing approaches.

Before discussing, classifying, and comparing methods for removing multiples, it will be useful to introduce and briefly discuss two important background topics/subjects that will enhance and facilitate understanding the sometimes counter-intuitive ideas we will be describing and attempting to convey.

Modeling and inversion are two entirely different enterprises

In this paper, we adopt an inclusive definition of inversion that includes any method that determines subsurface properties from measured surface data, or any intermediate task (e.g. multiple removal or depth imaging) toward that goal. Inversion methods can be direct or indirect, and these approaches are not in any practical or theoretical sense the same or equivalent. Modeling run backward, or model matching or iterative linear inverse model matching, or any form of indirect inversion, or solving a direct forward problem in an inverse sense, are not equivalent to direct inversion. Nor is any intermediate seismic processing objective, within a direct inversion algorithm, equivalent to solving for that same goal in some model-matching or indirect manner. That statement is true independent of: (1) the capability and speed of your computer, (2) the nature of the objective function, and (3) the local or global search engine. The only exception to that rule is when the direct inverse task is linear (e.g., when the goal is depth imaging and *you know the velocity field*, the direct inverse for depth migration is linear, and then modeling run backward is direct depth imaging). If the direct inverse is nonlinear in either the entire data set or a single event, then modeling run backward is not the equivalent of a direct inverse solution. There is widespread confusion on this fundamental and central point within math, physics, and geophysics "inversion" circles with significant and harmful conceptual and practical real-world consequence. See Weglein et al. (2009) for full detail and examples. And it is worth noting at this point that the inverse scattering series is the only direct inverse for a multidimensional acoustic, elastic, or inelastic heterogeneous Earth.

Prediction and subtraction: The plan to strengthen the prediction, and reduce the burden, dependence and mischief of the subtraction

Multiple removal is often described as a two-step procedure: prediction and subtraction. The subtraction step is meant to try to compensate for any algorithmic compromises, or real world conditions, outside the physical framework behind the prediction. In multiple-removal applications, the subtraction step frequently takes the form of energy-minimizing adaptive subtraction. The idea is that a section of data (or some temporally local portion of data) without multiples has less energy than the data with multiples. One often hears that the problem with multiple attenuation is not the prediction but the subtraction. In fact, the real problem is excessive reliance on the adaptive subtraction to solve too many problems, with an energy-minimizing criteria that can be invalid or fail with proximal or overlapping events. The breakdown of the energy-minimization adaptive subtraction criteria itself can occur precisely when the underlying physics behind, e.g., high-end inverse scattering series multiple prediction (that it is intended to serve) will have its greatest strength and will undermine rather than enhance the prediction.

The essence of ISS: An important prototype example

We will demonstrate some of these ideas (using a 1D plane-wave normal incidence case) for the inverse scattering free-surface multiple elimination method. There are other ways to derive the free-surface multiple-removal algorithm (e.g. Ware and Aki, 1968; Fokkema and van den Berg, 1990), but the ISS is unique in its message that all processing goals (e.g., internal multiple removal, depth imaging, nonlinear direct target identification, and Q-compensation without Q) can each be achieved in the same manner that the ISS removes free-surface multiples, i.e., directly without subsurface information. Hence, this analysis below carries much broader consequences beyond the immediate goal of the ISS removing free-surface multiples.

Figure 3 describes a situation in which a unit-amplitude downgoing wave leaves a source in the water column. The upper figure assumes that there is no free surface. $R(\omega)$ denotes the single temporal frequency of the upgoing recorded field. The lower figure corresponds to the same situation with the addition of the free surface. $R_f(\omega)$ is the single tempo-

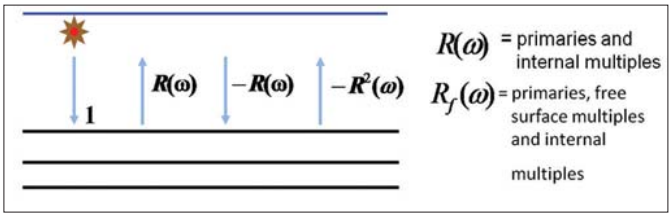

Figure 4. *The forward problem. Constructing free-surface multiples [i.e., from* R(ω) *to* $R_f(\omega)$*].*

ral frequency of the upgoing portion of the recorded data. $R(\omega)$ contains all primaries and internal multiples. $R_f(\omega)$, on the other hand, is the upgoing portion of the total measured wavefield and consists of primaries, internal multiples, and free-surface multiples. The downgoing source wavefield and the upgoing receiver wavefield would be realized in practice by source and receiver deghosting. Source and receiver deghosting is a critically important step to assure subsequent amplitude and phase fidelity of the ISS free-surface multiple-removal methods, whose derivation follows below.

Forward construction of data with free-surface multiples, $R_f(\omega)$ in terms of data without free-surface multiples, $R(\omega)$

The downgoing source wavefield of unit amplitude first impinges on the Earth and $R(\omega)$ emerges (consisting of all primaries and internal multiples). $R(\omega)$ hits the free surface and $-R(\omega)$ is the resulting downgoing wave (because the reflection coefficient is –1 for the pressure field at the free surface). This downgoing field, $-R(\omega)$, in turn enters the Earth as a "wavelet", and $-R^2(\omega)$ emerges, and this repeats in the manner shown in Figure 4.

The total upgoing wavefield in the presence of a free surface, $R_f(\omega)$, is expressed in terms of the total upgoing wavefield in the absence of the free surface, $R(\omega)$:

$$R_f(\omega) = R(\omega) - R^2(\omega) + R^3(\omega) + \cdots \quad (1)$$

$$R_f(\omega) = R(\omega)/[1 + R(\omega)] \quad (2)$$

Several points are worth noting about this result.

The inverse series for removing free-surface multiples corresponding to the forward series (Equation 1) that constructs free-surface multiples is found by rearranging Equation 2 into $R = R_f/(1-R_f)$ and then expressing R as the infinite series

$$R = R_f + R_f^2 + R_f^3 + \cdots \quad (3)$$

This expression is, indeed, the 1D normal-incidence version of the inverse scattering free-surface multiple-attenuation algorithm (Carvalho, 1992; Weglein et al., 1997). Notice that neither the forward (construction) series for R_f in terms of R nor the removal (elimination) series for R in terms of R_f depend on knowing anything about the medium below the receivers.

The ISS free-surface removal series derivation and algorithm (Equation 3) does not care about the Earth model type and is completely unchanged if the Earth is considered to be acoustic, elastic, or anelastic. That property is called "model type independence," (see Weglein et al., 2003).

The derivation of these series (Equations 1 and 3) was based on the difference in the physical circumstances that gives rise to the events we are trying to isolate and separate: free-surface multiples and the (–1) reflection coefficient at the free surface (the physical circumstance).

Both the construction and elimination process assume a wavelet deconvolution in the forward problem. The wavelet, $S(\omega)$, plays a role in the forward problem:

$$R_f(\omega) = S(\omega)R(\omega)/[1 + R(\omega)],$$

and in the inverse

$$R = (R_f/S)/(1-(R_f/S)) = R_f/S + R_f^2/S^2 + R_f^3/S^3 + \cdots.$$

where the meaning of the quantity R_f is $S(\omega)$ times R_f in Equations 1 and 2. Hence, for free-surface multiple removal, there is a critical need for the wavelet because the effectiveness of the series has a nonlinear dependence on $1/S(\omega)$.

Free-surface demultiple algorithm: Instructive analytic examples

We present an analytic 1D normal incidence example (Figure 5) to illustrate the inner workings of the ISS free-surface multiple-removal algorithm.

The reflection data in the time domain are expressed as

$$R_f(t) = R_1\delta(t-t_1) + R_2'\delta(t-t_2) - R_1^2\delta(t-2t_1) - R_2'^2\delta(t-2t_2) - 2R_1R_2'\delta(t-(t_1+t_2)) + \cdots,$$

where R_1 and R_2' are the amplitudes of the two primaries in this two reflector example. In the frequency domain,

$$R_f(\omega) = R_1e^{i\omega t_1} + R_2'e^{i\omega t_2} - R_1^2e^{2i\omega t_1} - R_2'^2e^{2i\omega t_2} - 2R_1R_2'e^{i\omega(t_1+t_2)} + \cdots,$$

and

$$R_f^2(\omega) = R_1^2e^{2i\omega t_1} + R_2'^2e^{2i\omega t_1} + 2R_1R_2'e^{i\omega(t_1+t_2)} + \cdots.$$

Hence $R_f(\omega) + R_f^2(\omega)$ precisely eliminates all free-surface multiples that have experienced one downward reflection at the free surface. The absence of low frequency (and in fact all other frequencies) plays absolutely no role in this prediction. This is a nonlinear direct inverse that removes free-surface multiples. There is no imaginable way that one frequency of data could be used to model and subtract one frequency of free-surface multiples. A single frequency of data cannot even locate the water bottom. This is an example of how a direct nonlinear inverse does not correspond to a forward problem run backward. Furthermore, model matching and subtracting multiples are inconceivable without knowing or caring about the Earth model type for the modeling step. This illustrates how model matching, iteratively or otherwise, modeling run backward, and all forms of indirect inversion are not equivalent to a direct inverse solution.

Recovering an invisible primary

Consider a free-surface example (Figure 6) with the following data, corresponding to two primaries and a free-surface multiple:

$$R_t(t) = R_1\delta(t-t_1) + R_2'\delta(t-t_2) - R_1^2\delta(t-2t_1). \quad (4)$$

Now assume for our example that

$$R_2' = R_1^2,$$

$$t_2 = 2t_1.$$

Then from Equation 4,

$$R_f(t) = R_1\delta(t - t_1).$$

The second primary and the free-surface multiple cancel, and

$$R_f(\omega) = R_1 e^{i\omega t_1}$$

$$R_f^2(\omega) = R_1^2 e^{2i\omega t_1}$$

$$R_f(\omega) + R_f^2(\omega) = R_1 e^{i\omega t_1} + R_1^2 e^{2i\omega t_1}$$

$$R(t) = R_1\delta(t - t_1) + R_1^2\delta(t - 2t_1) = R_1\delta(t - t_1) + R_2'\delta(t - 2t_1)$$

resulting in the two primaries by recovering the primary not "seen" in the original data.

The ISS free-surface multiple-removal algorithm, with deghosted and wavelet deconvolved data, can predict and subtract the hidden multiple and recover the hidden primary. If these obliquity factor deghosting and wavelet ingredients are compromised in the prediction, the amplitude and phase will be incorrect and the invisible primary will not be recovered. Furthermore, when the multiple is removed in the invisible reflector example, the energy goes up, not down, and the adaptive subtraction energy-minimization criterion fails and cannot "fix" the problem caused by missing obliquity factors, wavelet removal, and deghosting. The lesson: Don't compromise on prediction strengths and assume the subtraction (adaptive) will atone for any shortcomings. The ISS FS multiple prediction has no trouble recovering the hidden primary. Zhang (2007) demonstrates with a prestack example that with deghosted data the ISS free-surface algorithm precisely predicts the FS multiple without the need for adaptive subtraction. For these same examples and in general, the feedback loop free-surface multiple-attenuation algorithm, with its lack of an obliquity factor and retaining the source-side ghost, will not accurately predict the amplitude and phase of free-surface multiples.

ISS internal multiple-attenuation algorithm

The ISS internal-multiple-attenuation algorithm in 2D starts with the input data, $D(k_g, k_s, \omega)$, that is deghosted, wavelet deconvolved, and with free-surface multiples removed. The parameters, k_g, k_s, and ω, represent the Fourier conjugates to receiver, source, and time, respectively. The ISS internal-multiple-attenuation algorithm for first-order internal multiple prediction in a 2D Earth is (Araújo, 1994; Weglein et al., 1997).

In the previous Equation 5, the quantity $b_1(k_g, k_s, z)$ corresponds to an uncollapsed migration (Weglein et al., 1997) of an effective incident plane-wave data. The vertical wavenumbers for receiver and source, q_g and q_s are given by $q_i = \mathrm{sgn}(\omega)\sqrt{(\omega/c_0)^2 - k_i^2}$ for $i = (g,s)$; c_0 is the constant reference velocity; z_s and z_g are source and receiver depths; and z_i (i = 1, ... ,3) represents pseudodepth. $b_{3IM}(k_g, k_s, \omega)$ is a portion of a term in the ISS that performs prediction of all first-order internal multiples at all depths at once.

For a 1D Earth and a normal-incidence plane wave, Equation 5 reduces to

$$b_{3IM}(k) = \int_{-\infty}^{\infty} dz_1 b_1(z_1) e^{ikz_1} \int_{-\infty}^{z_1-\varepsilon} dz_2 b_1(z_2) e^{-ikz_2} \int_{z_2+\varepsilon}^{\infty} dz_3 b_1(z_3) e^{ikz_3} \quad (6)$$

For the example shown in Figure 6 with two primaries:

$$b_1(t) = R_1\delta(t - t_1) + R_2'\delta(t - 2t_2)$$

We transform the data into pseudodepth:

$$b_1(z) = R_1\delta(z - z_1) + R_2'\delta(z - 2z_2)$$

where $z_1 = \frac{c_0 t_1}{2}$ and $z_2 = \frac{c_0 t_2}{2}$. The integral in Equation 6 produces

$$b_{3IM}(k) = e^{2ikz_2 - ikz_1} R_1 R_2^2 T_{01}^2 T_{10}^2,$$

and in the time domain:

$$b_{3IM}(t) = \delta(t - (2t_2 - t_1)) R_1 R_2^2 T_{01}^2 T_{10}^2.$$

The actual internal multiple is

$$-\delta(t - (2t_2 - t_1)) R_1 R_2^2 T_{01} T_{10}.$$

Hence, Equations 5 and 6 predict the precise time and approximate amplitude of the internal multiple (i.e., it's an attenuator). There is a closed form subseries of the ISS that eliminates that multiple (Ramirez and Weglein, 2005).

Examples of 2D ISS free-surface and internal multiple removal with marine data

Figure 7 shows an example of the inverse scattering series internal-multiple-attenuation algorithm applied to a 2D synthetic data set. The data were computed using an Earth model characterized by rapid lateral variations (Figure 7a). In Figure 7, from left to right, the three panels show the input data, the predicted internal multiples, and the result of inverse scattering internal multiple attenuation, respectively.

Figures 8a and 8b illustrate the free-surface and internal multiple-attenuation algorithms applied to a data set from the Gulf of Mexico over a complex salt body. Seismic imaging beneath salt is a challenging problem due to the complexity of the resultant wavefield. In Figure 8a, the left panel is a

$$b_{3IM}(k_g, k_s, \omega) = \frac{1}{(2\pi)^2} \int_{-\infty}^{\infty} dk_1 e^{iq_2(z_g - z_s)} \int_{-\infty}^{\infty} dz_1 b_1(k_g, k_1, z_1) e^{i(q_g + q_1)z_1} \times \int_{-\infty}^{\infty} dk_2 e^{-iq_1(z_g - z_s)} \int_{-\infty}^{z_1-\varepsilon} dz_1 b_1(k_1, k_2, z_2) e^{-i(q_1 + q_2)z_2} \int_{z_2+\varepsilon}^{\infty} dz_3 b_1(k_2, k_s, z_3) e^{i(q_2 + q_g)z_3} \quad (5)$$

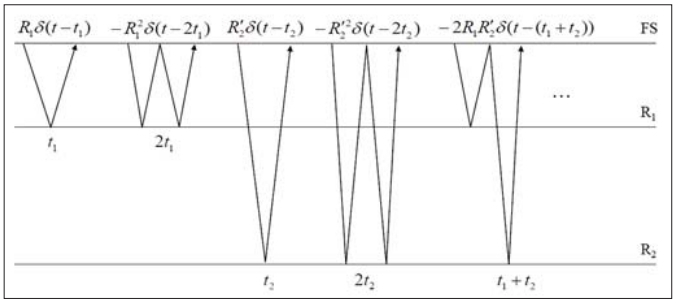

Figure 5. *An analytic 1D normal incidence example to illustrate the inner workings of the ISS free-surface multiple-removal algorithm.*

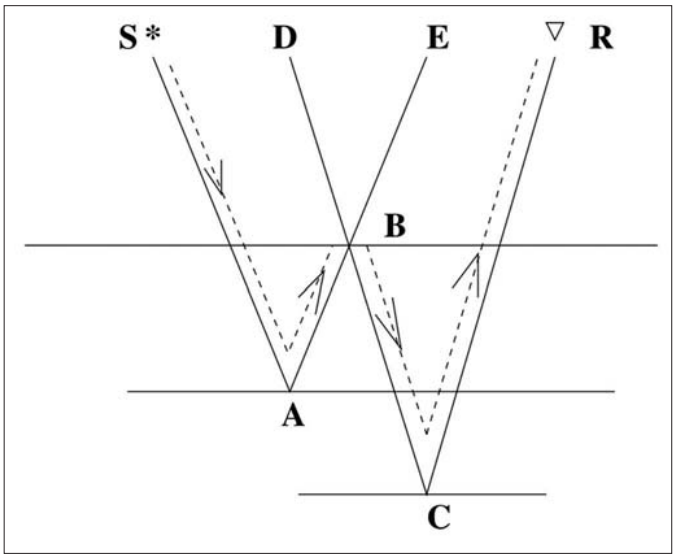

Figure 6. *A one-dimensional model with two interfaces.*

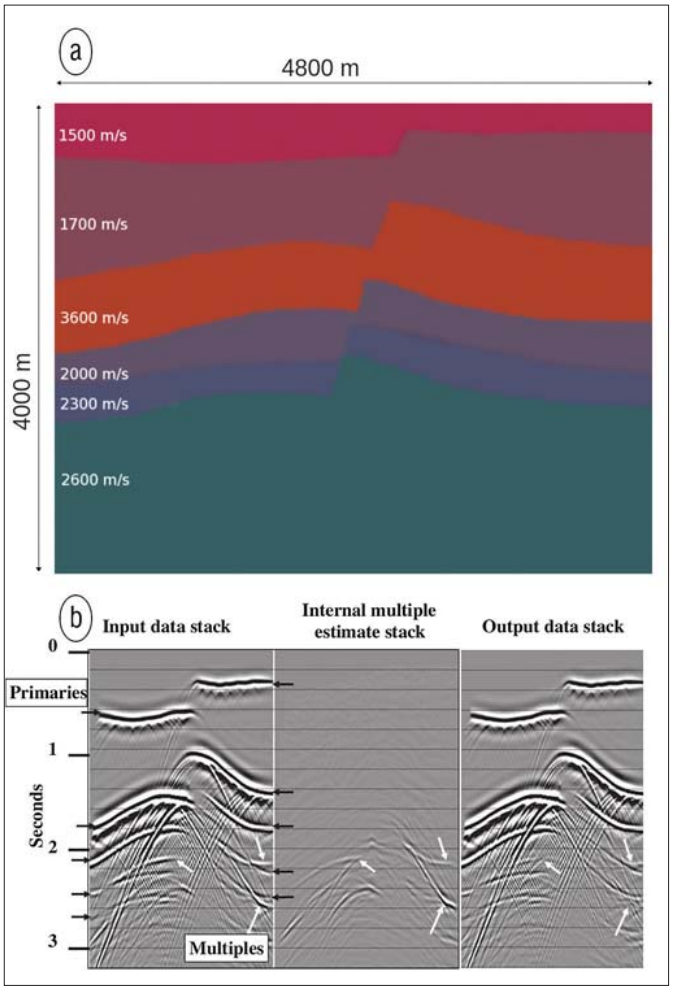

Figure 7. *(a) A 2D synthetic model characterized by gently curved reflectors intersected by a fault. (b) The left panel shows a common-offset display from the synthetic data set created using the model. The middle panel shows the predicted internal multiples and the right panel is the result after subtracting the predicted multiples from the input data set. (From Matson et al., 1999, and Weglein et al., 2003)*

stacked section of the input data and the right panel shows the result of the inverse scattering free-surface multiple-removal algorithm. Figure 8b illustrates the internal-multiple-attenuation method applied to the same Gulf of Mexico data set. An internal multiple that has reverberated between the top of the salt body and the water bottom (and interferes with the base salt primary) is well attenuated through this method.

ISS internal multiple application for land

Fu et al. (2010), along with Terenghi et al. and Luo et al., (in this special section) describe the motivation, evaluation, and comparison of different approaches to removing internal multiples on complex synthetic and onshore data. Fu et al. concluded that "Their (ISS internal multiple algorithm) performance was demonstrated with complex synthetic and challenging land field data sets with encouraging results, where other internal multiple suppression methods were unable to demonstrate similar effectiveness."

While the ISS internal multiple attenuator was unmatched in capability, in comparison with other internal multiple methods tested, an examination of the results shows that there are open issues yet to be addressed. A more complete understanding of the action of the ISS first-order internal multiple attenuator (Equation 5) when the input consists of all the events in the recorded data, and the anticipated need for further inclusion of ISS internal multiple-removal capability in our algorithm are our response to those issues, and are currently underway.

The Delft group, led by Berkhout, at some point several years ago took note and acknowledged the ISS internal multiple approach and then formulated several new and innovative DELPHI approaches that drew upon certain (but not all) aspects and properties of the ISS internal multiple algorithm. The differences between the latter DELPHI approaches and the ISS internal multiple method today remain significant and substantive. The comparisons to ISS internal multiple attenuation referred to in Fu et al. included the DELPHI approaches to internal multiple removal. The details behind the Fu et al. tests and results are described, explicated and further analyzed in Terenghi et al.

Discussion

We have described a "wish list" of qualities that the ideal response to multiple-removal challenges would satisfy, and

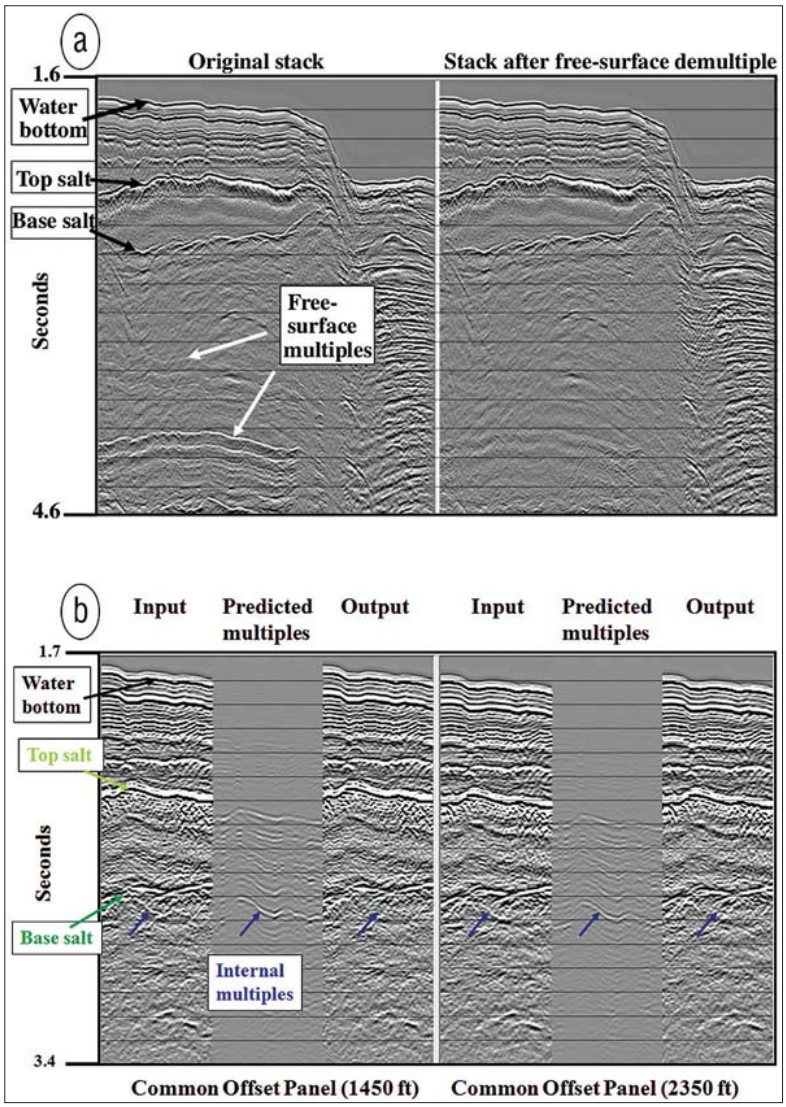

Figure 8. *(a) The left panel is a stack of a field data set from the Gulf of Mexico. The right panel is the result of ISS free-surface multiple removal. (b) The ISS internal multiple-attenuation method applied to the same data set after free-surface multiple removal. Data courtesy of WesternGeco. (From Matson et al., 1999, and Weglein et al., 2003)*

have shown that only the ISS multiple-removal methods are candidates toward reaching that high standard. All methods have strengths and shortcomings, and as we recognize the shortcomings of the current ISS attenuator, we also recognize that removing them resides within the ISS and that "upgrade" will never require subsurface information, picking events or any interpretive intervention or layer stripping. What all the ISS methods require is a reasonable source signature and deghosting, and we are developing onshore Green's theorem methods for that purpose (see Zhang and Weglein, 2005; Zhang and Weglein, 2006; and Mayhan et al., 2011).

Adaptive energy-minimizing criteria are often employed in an attempt to bridge the conditions and limitations of the real world and the physics behind what our algorithms are assuming. When first introduced by Verschuur et al. (1992) and Carvalho and Weglein (1994), the need was clear and good benefit was derived, especially with isolated primaries and free-surface multiples of first-order. But, as with all assumptions, today's reasonable and necessary assumption will invariably be tomorrow's impediment to progress and increased effectiveness. And that's the case with adaptive subtraction today, especially with land and complex marine internal multiples. We have advocated a three-pronged response to land and complex marine internal multiples: (1) seeking further capability for amplitude fidelity for all orders of internal multiples, including converted-wave internal multiples, (2) satisfying prerequisites for the source signature and radiation pattern, and (3) look for a new "bridge" to replace the energy-minimization adaptive criteria, a bridge consistent with the underlying physics rather than running at cross purposes with the greatest strength of the ISS prediction. For marine multiple removal, a key impediment for shallower-water exploration is the inability to extrapolate to near-source precritical angle traces when the nearest receiver is in the postcritical region. That can shut down free-surface multiple removal and can impede interpretation and drilling decisions. All methods for extrapolation—including *f-k*, Radon, interferometry (i.e., Green's theorem), and migrate demigrate data reconstruction—fail to provide that post- to precritical curve-jumping capability. One possibility with some ray of hope and optimism is to invert the postcritical data with model matching (Sen et al., 2001). That global search procedure and test, although positive and encouraging, was already pushing compute and algorithm capability with an initial 1D elastic test and application. Further attention and progress on this open issue is warranted and could pay significant dividends. Our plan is to progress each of these issues as a strategy to extend the current encouraging results and allow ISS multiple removal to reach its potential: to surgically remove all multiples without damaging primaries under simple or complex, daunting land and marine circumstances.

Summary

The strategy that we advocate is a tool-box approach, where the appropriate multiple-removal method is chosen, based on the given data set and the processing goal. The relative use of different methods within the tool box has shifted over time as exploration portfolios have focused on more remote, complex and difficult marine and land plays. That industry trend and need drives our orientation and continued interest in multiple removal. Its objectives are: (1) fidelity of both amplitude and phase prediction to allow surgical multiple removal of all multiples without damaging primaries; (2) including all relevant multiples in the algorithms; (3) using appropriate orders of multiple-removal terms from ISS multiple-removal subseries) in the prediction; (4) strengthen the prediction and reduce the burden on the adaptive subtraction, and (5) develop a replacement to the energy-minimization criteria that

will align with rather than impede the method it is meant to serve. The ISS methods for removing free-surface and internal multiples are an essential and uniquely qualified ingredient/component in this strategy. When other priorities (like cost) might reasonably override the interest in (1) amplitude and phase fidelity, (2) inclusion of all internal multiples, and/or when the generators of the relevant internal multiples can be reliably identified, then the DELPHI methods can be the appropriate and indicated choice.

The potential cost of drilling dry holes always has to be taken into account. The industry move to 3D acquisition and processing was not put forth to save money on acquisition and processing—it saved money by drilling fewer expensive dry holes. One exploratory well in the deepwater Gulf of Mexico can cost US $200 million—and we can significantly increase data acquisition investment and processing expenditure by the cost saving of avoiding dry holes and improving the exploration drilling success rate. Distinguishing between a multiple and a gas sand is a "drill no-drill" decision.

In summary, multiple-removal prediction methods have progressed and there is much to celebrate. The capability and potential that resides within the ISS for attenuating multiples has already shown differential added value. However, the trend to more complex and challenging marine and onshore plays demands inclusiveness of all troublesome multiples in the removal, along with: (1) stronger and more competent prediction, with amplitude and phase fidelity at all offsets, and (2) the development of fundamentally new concepts and criteria for subtraction, that align with rather than undermine the strengths of high-end prediction. There will always be a need for a subtraction step, attempting to deal with issues beyond the framework of the prediction, and there will always be those types of "beyond the framework" issues. We need a more sophisticated and capable subtraction criteria. The adaptive subtraction concept has been enormously useful, with a strong record of contribution but it is now too blunt an instrument for the more complicated and complex challenges. In the interim, the strategy is to build the strength of the prediction and to reduce the burden on the adaptive subtraction. The ISS is also the source of an effective response to outstanding open issues on amplitude and all orders of internal multiples which have moved from the back burner to center stage. The key to that strategy builds predictive strength from a direct inverse machinery, and wave-theory-deterministic Green's theorem prerequisite satisfaction, while seeking near-term reduction of the burden on the energy-minimization adaptive subtraction, and ultimately to replace the latter with an entirely consistent, comprehensive and more effective prediction and subtraction of multiples. The ISS multiple prediction, and the Green's theorem prerequisite satisfaction for the data wavelet and deghosting, are aligned and consistent. A subtraction on that same footing would provide an overall comprehensive and consistent methodology and a step improvement in multiple-removal capability. In this paper, we want to communicate our support and encouragement for that necessary future development and delivery.

The progress and success represented by advances in multiple-attenuation methods has given hope to heretofore areas that were previously "off-limits" and "no-go zones." That, in turn, has allowed our industry to imagine that yet more difficult exploration areas and targets could be accessible. In summary, that is the encouraging and positive response to the question "multiples or multiple removal; who is winning?"

References

Araújo, F., 1994, Linear and nonlinear methods derived from scattering theory: backscattered tomography and internal multiple attenuation: PhD thesis, Universidade Federal da Bahia.

Araújo, F., A. Weglein, P. Carvalho, and R. Stolt, 1994, Inverse scattering series for multiple attenuation: An example with surface and internal multiples: 64th Annual International Meeting, SEG, Expanded Abstracts, 1039–1041.

Carvalho, P. and A. Weglein, 1994, Wavelet estimation for surface multiple attenuation using a simulated annealing algorithm: 64th Annual International Meeting, SEG, Expanded Abstracts, 1481–1484.

Carvalho, P., 1992, Free-surface multiple reflection elimination method based on nonlinear inversion of seismic data: PhD thesis, Universidade Federal da Bahia.

Coates, R. and A. Weglein, 1996, Internal multiple attenuation using inverse scattering: Results from prestack 1 and 2D acoustic and elastic synthetics: 66th Annual International Meeting, SEG, Expanded Abstracts, 1522–1525.

Fokkema, J. and P. van den Berg, 1990, Removal of surface-related wave phenomena: The marine case: 60th Annual International Meeting, SEG, Expanded Abstracts, 1689–1692.

Fu, Q., Y. Luo, P. Kelamis, S. Huo, G. Sindi, S. Hsu, and A. Weglein, 2010, The inverse scattering series approach toward the elimination of land internal multiples. 80th Annual International Meeting, SEG, Expanded Abstracts, 3456–3461.

Kelamis, P., W. Zhu, K. Rufaii, and Y. Luo, 2006, Land multiple attenuation—The future is bright: 76th Annual International Meeting, SEG, Expanded Abstracts, 2699–2703.

Matson, K., D. Corrigan, A. B. Weglein, C. Y. Young, and P. Carvalho, 1999, Inverse scattering internal multiple attenuation: Results from complex synthetic and field data examples: 69th Annual International Meeting, SEG, Expanded Abstracts, 1060–1063.

Mayhan, J., P. Terenghi, A. Weglein, and N. Chemingui, 2011, Green's theorem derived methods for deghosting seismic data when the pressure P and its normal derivative are measured: 81st Annual International Meeting, SEG, Expanded Abstracts, 2722–2726.

Morley, L. and J. Claerbout, 1983, Predictive deconvolution in shot-receiver space: Geophysics, **48**, no. 5, 515–531, doi:10.1190/1.1441483.

Ramírez, A. and A. Weglein, 2005, An inverse scattering internal multiple elimination method: Beyond attenuation, a new algorithm and initial tests: 75th Annual International Meeting, SEG, Expanded Abstracts, 2115–2118.

Sen, M., A. B. Weglein, and P. Stoffa, 2001, Prediction of precritical seismograms from postcritical traces, University of Texas Institute for Geophysics Research Project Report: M-OSRP report year 2009.

Shaw, S. A. and H. Zhang, 2003, Inverse Scattering Series and Seismic Exploration, Inverse Problems: R27–R83.

Terenghi, P., S. Hsu, A. B. Weglein, and X. Li, 2011, Exemplifying the specific properties/characteristics of the ISS internal multiple method that reside behind its capability for complex on-shore and marine multiples: in this issue.

Verschuur, D., A. J. Berkhout, and C. P. A. Wapenaar, 1992, Adap-

tive surface-related multiple elimination: Geophysics, **57**, no. 9, 1166–1177, doi:10.1190/1.1443330.

Ware, J. A., and K. Aki, 1968, Continuous and discrete inverse scattering problems in a stratified elastic medium. I. Plane waves at normal incidence: The Journal of the Acoustical Society of America, **45**, no. 4, 911–921, doi:10.1121/1.1911568.

Weglein, A., F. Araújo, P. Carvalho, R. Stolt, K. Matson, R. Coates, D. Corrigan, D. Foster, S. Shaw, and H. Zhang, 2003, Inverse scattering series and seismic exploration: Inverse Problems, **19**, no. 6, R27–R83, doi:10.1088/0266-5611/19/6/R01.

Weglein, A. and W. Dragoset, eds., 2005, Multiple attenuation: SEG Geophysics Reprint Series.

Weglein, A., 1999, Multiple attenuation: an overview of recent advances and the road ahead: The Leading Edge, **18**, no. 1, 40–44, doi:10.1190/1.1438150.

Weglein, A., F. Araújo Gasparotto, P. Carvalho, and R. Stolt, 1997, An inverse-scattering series method for attenuating multiples in seismic reflection data: Geophysics, **62**, no. 6, 1975–1989, doi:10.1190/1.1444298.

Weglein, A., H. Zhang, A. Ramírez, F. Liu, and J. Lira, 2009, Clarifying the underlying and fundamental meaning of the approximate linear inversion of seismic data: Geophysics, 74, no. 6, WCD1–WCD13, doi:10.1190/1.3256286.

Wiggins, J., 1988, Attenuation of complex water-bottom multiples by wave-equation-based prediction and subtraction: Geophysics, **53**, no. 12, 1527–1539, doi:10.1190/1.1442434.

Zhang, J., 2007, Wave theory based data preparation for inverse scattering multiple removal, depth imaging and parameter estimation: analysis and numerical tests of Green's theorem: PhD thesis, University of Houston.

Zhang, J., and A. Weglein, 2005, Extinction theorem deghosting method using towed streamer pressure data: analysis of the receiver array effect on deghosting and subsequent free-surface multiple removal: 75th Annual International Meeting, SEG, Expanded Abstracts, 2095–2098.

Zhang, J. and A. Weglein, 2006, Application of extinction theorem deghosting method on ocean bottom data: 76th Annual International Meeting, SEG, Expanded Abstracts, 2674–2678.

Acknowledgments: The authors express our deepest appreciation and gratitude to Dolores Proubasta, James D. Mayhan, and Hong Liang for their excellent technical suggestions and advice that have greatly benefited this paper. All authors wish to thank all M-OSRP sponsors, NSF (Award DMS-0327778) and DOE (BES Award DE-FG02-05ER15697) for their encouragement and support. We thank Bill Dragoset and WesternGeco for providing the data shown in example 2 and for permission to publish the results.

Corresponding author: aweglein@uh.edu

Reflector Spectrum for Relating Seismic Arrivals to Reflectors

Hong Liang[2], Yi Luo[1], Panos G. Kelamis[1] and Arthur B. Weglein[2]

[1]EXPEC Advanced Research Center, Saudi Aramco, Saudi Arabia

[2]University of Houston, USA

ABSTRACT

When interpreting seismic images or suppressing multiples in seismic data, it is important to identify which reflectors the multiples, especially the internal multiples, originated from. In this paper, we present a method to relate all seismic arrivals, including primaries and multiples, to their originating reflectors. The method makes use of the reflectivity forward modeling method to isolate reflectors and determines the contribution of an individual reflector to arrivals in a seismic trace. Repeating this process for all reflectors produces a reflector spectrum, which shows quantitatively the relative contribution of each reflector to all arrivals in a trace. Then we modify the reflector spectrum to relate seismic arrivals only to their shallowest reflectors. We apply the reflector spectrum and the modified reflector spectrum for a velocity model constructed from a field sonic log. Our study provides an indication of the minimum number of reflectors responsible for multiples, and demonstrates that internal multiples originate from many reflectors distributed throughout the model, rather than from a few major ones.

INTRODUCTION

When interpreting seismic data, we often make synthetic traces generated from 1D velocity models derived from sonic logs. This trace is useful for interpreters to associate seismic events with well information, and to distinguish primaries from multiples. It will be helpful that we

relate seismic arrivals in these traces to their reflectors. Building the relations between seismic arrivals and corresponding reflectors will help us to develop multiple reduction methods.

Others (Foster and Yin, 1995; Resnick, et al., 1986) have proposed methods to determine how seismic reflections are generated and propagate in finely laminated thin layers. One method for identifying reflectors that generate internal multiples follows a trial and error approach. The method first sets impedance contrasts to zero at selected depths in a velocity model, and then the resulting wavefield is observed. If certain internal multiples disappear after an impedance contrast is removed, then it is concluded that the removed impedance contrast generated the multiples. The disadvantage of this method is that altering the velocity model affects not only the impedance contrasts of reflectors, but also the traveltimes of seismic waves.

In this paper, we propose a method, referred as to reflector spectrum, for analyzing individual reflectors and the arrivals they generate, without changing the velocity model. This reflector spectrum method allows us to quantify the contribution of a single reflector to all arrivals in a seismic trace, or conversely, to identify all contributing reflectors for a single arrival.

METHOD

The reflector spectrum method is built based on the reflectivity forward modeling algorithm (Kennett, 2003). For a given velocity function $v(z_i)$, where z_i is the depth of the i^{th} reflector and i is the layer index taking value from 1 to N, the reflection and transmission coefficients due to velocity contrasts of two adjacent layers $v(z_i)$ and $v(z_{i+1})$ are given by

$$r_d(z_i) = \frac{v(z_{i+1}) - v(z_i)}{v(z_{i+1}) + v(z_i)} \tag{1}$$

$$r_u(z_i) = \frac{v(z_i) - v(z_{i+1})}{v(z_{i+1}) + v(z_i)} \tag{2}$$

$$t_d(z_i) = 1 + r_d(z_i) \tag{3}$$

$$t_u(z_i) = 1 + r_u(z_i) \tag{4}$$

where $r_d(z_i)$ and $t_d(z_i)$ are reflection and transmission coefficients for incident downgoing waves, respectively, $r_u(z_i)$ and $t_u(z_i)$ are the corresponding coefficients for incident upgoing waves, and i is taking value from 1 to N-1. The density is ignored for simplifying the symbols in description, even though it plays a role in the coefficient. Besides defining the reflectivity coefficients, the velocity $v(z_i)$ also determines the traveltimes for waves traveling in between interfaces.

Since the reflectivity method separates the roles of reflectivity and traveltimes (see details in Appendix A), it allows us to change a single reflection coefficient while keeping the remaining coefficients as well as the velocity $v(z_i)$, hence, the traveltime, unchanged. As a result, we can simply set one of the reflection coefficients to zero without changing the velocity function itself. In this way, the effect of the corresponding reflector is isolated.

Figure 1 shows a simple example to illustrate this concept. The velocity function is shown in Figure 1a, and the calculated reflection coefficients are shown in Figure 1b. Using the velocity, reflectivity, and a wavelet, we compute the synthetic trace shown in Figure 1c. Zeroing the reflection coefficient corresponding to the first interface (setting $r_d(z_1) = r_u(z_1) = 0$ while keeping everything else unchanged) shown in Figure 1d produces a new trace (Figure 1e). The subtraction of this new trace from the original trace (Figure 1a) generates the difference trace shown in Figure 1f. The events seen in the difference trace originate from the reflector located at the first interface, and include the primary reflection at top of the layer (at 400 ms) and all related internal multiples, although only the first order internal multiple (at 1000 ms) is shown here.

Similarly, we can dim the reflection coefficient at the bottom of the layer, then the second primary and the associated internal multiples (including the same one at 1000 ms as in Figure 1c) will become disappeared. Note that the very same multiples can be erased by muting either the top (at 400 m) or bottom reflector (at 1000 m), and this is because we removed or dimmed both reflection coefficients ($r_d(z_i)$ and $r_u(z_i)$) simultaneously for an interface in this example. If only one type of coefficient, e.g., $r_u(z_1)$, is muted, this internal multiple will disappear only once by dimming the top reflector. We will show, in the section of shallow-reflector spectrum, that such surgical muting is useful for simplifying the relationships between multiples and their generators.

Figure 1 showed that muting reflection coefficients of an interface produces a difference trace, which contains reflections originated from this muted reflector. Next, by individually zeroing reflection coefficients for interfaces 1 to $N-1$, we obtain $N-1$ difference traces. These $N-1$ traces can be displayed in an image, named a reflector spectrum. In summary, the reflector spectrum is achieved by the following steps:

1) Compute the original synthetic trace $Tr_{all}(t)$ where no reflection coefficient is set to zero;
2) For the i^{th} reflector at depth z_i (beginning with $i=1$), set the reflection coefficients $r_d(z_i)=r_u(z_i)=0$, to obtain a new synthetic trace $Tr_i(t)$;
3) Subtract $Tr_i(t)$ from $Tr_{all}(t)$ to obtain a difference trace $Tr_{diff}(t,z_i)=Tr_{all}(t)-Tr_i(t)$, which contains all the seismic arrivals that have experienced at least one reflection at the i^{th} reflector (at depth z_i);
4) Repeat (2) and (3) for each reflector i taking values $2 \le i \le N-1$ to get a group of difference traces $Tr_{diff}(t,z_i)$, which constitutes the reflector spectrum.

Reflector Spectrum

Figure 2 illustrates an example of the reflector spectrum, in which each column is a difference trace after setting each interface reflection coefficient, in turn, to zero. The leftmost panel in the figure shows the full synthetic trace $Tr_{all}(t)$ including all reflection coefficients. For simplicity, only primary reflections are modeled in the reflector spectrum in Figure 2, so this spectrum shows where the primaries are generated. This method for identifying reflectors corresponding to primary reflections can also be used to identify those for other types of reflections such as surface-related multiples or internal multiples. Note that since primaries reflect only once and each primary reflection is only associated with one reflector, summing the reflector spectrum in Figure 2 over the horizontal axis will produce the synthetic trace shown on the left in the figure.

Just as a velocity spectrum relates seismic events to velocities—that are the best fits of the moveout of these events, the reflector spectrum allows us to easily relate arrivals in a seismic trace to their corresponding reflectors. For any event in the reflector spectrum, the vertical coordinate indicates the arrival time of the reflection, while the horizontal coordinate indicates the depth of the corresponding reflector. Values in the reflector spectrum have units of seismic amplitude, and the color at a point (t,z) in the spectrum represents the seismic amplitude contributed by the reflector at depth z to the seismic arrival at time t. Thus, a horizontal trace in a reflector spectrum at time t (a common time trace) identifies contributions of all reflectors to the arrival at time t in the full seismic trace, while a vertical trace in a reflector spectrum at depth z (a common depth trace) shows all seismic arrivals generated by the reflector at that depth. Therefore, muting a single reflector will mute the entire vertical trace in the reflector spectrum. As we will show later, muting the single reflector at the free surface will remove all

surface-related multiples, and that is what have been done by the well-known SRME technology.

In a first glance of Figure 2, we might think that the reflector spectrum looks like a display of VSP data which also has the two coordinates of time and depth. However, they are very different. Each traces at depth z in VSP is a record of the wave field at that depth, however, as we mentioned before, a vertical trace in a reflector spectrum at depth z shows all seismic arrivals generated by the reflector at that depth. For example, if Figure 2 were showing VSP data, we would have seen many events traceable from the generating depth all the way to the surface, so along with the first arrival, many "V" shape patterns (with 90-degree anti clock wise rotation) would have been observed. In a display of VSP data the reflected waves can be recorded and shown at all locations shallower than the depths where they are reflected; in contrast, in the reflector spectrum they are only shown at the depths where they are reflected.

The reflector spectrum can be viewed as a well-known mathematical operator—the Fréchet derivative, i.e., the derivative of the calculated trace with respect to each individual reflection coefficient. Further investigation of this property could lead to an inversion scheme for primary reflections only, for example.

REFLECTOR SPECTRUM

In the following examples, a more complex velocity function derived from a sonic log is used to compute seismic waves. The reflectivity algorithm uses a same set of parameters in all examples: sample interval in time dt=0.004 s, number of samples in time nt=500, sample interval in space dz=5 m, number of samples in space nz=200, peak frequency of Ricker wavelet f_p=20 Hz.

Reflector Spectrum

Figure 3a and Figure 3b show the reflector spectrums for primaries only and internal multiples only, respectively. Figure 4 shows two common depth traces extracted from Figures 3a and 3b at the locations indicated by the blue arrows. From Figure 4, we see that the reflector at depth 400 m generates one primary reflection (Figure 4a) and many internal multiples (Figure 4b).

Similarly, Figure 5 shows two common time traces extracted from Figures 3a and 3b at the locations indicated by the red arrows. Not surprisingly, we see that the primary reflections at time 800 ms originate from reflectors confined to a small region in depth (primaries generated at these reflectors interfere with each other due to the effect of wavelet), while the internal multiples at 800 ms originate from many reflectors over a wide range of depths ranging from shallow to deep.

Figure 4 shows that the arrival time of the first arrival of multiple reflections (Figure 4b) is nearly the same as that of primary reflections (4a). This similarity can be explained with refence to Figure 6, where we can see three primaries (S_1-Z_2-Z_1-R_1, S_2-Z_1-R_1, and S_2-Z_1-Z_3-R_2) and one internal multiple (S_1-Z_2-Z_1-Z_3-R_2), and all these reflections have nearly the same traveltime if the three reflectors are close to each other. Note that all the symbols of S_1, S_2, R_1 and R_2 are actually representing the same spatial point in the 1D case. From Figure 5 we know that that the primaries (near 900 m in Figure 5a) and the internal multiples (near 900 m in Figure 5b) will be mixed in a synthetic trace consisting of all kinds of reflections. These phenomena indicate the fact that a classical primary reflection (which is considered to be the result of a process in which a downgoing wave travels to a reflector, reflects once and returns to the surface) is associated with a set of multiple reflections. Therefore, in a thin layer model, the observed 'primary' is often the

result of interference between a classical primary reflection and multiple reflections (O'doherty and Anstey, 1971; Foster and Yin, 1995).

The traces in Figure 5, along with the reflector spectrum in Figure 3b, suggest that an internal multiple is related to many reflectors. This is to be expected, since an internal multiple involves at least two, often three, reflectors. For example, in Figure 6, muting any one of the three reflectors the first order internal multiple will disappear, so this first order internal multiple is related to all of the three reflectors. Although the reflector spectrum relates an internal multiple to all contributing reflectors, which is the physical truth, the fact that each multiple can appear numerous times may be undesirable for multiple elimination techniques, and summing the reflector spectrum over the horizontal axis will not produce the original synthetic trace shown on the left. For this reason, we propose to modify the reflector spectrum so that each multiple appears only once.

SHALLOW-REFLECTOR SPECTRUM

Here we introduce the shallow-reflector spectrum, which is a modified reflector spectrum that provides a simplified view of how multiples are generated. In a shallow-reflector spectrum, multiples are related only to the shallowest corresponding reflectors. For example, in Figure 6, the first-order internal multiple will be only related to the reflector at depth z_1. This is typical in land seismic datasets (Luo et al., 2011; Kelamis et al., 2008). As a result, each multiple will appear only once in this spectrum, unlike the reflector spectrum for internal multiples shown, for example, in Figure 3b, where each multiple can appear more than once. The shallow-reflector spectrum can be obtained by the following steps:

Reflector Spectrum

1) Compute the original synthetic trace $Tr_{all}(t)$ where no reflection coefficient is set to zero;
2) For the i^{th} reflector at depth z_i (beginning with $i=1$), set the reflection coefficients for the incident upgoign waves $r_u(z_k)=0$ for every k satisfying $1 \le k \le i$, to obtain a new synthetic trace $Tr_i(t)$;
3) Subtract $Tr_i(i)$ from $Tr_{all}(t)$ to obtain a difference trace $Tr_{diff}(t,z_i) = Tr_{all}(t) - Tr_i(t)$;
4) Repeat (2) and (3) for each reflector i taking value $2 \le i \le N-1$, to obtain a set of difference traces $Tr_{diff}(t,z_i)$. The resulting trace $Tr_{diff}(t,z_i)$ contains all the multiples that have experienced at least one downward reflection, which turns upgoing waves into downgoing, at or above the i^{th} reflector;
5) For $2 \le i \le N-1$, calculate $Tr_{shallow}(t,z_i) = Tr_{diff}(t,z_i) - Tr_{diff}(t,z_{i-1})$, to obtain a shallow-reflector trace which contains all multiples that have experienced at least one reflection at the i^{th} reflector. For this trace, no reflection occurs above the i^{th} reflector, i.e., the i^{th} reflector is the shallowest reflector. For $i=1$, we have $Tr_{shallow}(t,z_1) = Tr_{diff}(t,z_1)$ according to the definition of shallow-reflector trace. The group of shallow-reflector traces $Tr_{shallow}(t,z_i)$ constitutes the so-called shallow-reflector spectrum.

Figures 7a and 7b show the reflector spectrum and shallow-reflector spectrum for surface-related multiples only, respectively. Figure 7a reveals the true physics and indicates where all surface-related multiples originated. In comparison, Figure 7b indicates only the shallowest reflector for each surface-related multiple.

Figure 7b suggests that all surface-related multiples can be eliminated if the influence of the surface reflector can be somehow removed. In fact, others (Verschuur and Berkhout, 1997; Weglein et al., 1997; Moore and Dragoset, 2008) have developed methods to do exactly this. The success of these surface–related multiple elimination techniques is perhaps due in part to the simplicity of the shallow–reflector spectrum for surface–related multiples (e.g., Figure 7b), which indicates that *all* surface–related multiples can be removed simply by removing the surface reflector.

Figure 8 shows the shallow-reflector spectrum for internal multiples only. It is worth to remind that the corresponding reflector spectrum have been shown in Figure 3b. Figure 9 illustrates the contributions from reflectors at all depths to the internal multiple at 800 ms in the shallow-reflector spectrum. Note that because each internal multiple appears only once in a shallow-reflector spectrum, we can conclude from Figures 8 and 9 that the internal multiples originate from many reflectors. Not surprisingly, we cannot hope to eliminate all internal multiples by simply removing a single reflector, as was the case for surface-related multiples.

Perhaps the most attractive feature of the shallow-reflector spectrum is that summation of, for example, the spectrum shown in Figure 8 over horizontal axis will produce the full synthetic trace $Tr_{all}(t)$ shown in the left panel in the figure. This property could prove useful when developing internal multiple elimination techniques.

Using the shallow-reflector spectrum, our study demonstrates that internal multiples originate from many reflectors distributed throughout a model, rather than a few major reflectors. The shallow-reflector spectrum provides an indication of the minimum number of reflectors responsible for multiples, or, in other words, the minimum number of reflectors we have to remove in order to eliminate the multiples. For surface-related multiples, the shallow-reflector

spectrum confirms that only one reflector, i.e., the free surface, is responsible for the multiples, and so we can eliminate all surface-related multiples by removing the free surface. For internal multiples, however, the shallow-reflector spectrum shows that many reflectors are responsible for the multiples. Thus, we cannot eliminate all internal multiples by removing any single reflector or even a few of the strongest reflectors.

CONCLUSIONS

We have presented a new method for generating a reflector spectrum, which relates seismic arrivals or events to the reflectors from which they originated. We have also proposed a shallow-reflector spectrum, which relates seismic arrivals only to the shallowest corresponding reflector. Our study confirms that internal multiples originate from many reflectors. Thus, internal multiples cannot be eliminated by removing any single reflector or even a few major reflectors. The reflector spectrum can give new leverage to interpreters to relate seismic events to their generators, and developer to get insight into the fundamental physics of multiples generation.

ACKNOWLEDGEMENTS

The authors thank the Saudi Arabian Oil Company (Saudi Aramco) and its Advanced research Center (EXPEC ARC) for support and permission to present this research.

APPENDIX A

REFLECTION FROM A STACK OF UNIFORM LAYERS

We follow the reflectivity method in Kennett (2003) to build up the combined reflection response of an N-layer velocity model to normal incident downgoing waves. Figure A-1shows

the N-layer velocity model $v(z_i)$, where z_i is the depth of the i^{th} reflector and i is the layer index taking value from 1 to N,

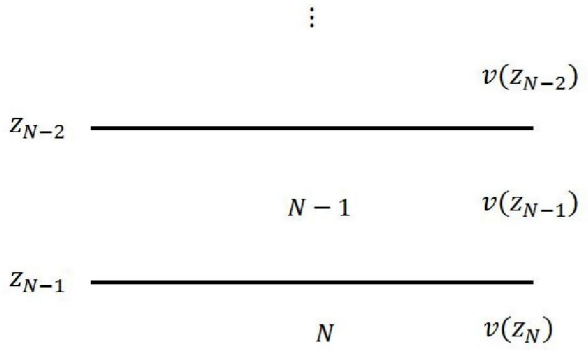

Figure A-1: An illustration of an N-layer velocity model

The reflection coefficient at depth z_{N-1}^- is given

$$R_D(z_{N-1}^-) = r_d(z_{N-1}) \tag{A-1}$$

where $r_d(z_{N-1})$ is given by equation 1 in the text. The minus superscript in z_{N-1}^- indicates the depth just above z_{N-1}; and $R_D(z_{N-1}^-)$ is the amplitude of the reflected waves at depth z_{N-1}^- for a downgoing wave with unit amplitude incident at depth z_{N-1}^-. The reflectivity $R_D(z_{N-1}^-)$ can be extrapolated upwards,

$$R_D(z_{N-2}^+) = E_D^{N-1} R_D(z_{N-1}^-) E_U^{N-1} \tag{A-2}$$

Here, the plus superscript in z_{N-2}^+ indicates the depth just below z_{N-2}, and the phase terms depend on the frequency and velocity,

$$E_D^{N-1} = E_U^{N-1} = e^{i\omega(z_{N-1}-z_{N-2})/v(z_{N-1})} \tag{A-3}$$

Reflector Spectrum

The reflectivity at depth z_{N-2}^{+} has not included the effect of the interface at z_{N-2} yet. After incorporating this interface at z_{N-2}, the reflectivity becomes:

$$R_D(z_{N-2}^{-}) = r_d(z_{N-2}) + t_d(z_{N-2})R_D(z_{N-2}^{+})[1 - r_u(z_{N-2})R_D(z_{N-2}^{+})]^{-1}t_u(z_{N-2}) \quad \text{(A-4)}$$

The equations of A-2 A-3 and A-4 work together to recursively construct, starting from bottom, the reflection response for multi-layer velocity model. Finally, a synthetic seismic trace is produced by inverse Furious transform of the products of the reflection response and wavelet spectrum. Note that the term in the square bracket in equation A-4, $[1 - r_u(z_{N-2})R_D(z_{N-2}^{+})]^{-1}$, represents the cumulative effect of a sequence of internal reverberations; that means all primaries and internal multiples are included in the modeling. A Tyler expansion of this term will give separate terms for primary reflections, first and higher orders of multiples.

REFERENCES

Foster, D. J., and C. S. Yin, 1995, Wave propagation in elastic thin layers: Proc. SPIE, Mathematical Methods in Geophysical Imaging III, **2571**, 25-42.

Kelamis, P. G., Y. Luo, W. Zhu, and K. O. Al-Rufaii, 2008, Two pragmatic approaches for attenuation of land multiples: 70th EAGE Conference & Exhibition.

Kennett, B. L. N, 2003, The seismic wavefield: Introduction and theoretical development: Cambridge University Press.

Luo, Y., P. G. Kelamis, Q. Fu, S. Huo, G. Sindi, S. Hsu and A. B. Weglein, 2011, Elimination of land internal multiples based on the inverse scattering series: The Leading Edge, 30, 884-889.

Moore, I., and B. Dragoset, 2008, General surface multiple prediction (GSMP): A flexible 3D SRME algorithm: 70th Annual International Conference and Exhibition, EAGE, Extended Abstracts, G043.

O'doherty, R. F. and N. A. Anstey, 1971, Reflections on amplitudes: Geophysical Prospecting, 19, 430-458.

Resnick, J. R., I. Lerche, and R. T. Shuey, 1986, Reflection, transmission, and the generalized primary wave: Geophys. J. Roy. Astr. Soc., **87**, 349-377.

Verschuur, D. J., and A. J. Berkhout, 1997, Estimation of multiple scattering by iterative inversion, part II—Practical aspects and examples: Geophysics, **62**, 1596–1611.

Weglein, A. B., F. A. Gasparotto, P. M. Carvalho, and R. H. Stolt, 1997, An inverse scattering series method for attenuating multiples in seismic reflection data: Geophysics, **62**, 1975–1989.

Figure Captions

Figure 1: A synthetic example showing (a) the velocity function, (b) reflection coefficients, (c) synthetic trace computed from (b) and (a), (d) zeroing of the reflection coefficient of the first interface, (e) synthetic trace computed from (d) and (a), and (f) difference between (c) and (e).

Figure 2: Reflector spectrum for primaries only. The top panel shows the velocity function, while the left panel shows the trace containing all primary reflections. A common depth trace in the spectrum shows seismic reflections originated from the depth where the trace is located.

Figure 3: Reflector spectrums for primaries only (a) and internal multiples only (b). The top panel shows the velocity function, while the left panel shows the trace containing all reflections. Any common depth trace at depth z in these spectrums contains all seismic waves reflected at that depth.

Figure 4: Primaries (a) and internal multiples (b) originating from the reflector at depth 400 m. These two traces are extracted from Figures 3a and 3b, respectively, and they include the waves reflected at the interface at depth 400m.

Figure 5: The contributions from all reflectors at all depths to the primaries (a) and internal multiples (b) at time 800 ms. The two traces are extracted from the reflection spectrums shown in Figures 3a and 3b, respectively, and they show the contributors to the seismic arrival at time 800 ms.

Figure 6: An illustration of three primaries and a first order internal multiple. The three primaries are S_1-Z_2-Z_1-R_1, S_2-Z_1-R_1, and S_2-Z_1-Z_3-R_2, the multiple is S_1-Z_2-Z_1-Z_3-R_2. All four reflections will be mixed together as an observed effective primary if the reflectors Z_1, Z_2 and Z_3 are close enough. Note, S_1, S_2, R_1 and R_2 are the same point for a 1D model.

Figure 7: (a) Reflector spectrum for surface-related multiples only, which indicates that not only the free surface, but also many deeper reflectors, contribute to the surface-related multiples. (b) Shallow-reflectorspectrum for surface-related multiples only, where all surface-related multiple can be attributed to the surface, and all surface-related multiples can be eliminated by removing the free surface reflector.

Figure 8: Shallow-reflector spectrum for internal multiples only. Internal multiples cannot be attributed to a single (i.e., the shallowest) reflector, as was the case for the surface-related multiples shown in Figure 7b.

Figure 9: The contributions from reflectors at all depths to the internal multiple at time 800 ms in the Shallow-reflector spectrum in Figure 8.

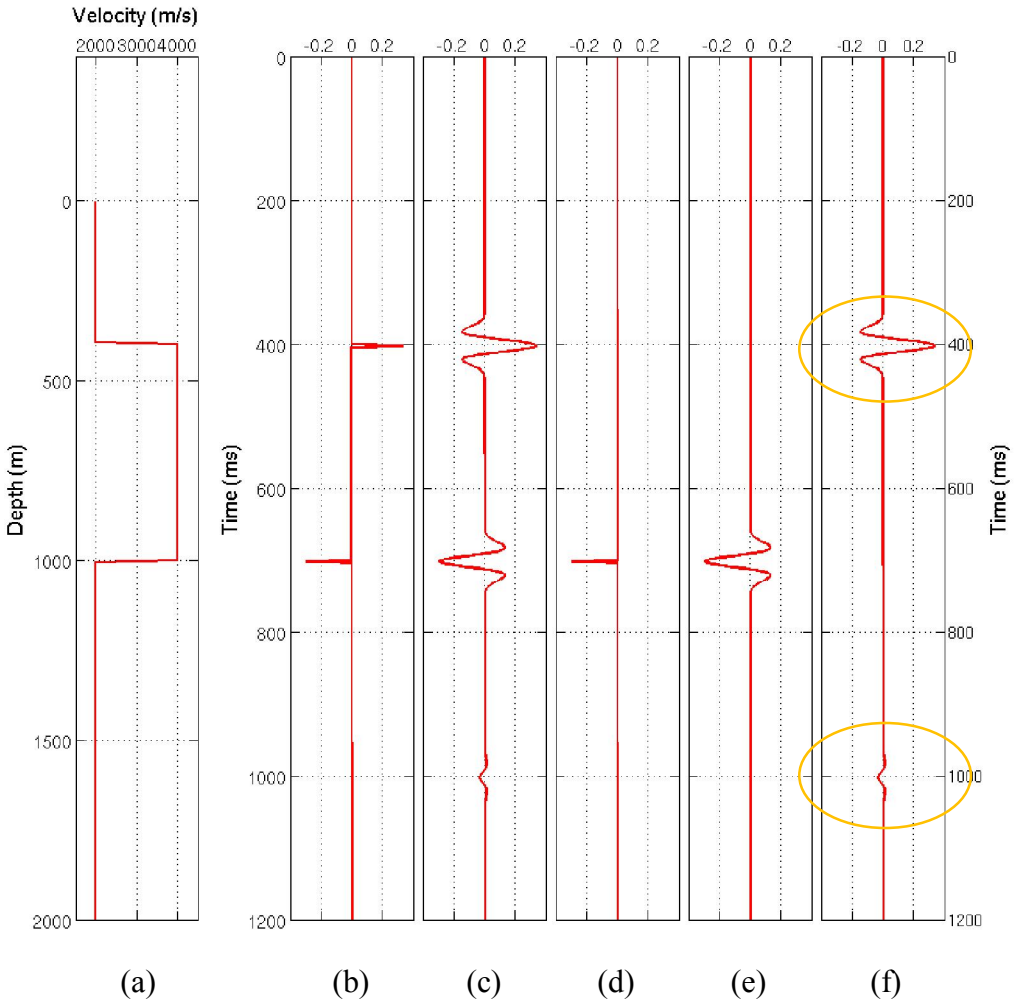

Figure 1: A synthetic example showing (a) the velocity function, (b) reflection coefficients, (c) synthetic trace computed from (b) and (a), (d) zeroing of the reflection coefficient of the first interface, (e) synthetic trace computed from (d) and (a), and (f) difference between (c) and (e).

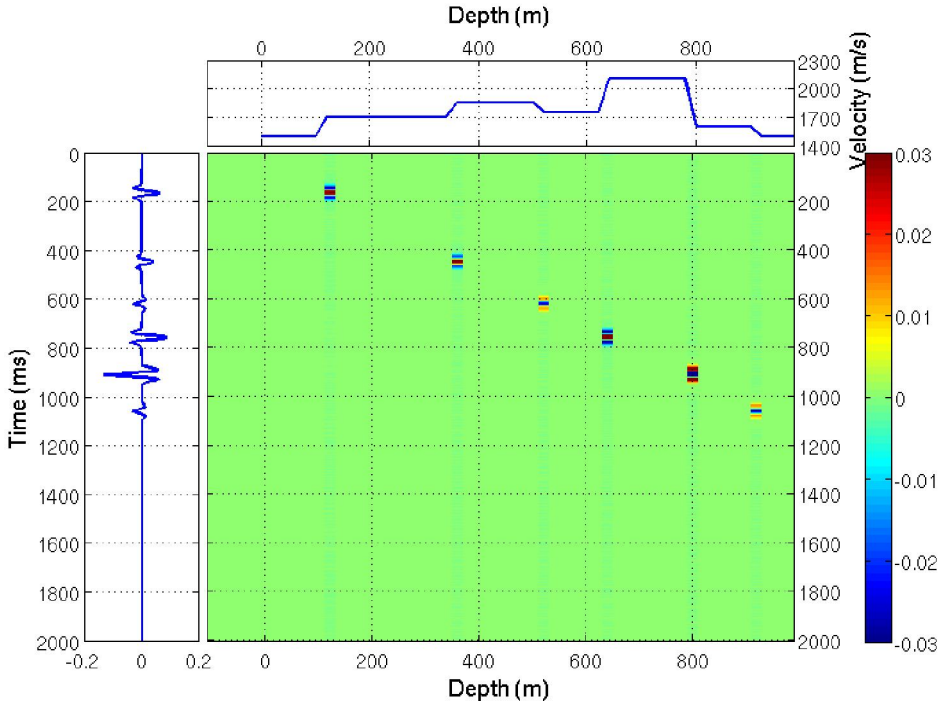

Figure 2: Reflector spectrum for primaries only. The top panel shows the velocity function, while the left panel shows the trace containing all primary reflections. A common depth trace in the spectrum shows seismic reflections originated from the depth where the trace is located.

Reflector Spectrum

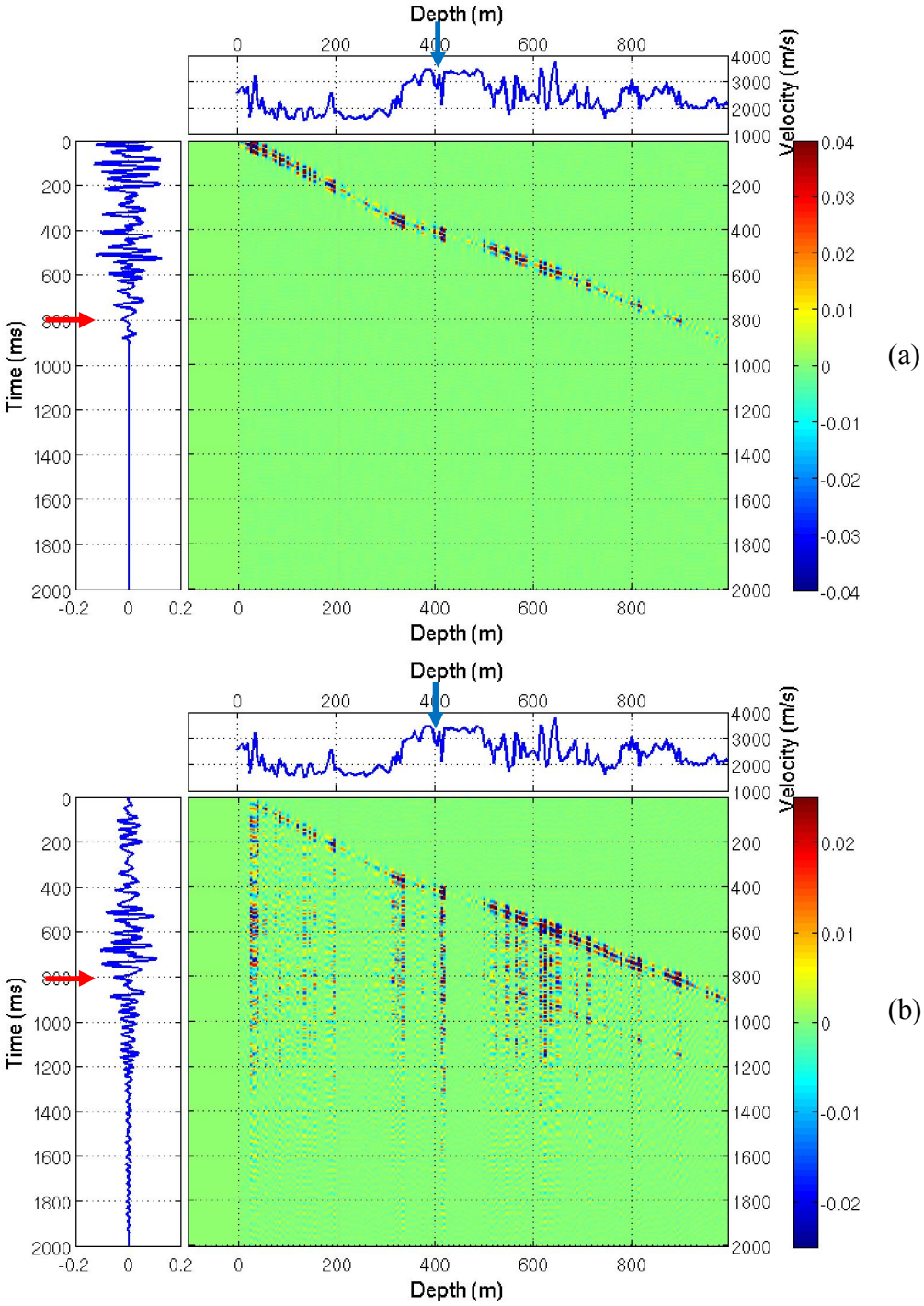

Figure 3: Reflector spectrums for primaries only (a) and internal multiples only (b). The top panel shows the velocity function, while the left panel shows the trace containing all reflections. Any common depth trace at depth z in these spectrums contains all seismic waves reflected at that depth.

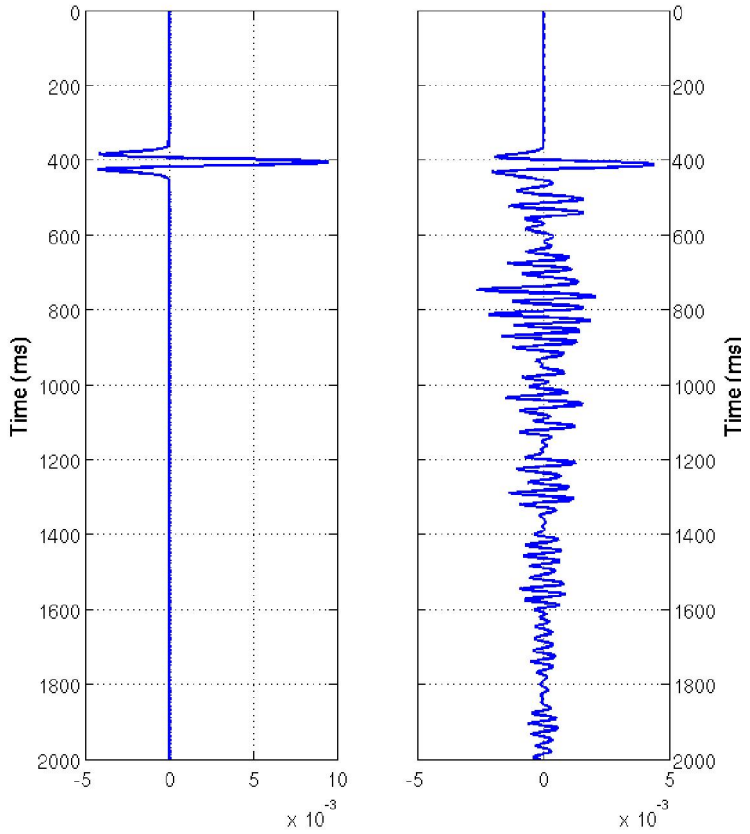

(a) (b)

Figure 4: Primaries (a) and internal multiples (b) originating from the reflector at depth 400 m. These two traces are extracted from Figures 3a and 3b, respectively, and they include the waves reflected at the interface at depth 400m.

Reflector Spectrum

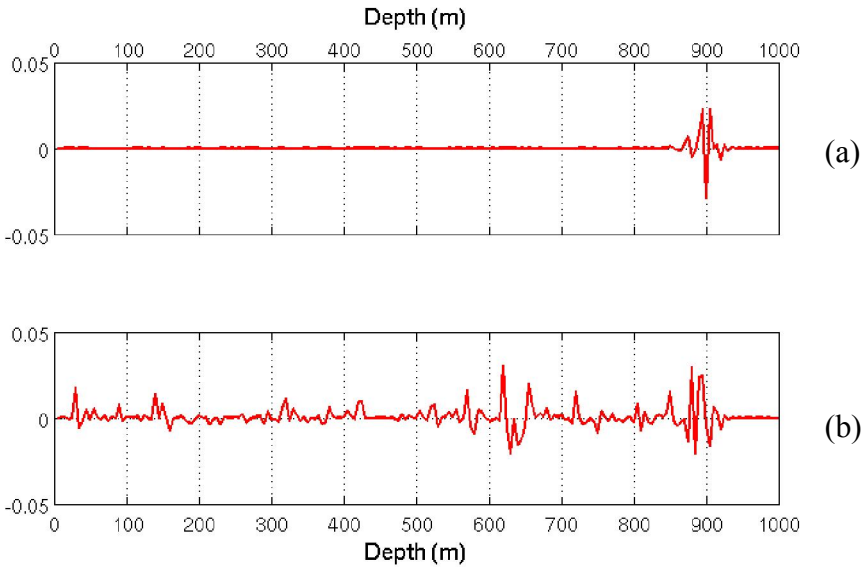

Figure 5: The contributions from all reflectors at all depths to the primaries (a) and internal multiples (b) at time 800 ms. The two traces are extracted from the reflection spectrums shown in Figures 3a and 3b, respectively, and they show the contributors to the seismic arrival at time 800 ms.

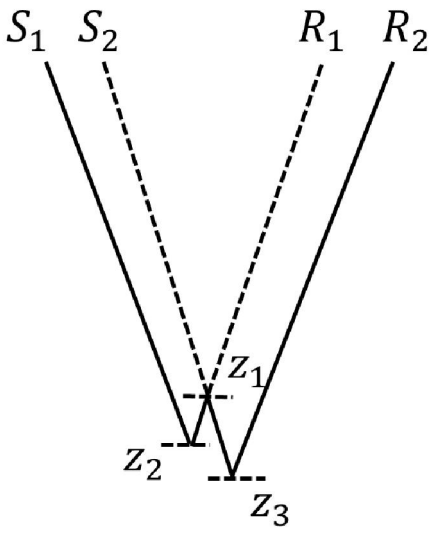

Figure 6: An illustration of three primaries and a first order internal multiple. The three primaries are S_1-Z_2-Z_1-R_1, S_2-Z_1-R_1, and S_2-Z_1-Z_3-R_2, the multiple is S_1-Z_2-Z_1-Z_3-R_2. All four reflections will be mixed together as an observed effective primary if the reflectors Z_1, Z_2 and Z_3 are close enough. Note, S_1, S_2, R_1 and R_2 are the same point for a 1D model.

Reflector Spectrum

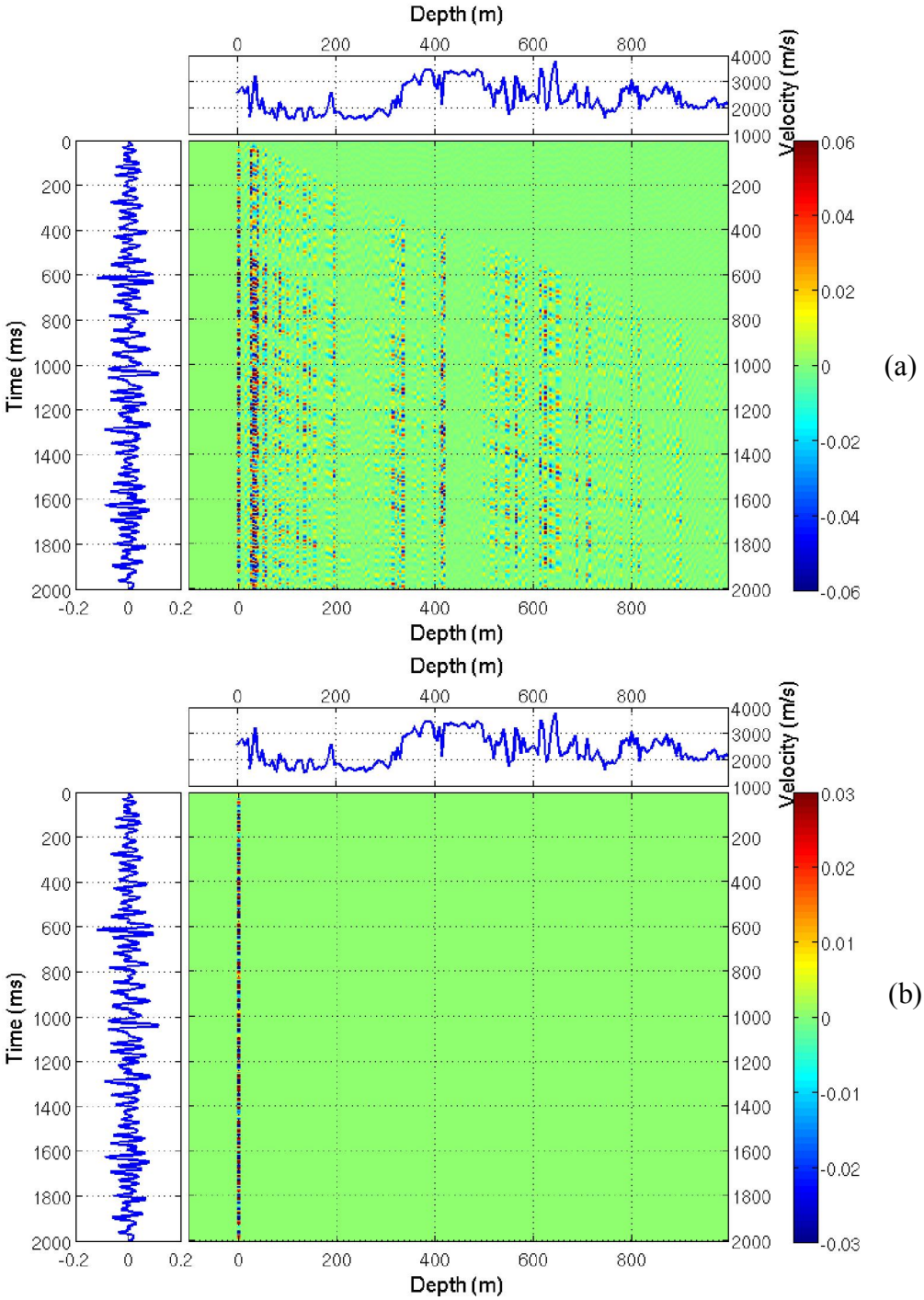

Figure 7: (a) Reflector spectrum for surface-related multiples only, which indicates that not only the free surface, but also many deeper reflectors, contribute to the surface-related multiples. (b) Shallow-reflector spectrum for surface-related multiples only, where all surface-related multiple can be attributed to the surface, and all surface-related multiples can be eliminated by removing the free surface reflector.

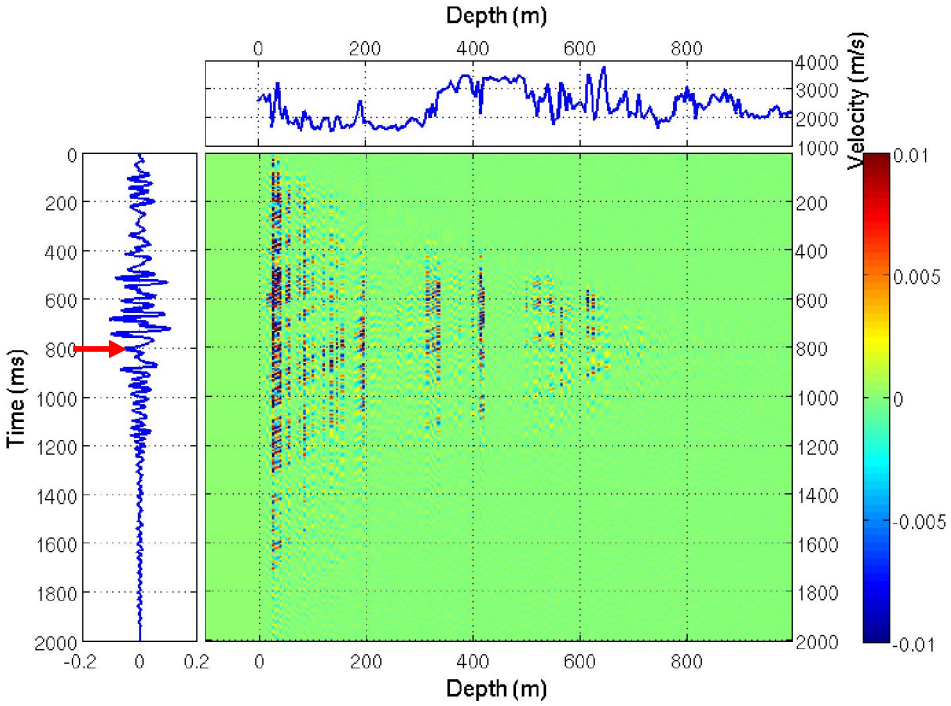

Figure 8: Shallow-reflector spectrum for internal multiples only. Internal multiples cannot be attributed to a single (i.e., the shallowest) reflector, as was the case for the surface-related multiples shown in Figure 7b.

Reflector Spectrum

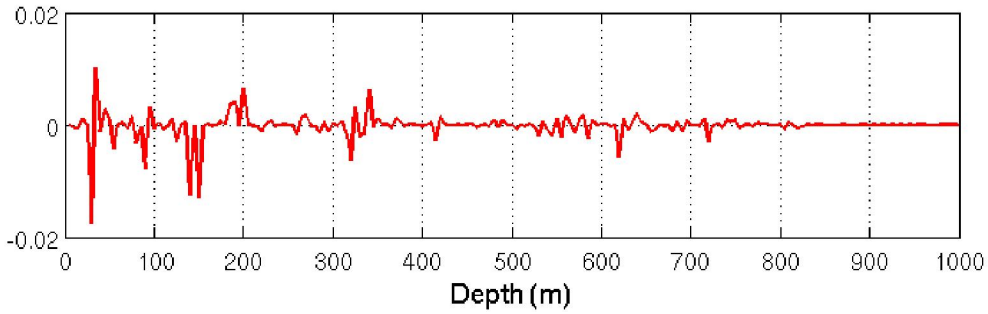

Figure 9: The contributions from reflectors at all depths to the internal multiple at time 800 ms in the Shallow-reflector spectrum in Figure 8.

Prediction of distinguishable internal multiples

Hong Liang[2], Yi Luo[1], Panos G. Kelamis[1] and Arthur B. Weglein[2]

[1]EXPEC Advanced Research Center, Saudi Aramco, Saudi Arabia

[2]University of Houston, USA

ABSTRACT

This paper demonstrates that the kinematics or arrival times of some internal multiples in a finely laminated thin-layer velocity model can be predicted by a completely data-driven method, the inverse scattering series (ISS) method. The ISS method is used because it assumes that each and every sample in the input data represents a reflector; this assumption is consistent with the correct physical mechanism for the generation of internal multiples found in our previous work by using the reflector spectrum method. We found that only a portion of the entire internal multiples can be predicted: the portion whose traveltime is at least a period of time longer than that of the relevant primaries. The non-predicted ones are so close to the primaries that they can be treated as a part of the "effective primaries". We also recognized that even though the first-order internal multiples are the main components of all internal multiples, higher orders must be taken into account to make the modeled/true and predicted multiples match each other. The velocity model used in this study is constructed from a real sonic logging, so our study suggests that the ISS method could be useful for internal-multiple reduction of field seismic data.

INTRODUCTION

Multiple elimination, especially internal-multiple elimination, is a long-standing problem in exploration reflection seismology. This challenge is even more essential for land seismic data processing due to the fact that strong internal multiples are often generated at near surface zones

(Kelamis et al., 2006). It has been well known, from countless sonic well logging, that the subsurface media are composed of many finely laminated thin layers, and each layer has seismic velocity (or impedance) different from its neighboring layers. Not many published papers have studied how the internal multiples are formed in thin layers, and how these internal multiples can be predicted from data. Luo and Liang (2012) presented a new method (named as the reflector spectrum) that illustrates where internal multiples are generated. In this paper, we study whether and what internal multiples in the thin-layer velocity model could be predicted, and show how they can be predicted. In our study, the thin-layer velocity model is constructed from a field sonic log, so this study could provide useful information for practical applications.

Many different approaches have been developed for internal-multiple elimination and have demonstrated applicability for synthetic and field data sets (Weglein et al., 1997; Verschuur and Berkhout, 2001; Kelamis et al., 2006; Luo et al., 2007). Among them, the ISS method is an internal-multiple-attenuation algorithm that does not require any subsurface information or user-provided a priori knowledge (Luo et al., 2011; Weglein et al., 2011). The ISS method can predict internal multiples generated at all depths at once. Most importantly, this method assumes each sample in seismic data associating a reflector, and interfering stacking of seismic waves from all these reflectors yields the observed internal multiples. This hypothesis was recently confirmed in our previous work (Luo and Liang, 2012) by using a newly developed method – the reflector spectrum method. With these in mind, we employ the ISS method for internal-multiple prediction in this paper.

In this paper, we will (1) introduce the reflectivity method for modeling 1D synthetic traces, (2) describe the ISS internal-multiple algorithm, (3) discuss prediction of first-order internal

multiples using the ISS method, (4) exemplify prediction of full internal multiples, and (5) discuss our results and summarize our conclusions.

MODELING METHOD

We follow the reflectivity method (Kennett, 2003) to build the reflection response for a stack of uniform layers. For a given velocity function $v(z_i)$, where z_i is the depth of the i^{th} reflector and i is the layer index taking its value from 1 to N, the reflection and transmission coefficients resulting from velocity contrasts of two adjacent layers $v(z_i)$ and $v(z_{i+1})$ are given by

$$r_d(z_i) = \frac{v(z_{i+1}) - v(z_i)}{v(z_{i+1}) + v(z_i)}, \tag{1}$$

$$r_u(z_i) = \frac{v(z_i) - v(z_{i+1})}{v(z_{i+1}) + v(z_i)}, \tag{2}$$

$$t_d(z_i) = 1 + r_d(z_i), \tag{3}$$

$$t_u(z_i) = 1 + r_u(z_i), \tag{4}$$

where $r_d(z_i)$ and $t_d(z_i)$ are reflection and transmission coefficients for incident downgoing waves, respectively, $r_u(z_i)$ and $t_u(z_i)$ are the corresponding coefficients for incident upgoing waves, and i is taking its value from 1 to N-1. The density is ignored for simplifying the symbols in our description, even though it plays a role in the coefficient.

We take the model in Figure 1 as a simple example, in which a uniform layer is bounded by interfaces at z_1 and z_2. The reflection and transmission coefficients for the two interfaces are $r_d(z_i)$, $t_d(z_i)$, $r_u(z_i)$ and $t_u(z_i)$ (i=1, 2). The reflection coefficient just above z_2 is equal to the interface coefficient and is given by

$$R_D(z_2^-) = r_d(z_2), \tag{5}$$

where the minus superscript in z_2^- indicates the depth above z_2 for a infinite small distance, and $R_D(z_2^-)$ is the amplitude of the reflected upgoing wave at depth z_2^- for a downgoing wave with unit amplitude incident at depth z_2^-. The reflectivity $R_D(z_2^-)$ can be extrapolated upward to the depth just below the top interface

$$R_D(z_1^+) = E_D R_d(z_2^-) E_U, \tag{6}$$

where the plus superscript in z_1^+ indicates the depth below z_1 for an infinite small distance, and $R_D(z_1^+)$ represents the reflectivity at depth z_1^+, which does not include the effect of the interface at z_1 yet. The phase terms in transmission through the uniform layer, E_U and E_D, depend on the frequency and velocity

$$E_U = E_D = e^{i\omega(z_2 - z_1)/v(z_2)}. \tag{7}$$

Consider a normal incident downgoing wave with unit amplitude impinging on the interface z_1, as shown in Figure 1. There will be a reflection from the interface at z_1 with amplitude $r_d(z_1)$, accompanied by a transmission into the uniform layer with amplitude $t_d(z_1)$. The transmitted wave will reach the interface at z_2 with a phase shift E_D and then will be reflected back into the layer with amplitude $t_d(z_1)E_D r_d(z_2)$. The reflected upgoing wave will reach the interface at z_1 with a further phase shift E_U. There is again a transmission and a reflection at the interface z_1. The whole propagation process contains a sequence of transmissions and internal reflections. Thus, as is shown in Figure 1, the amplitude of the cumulative upgoing waves just above the interface at z_1 is

$$R_D(z_1^-) = r_d(z_1) + t_d(z_1)E_D r_d(z_2)E_U t_u(z_1) + t_d(z_1)E_D r_d(z_2)E_U r_u(z_1)E_D r_d(z_2)E_U t_u(z_1) + \\ + t_d(z_1)E_D r_d(z_2)E_U r_u(z_1)E_D r_d(z_2)E_U r_u(z_1)E_D r_d(z_2)E_U t_u(z_1) + \cdots, \tag{8}$$

where $R_D(z_1^-)$ represents the total reflectivity at depth z_1^-, which includes the effect of interfaces at z_1 and z_2 and transmission through the uniform layer.

With the aid of equations 5 and 6, we can rewrite equation 8 as

$$\begin{aligned} R_D(z_1^-) &= r_d(z_1) + t_d(z_1)R_D(z_1^+)t_u(z_1) + t_d(z_1)R_D(z_1^+)r_u(z_1)R_D(z_1^+)t_u(z_1) + \\ &\quad + t_d(z_1)R_D(z_1^+)r_u(z_1)R_D(z_1^+)r_u(z_1)R_D(z_1^+)t_u(z_1) + \cdots \\ &= r_d(z_1) + t_d(z_1)R_D(z_1^+)[1 + r_u(z_1)R_D(z_1^+) + r_u(z_1)R_D(z_1^+)r_u(z_1)R_D(z_1^+) + \cdots]t_u(z_1). \end{aligned} \tag{9}$$

Note that the terms within the square brackets in equation 9 represent the cumulative effect of a sequence of internal reverberations and can be rewritten as

$$[1 + r_u(z_1)R_D(z_1^+) + r_u(z_1)R_D(z_1^+)r_u(z_1)R_D(z_1^+) + \cdots] = [1 - r_u(z_1)R_D(z_1^+)]^{-1}. \tag{10}$$

With the aid of equation 10 we can rewrite equation 9 as

$$R_D(z_1^-) = r_d(z_1) + t_d(z_1)R_D(z_1^+)[1 - r_u(z_1)R_D(z_1^+)]^{-1}t_u(z_1). \tag{11}$$

Equations 6, 7, and 11 together can be extended to recursively construct, starting from the bottom, the reflection response for a multi-layer velocity model. Finally, a synthetic seismic trace can be produced by an inverse Fourier transform of the products of the reflection response and the wavelet spectrum. Note that the term in the square brackets in equation 11, $[1 - r_u(z_1)R_D(z_1^+)]^{-1}$, includes a full set of internal reflections. Therefore, all primary and multiple reflections can be modeled using the cascaded construction scheme of equations 6 and 7 followed by equation 11. The Tyler expansion of this term, in equation 9, gives separate terms for primary reflections, and for first and higher orders of internal reflections. By purposefully selecting the terms in the Tyler expansion, we have developed modeling methods for primaries only and internal multiples only (including first-order, second-order, and total internal multiples).

The modeled internal multiples will be compared with the predicted multiples in the later sections.

PREDICTION METHOD

The inverse scattering series (ISS) internal-multiple-attenuation method is a data-driven algorithm (Araújo et al., 1994; Weglein et al., 1997). It does not require any subsurface information about the medium where the internal multiples propagate, and predicts the exact traveltime and approximated amplitude of internal multiples. The algorithm predicts internal multiples for all depths at once.

The ISS internal-multiple-attenuation algorithm starts with the deghosted data D with all free-surface multiples eliminated. The second term in the algorithm in a 2D earth is given by Araújo et al. (1994) and Weglein et al. (1997) (equation 37); for a 1D earth and a normal incident wave the equation reduces to (Weglein et al., 2003)

$$b_3(k) = \int_{-\infty}^{\infty} dz_1 e^{ikz_1} b_1(z_1) \int_{-\infty}^{z_1-\varepsilon} dz_2 b_1(z_2) e^{-ikz_2} \int_{z_2+\varepsilon}^{\infty} dz_3 e^{ikz_3} b_1(z_3) \qquad (12)$$

where the deghosted data, $D(t)$, for an incident plane wave, satisfies $D(\omega) = b_1(k)$, $b_1(z) = \int_{-\infty}^{\infty} e^{-ikz} b_1(k) dk$, $k = 2\omega / c_0$ is the vertical wavenumber, and c_0 is the reference velocity; $b_1(z)$ corresponds to an uncollapsed FK migration of effective incident plane-wave data; z_i ($i = 1,2,3$) represents three pseudo-depths; ε is a positive quantity and it is chosen to be the width of the source wavelet.

The parameter ε ensures that the three pseudo-depths satisfy $z_2 < z_1$ and $z_2 < z_3$; this allows the 'lower-higher-lower' combination of subevents to construct first-order internal multiples as shown in Figure 2. The output of equation 12 is transformed back to the space-time domain.

When subtracting the estimated internal multiples from the input data, all first-order internal multiples are suppressed and all higher-order internal multiples are altered.

PREDICTION OF FIRST-ORDER INTERNAL MULTIPLE

In this section we will evaluate the performance of the ISS method by compared with that of the predicted and modeled first-order internal multiples. Because the ISS internal-multiple algorithm requires three integrals of the data (see equation 12), the predicted internal multiples contains three convolved source wavelets. Therefore, we artificially include three wavelets in the modeling process when we compare the predicted internal multiples with the modeling result. In other cases where only modeling results are shown, only one source wavelet is included in the forward modeling.

The reflectivity method discussed earlier is employed to model the synthetic traces for a complex velocity model. The velocity model is derived from a sonic log and is shown in Figure 3. The same set of parameters is used by the reflectivity algorithm in all the following examples: sample interval in time dt =0.004 s, number of samples in time nt =500, sample interval in space dz =5 m, number of samples in space nz =200, and peak frequency of Ricker wavelet f_p =20 Hz.

Figure 4 shows the comparison of the first-order internal multiples modeled by the reflectivity method (red) and those predicted by the ISS method (blue). In this example, the modeled result contains all first-order internal multiples and the ISS method takes the primaries-only trace as input. From the result, it appears as though that the ISS method failed to predict the first-order internal multiples. However, note that the velocity model studied here (Figure 3) is composed of many thin layers (200 layers, each 5 m thick), and the velocity tends to alternate between high values and low values which implies the cyclic polarity change of the interface

reflectivity (i.e., the sign change of the reflection coefficient). For such a medium, the behavior and the significance of the very-short-delay multiple reflections shown in Figure 5 have been studied by Anstey (1960) and O'Doherty and Anstey (1971). It is concluded that such very-short-delay multiple reflections are indistinguishable from the primary reflections and should be treated as part of "effective primaries" (Trorey, 1962). This also suggests to us that in such a thin-layer model an observed "primary" consists of a classical primary reflection, which reflected only once, and a set of associated multiple reflections (Foster and Yin, 1995; Resnick et al., 1986).

On the basis of the above discussion, we modify the reflectivity modeling method by introducing a parameter ε into the modeling process. The parameter ε defines a time window and the forward modeling of internal multiples with the parameter ε excludes the multiple reflections within a short time interval (a period of source wavelet) after the primary reflections, i.e., it excludes the very-short-delay multiple reflections. Trorey (1962) presented another approach to choosing the appropriate group of multiples to add in with the primaries and also pointed out that the choice was largely a matter of experience.

Figure 6 shows the comparison between the modeled primary reflections (blue) and the modeled primary plus the very-short-delay first-order multiple reflections (red). It shows that the very-short-delay first-order multiple reflections reinforce the primary reflections and it also confirms that these multiple reflections should be considered as part of effective primaries.

Using the forwarding modeling method with parameter ε, the modeled first-order internal multiples with the very short-delay ones excluded are shown in red in Figure 7, whereas the first-order internal multiples predicted by the ISS method are again shown in blue in Figure 7 (and are the same as the blue in Figure 4). From this figure we can see that the two results match fairly

well. By taking the primaries-only trace as input, the ISS internal-multiple method can predict the first-order internal multiples whose travel times are distinguishable from primary reflections.

PREDICTION OF FULL INTERNAL MULTIPLES

In this section, we consider the modeling and prediction of full internal multiples (including the first-order and higher-order internal multiples). We first study the effect of higher-order internal multiples from the point of view of forward modeling. Figure 8 shows the total internal multiples (blue in 8a and 8b), first-order internal multiples (red in 8a), and first-order plus second-order internal multiples (green in 8b), all of which are generated by the reflectivity modeling method. The first-order internal multiples (red in 8a) match the total internal multiples (blue) well, prior to time 1000 ms; adding the second-order internal multiples to the first-order internal multiples improves their match with the total internal multiples before time 1400 ms. After a longer time (after 1400 ms) there is still a mismatch between the total internal multiples and the first-order plus second-order internal multiples. The above results imply that higher-order internal multiples are nonnegligible if the longer time period is our interest.

In the previous section we confirmed that the distinguishable first-order internal multiples can be predicted by the ISS method which takes the primaries-only trace as input. However, there is no primaries-only trace in practice. One of our goals is to study whether the ISS method can still predict internal multiples by taking the full trace (including all primary and multiple reflections) as input.

We employ the reflectivity modeling method with parameter ε to generate the distinguishable total internal multiples, which are shown in red in Figure 9. The total internal multiples predicted by the ISS method are shown in blue in Figure 9, where the ISS method takes

the full trace as input. The close match between the predicted internal multiples and the modeled ones shown in Figure 9 indicates that the distinguishable total internal multiples can be predicted by the ISS method by taking the full trace as input. The predicted multiples successfully match the model ones because ISS can predict the nth-order multiples from those with one order lower, existing in the full trace.

CONCLUSIONS

In this paper, we apply the inverse scattering series theory to predict internal multiples in thin layers. The prediction results are compared with the internal multiples modeled by the reflectivity method. We found that not all the internal multiples can be predicted by the ISS method. Further investigation indicates that the non-predicted internal multiples are indistinguishable from the primary reflections, and they could be treated as part of effective primaries. Taking the effective primaries as the desirable signals, the rest of the internal multiples become distinguishable from primaries and can be predicted by the ISS internal-multiple-attenuation algorithm.

ACKNOWLEDGEMENTS

The authors thank the Saudi Arabian Oil Company (Saudi Aramco) and its Advanced research Center (EXPEC ARC) for support and permission to present this research.

REFERENCES

Anstey N. A., 1960, Attacking the problems of the synthetic seismogram: Geophysical prospecting, **8**, 242-259.

Araújo, F. V., A. B. Weglein, P. M. Carvalho, and R. H. Stolt, 1994, Inverse scattering series for multiple attenuation: An example with surface and internal multiples: 64th Annual International Meeting, SEG, Expanded Abstracts, 1039–1041.

Foster, D. J., and C. S. Yin, 1995, Wave propagation in elastic thin layers: Proceedings of SPIE, Mathematical Methods in Geophysical Imaging III, **2571**, 25-42.

Kelamis, P. G., Y. Luo, W. Zhu, and K. O. Al-Rufaii, 2008, Two pragmatic approaches for attenuation of land multiples: 70th EAGE Conference & Exhibition, Extended Abstracts.

Kelamis, P. G., W. Zhu, K. O. Rufaii, and Y. Luo, 2006, Land multiple attenuation-The future is bright: 76th Annual International Meeting, SEG, Expanded Abstracts, 2699–2703.

Kennett, B. L. N, 2003, The seismic wavefield: Introduction and theoretical development: Cambridge University Press.

Luo, Y., P. G. Kelamis, Q. Fu, S. Huo, G. Sindi, S. Hsu and A. B. Weglein, 2011, Elimination of land internal multiples based on the inverse scattering series: The Leading Edge, 30, 884-889.

Luo, Y., H. Liang, P. G. Kelamis, A. B. Weglein, 2012, Unraveling internal multiples via the reflector spectrum concept: submitted to SEG, Expanded Abstract.

Luo, Y., W. Zhu, and P. G. Kelamis, 2007, Internal multiple reduction in inverse-data domain: 77th Annual International Meeting, SEG, Expanded Abstracts, 2485–2489.

O'doherty, R. F. and N. A. Anstey, 1971, Reflections on amplitudes: Geophysical Prospecting, 19, 430-458.

Resnick, J. R., I. Lerche, and R. T. Shuey, 1986, Reflection, transmission, and the generalized primary wave: Geophysical Journal of Royal Astronomical Society, **87**, 349-377.

Trorey, A. W., 1962, Theoretical seismograms with frequency and depth dependent absorption: Geophysics, **27**, 766-785.

Verschuur, D. J. and A. J. Berkhout, 2001, CFP-based internal multiple removal, the layer-related case: 71st Annual International Meeting, SEG, Expanded Abstracts, 1997–2000.

Weglein, A. B., F. V. Araújo, P. M. Carvalho, R. H. Stolt, K. H. Matson, R. T. Coates, D. Corrigan, D. J. Foster, S. A. Shaw, and H. Zhang, 2003, Inverse scattering series and seismic exploration: Inverse Problems, **19**, no. 6, R27–R83.

Weglein, A. B., F. A. Gasparotto, P. M. Carvalho, and R. H. Stolt, 1997, An inverse scattering series method for attenuating multiples in seismic reflection data: Geophysics, **62**, 1975–1989.

Weglein A. B., S. Hsu, P. Terenghi, X. Li and R. H. Stolt, 2011, Multiple attenuation: Recent advances and the road ahead (2011): The Leading Edge, **30**, 864-875.

Figure Captions

Figure 1: An illustration of a sequence of transmission and reflection processes for a uniform layer.

Figure 2: An internal multiple (S_1-z_1-z_2-z_3-R_2) constructed by three subevents (S_1-z_1-z_2-R_1, S_2-z_2-R_1**,** S_2-z_2-z_3-R_2).

Figure 3: A velocity model derived from a sonic log**.**

Figure 4: The first-order internal multiples modeled by the reflectivity method (red) and those predicted by the ISS method (blue). The modeled result includes all first-order internal multiples, and the ISS internal-multiple-prediction method takes only primaries as input. .

Figure 5: An illustration of three very-short-delay multiple reflections (A, B, and C) and a primary reflection (D) for thin layers.

Figure 6: The modeled primary reflections (blue) and the modeled primary plus the very-short-delay first-order multiple reflections (red).

Figure 7: The first-order internal multiples generated by the reflectivity modeling method with the parameter ε (red) and those predicted by the ISS method (blue). The modeled first-order internal multiples exclude the very-short-delay multiples shown in Figure 4, and the ISS internal-multiple prediction result is the same as that in Figure 3.

Figure 8: The total internal multiples (blue in (a) and (b)), first-order internal multiples (red in (a)), and first-order plus second-order internal multiples (green in (b)), all of which are generated by the reflectivity modeling method.

Figure 9: The total internal multiples generated by the reflectivity modeling method with ε (red) and those predicted by the ISS method (blue). The reflectivity modeling method with ε

excludes the very-short-delay multiples, and the ISS internal-multiple-prediction method takes the full trace (including all primary and multiple reflections) as input.

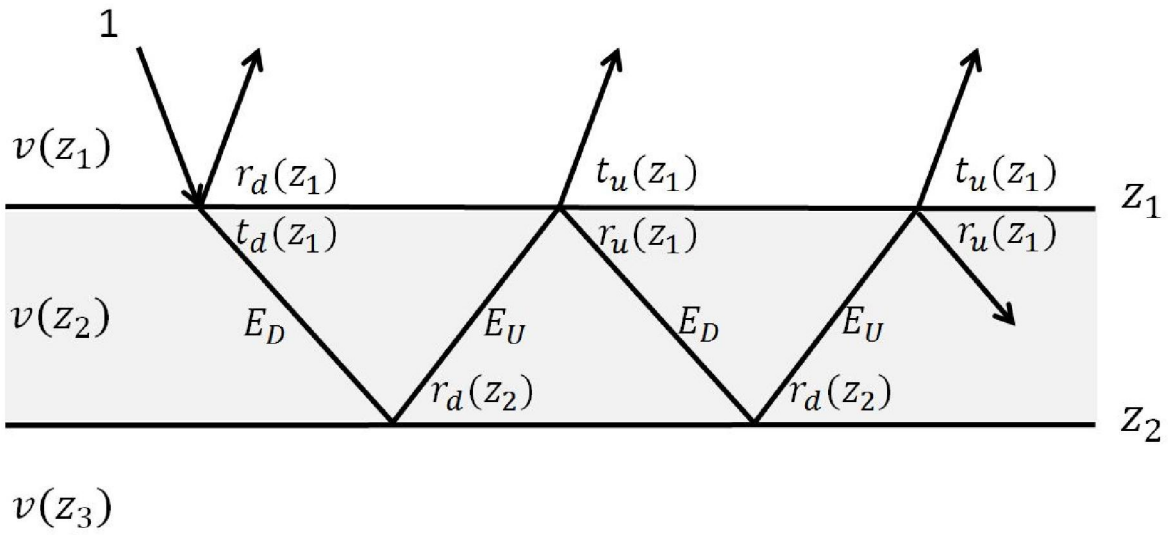

Figure 1: An illustration of a sequence of transmission and reflection processes for a uniform layer.

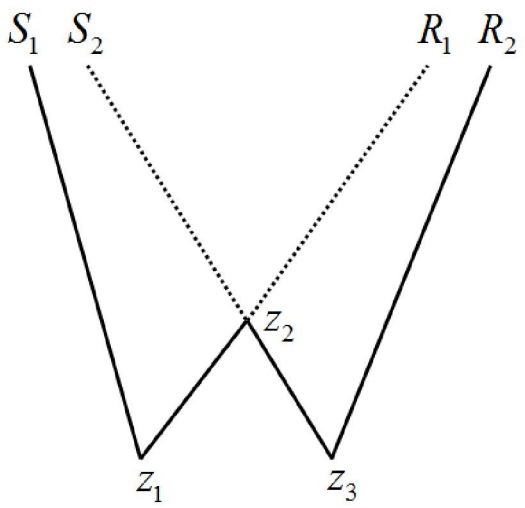

Figure 2: An internal multiple (S_1-z_1-z_2-z_3-R_2) constructed by three subevents (S_1-z_1-z_2-R_1, S_2-z_2-R_1, S_2-z_2-z_3-R_2).

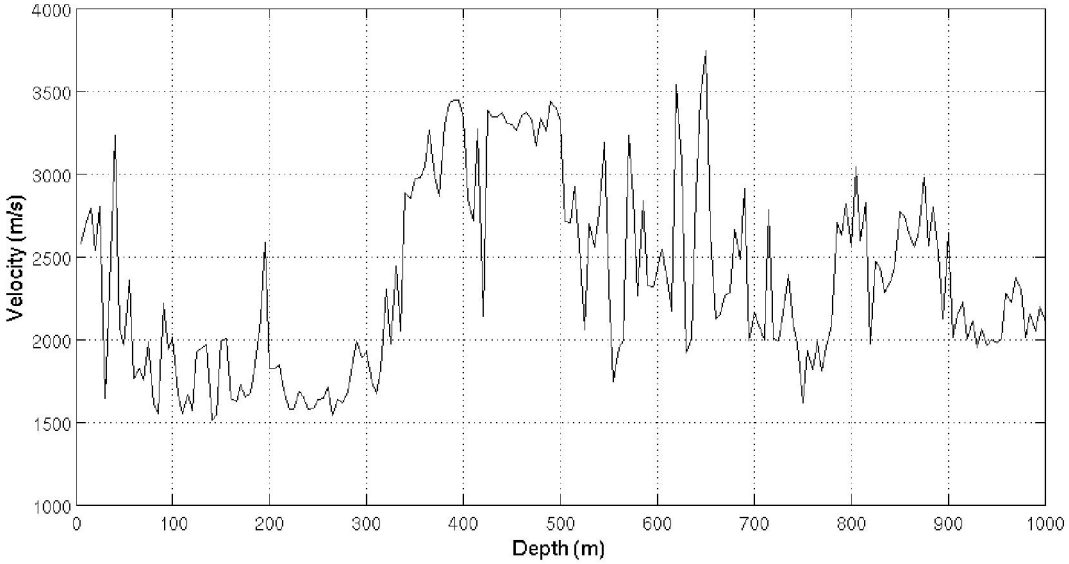

Figure 3: A velocity model derived from a sonic log.

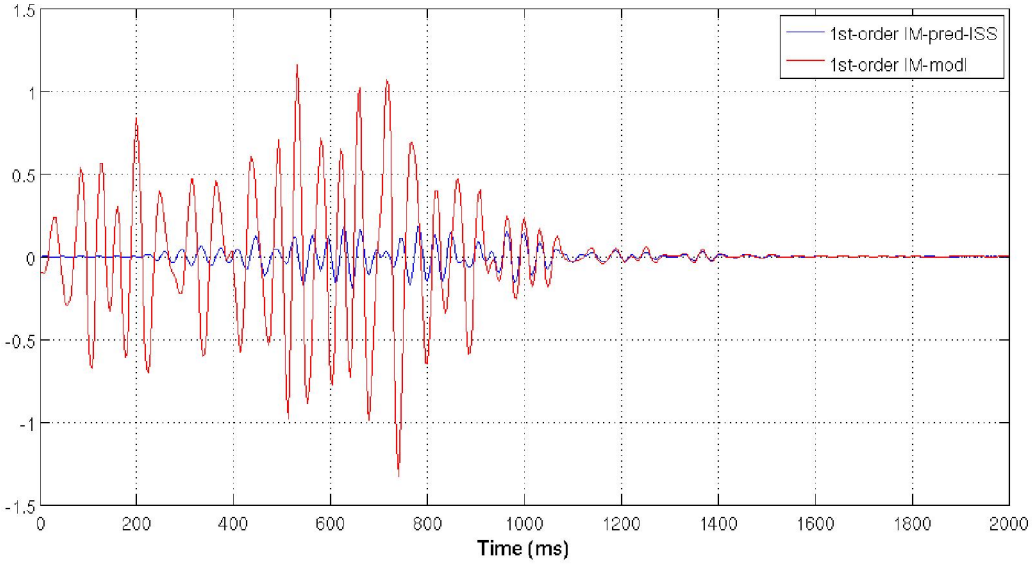

Figure 4: The first-order internal multiples modeled by the reflectivity method (red) and those predicted by the ISS method (blue). The modeled result includes all first-order internal multiples, and the ISS internal-multiple-prediction method takes only primaries as input.

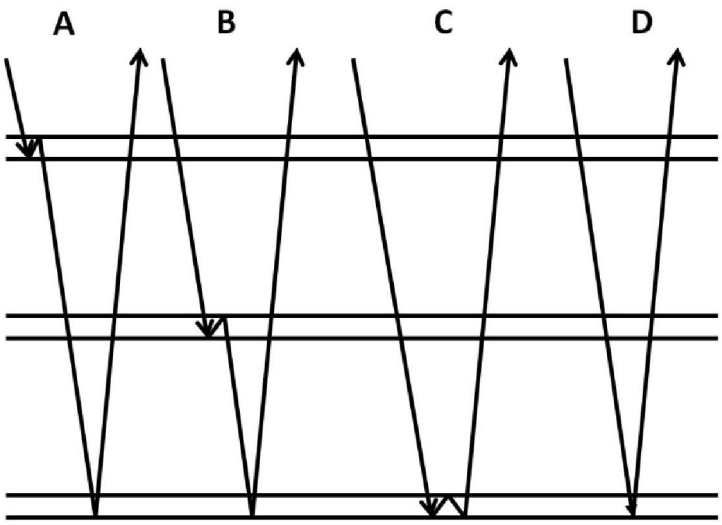

Figure 5: An illustration of three very-short-delay multiple reflections (A, B, and C) and a primary reflection (D) for thin layers.

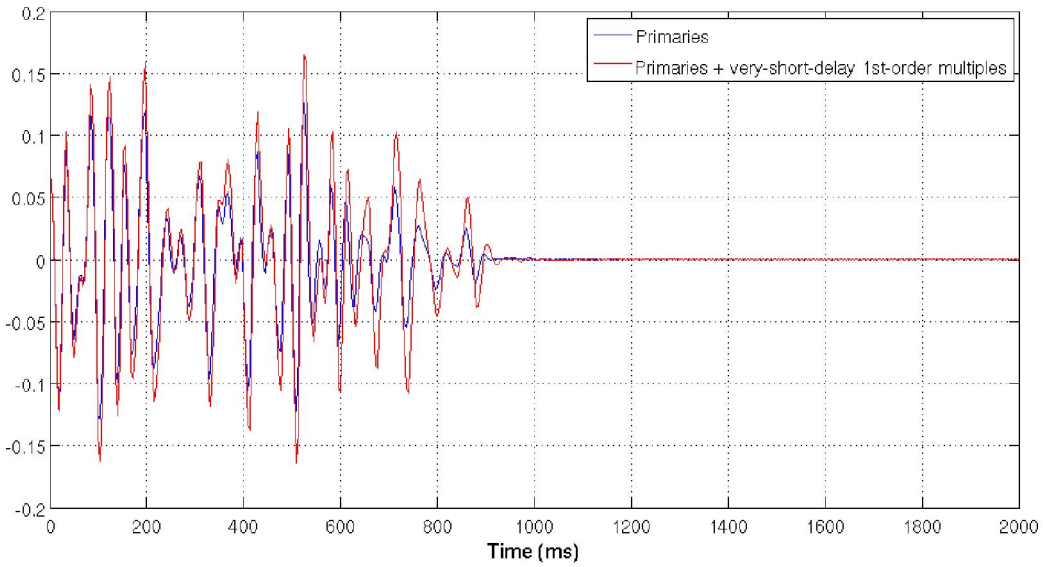

Figure 6: The modeled primary reflections (blue) and the modeled primary plus the very-short-delay first-order multiple reflections (red).

INVERSE SCATTERING SERIES DIRECT DEPTH IMAGING WITHOUT THE VELOCITY MODEL: FIRST FIELD DATA EXAMPLES

ARTHUR B. WEGLEIN[1], FANG LIU[1], XU LI[1], PAOLO TERENGHI[1], ED KRAGH[2], JAMES D. MAYHAN[1], ZHIQIANG WANG[1], JOACHIM MISPEL[3], LASSE AMUNDSEN[3], HONG LIANG[1], LIN TANG[1] and SHIH-YING HSU[1]

[1] *M-OSRP, University of Houston, 617 Science & Research Bldg. 1, Houston, TX 77004, U.S.A.*
[2] *SCR/Schlumberger, Schlumberger Cambridge Research Center High Cross, Madingley Road, Cambridge CB3 0EL, U.K.*
[3] *Statoil ASA, Statoil Forskningssenter, Arkitekt Ebbells veg 10, 7053 Ranheim, Norway.*

(Received September 3, 2011; revised version accepted November 24, 2011)

ABSTRACT

Weglein, A.B., Liu, F., Li, X., Terenghi, P., Kragh, E., Mayhan, J.D., Wang, Z., Mispel, J., Amundsen, L., Liang, H., Tang, L. and Hsu, S.-Y., 2012. Inverse scattering series direct depth imaging without the velocity model: First field data examples. *Journal of Seismic Exploration*, 21: 1-28.

In Weglein et al. (2010) an update and status report were provided on the progress on the inverse scattering series (ISS) direct depth imaging without the velocity model. In that article, results on synthetics with sufficient realism indicated that field data tests were warranted. This paper documents those first field data tests. These first early tests are encouraging and indicate that ISS direct depth imaging on field data is possible. Each member of a set of three distinct data or algorithmic conditions and requirements are identified and shown to be necessary for inverse scattering direct depth imaging, without a velocity model, to be effective and to produce the accurate structural configuration of reflectors and interfaces in the subsurface. Taken together, that set represents both necessary and sufficient conditions. In addition, for ISS imaging, the CIG flatness condition is a necessary and sufficient indication that an accurate depth image has been reached. The latter property is in contrast to conventional velocity dependent imaging methods where common image gather (CIG) flatness is a necessary but not a sufficient condition that a correct depth image has been achieved. The next steps, and open issues, on the road between viable and providing relevant and differential added value to the seismic tool-box are described and discussed.

KEY WORDS: imaging, migration, inverse scattering series, field data, velocity, CIG flatness.

0963-0651/12/$5.00

INTRODUCTION/BACKGROUND

For the purposes of this paper, an accurate depth image means a correct spatial location and configuration of interfaces/reflectors in the earth. All currently applied direct depth imaging methods and indirect imaging concepts firmly believe that depth and velocity are inextricably linked. That cornerstone of all current imaging means that any direct imaging method requires an accurate velocity model to produce an accurate image in depth.

DIRECT AND INDIRECT METHODS FOR IMAGING AND/OR INVERSION ARE NOT EQUIVALENT

It is essential to understand the significance of the term 'direct' in 'direct depth imaging'. Given an accurate velocity model (with an appropriate imaging method that can accurately backpropagate in space, or time, down through the velocity model), all current leading-edge imaging methods (e.g., Kirchhoff, FK, Beam and RTM) are able to directly output the depth (the actual spatial configuration) of reflectors. Within the framework of RTM methods, which assume an accurate velocity model, a recent set of papers (Weglein et al., 2011b, and Weglein et al., 2011c), advanced RTM concepts and methods, to address fundamental issues and shortcomings within current RTM practice, including the removal of the need for Perfectly Matched Layers (PML) and issues associated with that approach.

Indirect imaging methods (e.g., examining move-out trajectories and seeking flat common image gathers (CIG), Common Focus Point (CFP), Common Reflection Surface (CRS) and 'path integral' approaches) seek to satisfy a property or condition that an image with an accurate velocity would satisfy. Those properties are necessary conditions, but not sufficient, and hence satisfying the indirect proxy for an adequate velocity model is not equivalent to knowing the velocity and direct depth imaging. Therefore, satisfying these indirect criteria is no guarantee, and can lead to the correct depth or to any one of a set of incorrect depths. The latter truth is rarely (if ever) spoken and even rarer to find mentioned or exemplified in print. Most importantly, these indirect approaches fervently believe that a direct depth imaging method would require and demand a velocity model, and that there is absolutely no way around it, and that depth and velocity are innately linked and coupled on a very basic and fundamental level. That thinking is clear, and 100% correct within the framework of current imaging concepts and methods. However, that conventional mainstream thinking is limited from another broader perspective, and is superseded by the new broader framework for imaging provided by the inverse scattering series (ISS). Amundsen et al. (2005, 2006, 2008) have developed direct inversion methods for 1D acoustic and elastic media. The ISS is the only

direct inversion for both a 1D and a multi-dimensional acoustic, elastic and anelastic earth.

In addition to being direct and applicable for a multi-dimensional earth, the ISS (Weglein et al., 2003) is further unique in allowing for all processing objectives (including multiple removal, depth imaging, target identification, and Q compensation) to be achieved directly and without subsurface information.

In the same 'direct' sense that current imaging methods can directly output the spatial configuration of reflectors with a velocity model, ISS imaging algorithms can directly output the correct spatial configuration without the velocity model. It is the only method with that potential and capability.

Within the tool-box of multiple removal methods, the ISS internal multiple method is the only algorithm that predicts the removal of all internal multiples directly, and without subsurface information. The latter claim of ISS multiple removal capability was once highly controversial, incredulous and widely considered impossible. However, now it's not only understood to be possible, it has been documented and reported to have stand-alone capability in comparison with all other internal multiple methods (see, e.g., Luo et al., 2011). There is one set of unchanged ISS equations that at once communicates that all multiples can be removed, and all primaries can be accurately depth imaged - directly and without any subsurface information, including velocity. If one believes that it is impossible to directly depth image without the velocity using the ISS, then one is forced to also believe that it is impossible to remove internal multiples without subsurface information. They come from the exact same set of equations and logic.

The ISS subseries for direct depth imaging communicates that depth and velocity are not inextricably and fundamentally linked. The ISS provides a new superseding theory that views the current velocity-depth relationship and framework as a special limiting case, as quantum mechanics and relativity view classical physics as limiting and special cases, within a new comprehensive and broader platform and framework. The new broader ISS framework for imaging reduces to current imaging algorithms when the velocity model is adequate, a property that a superseding theory must satisfy, and most amazingly it determines automatically on its own for any particular data set, or portion of a data set (and a given velocity model and migration algorithm), whether the new framework is needed, or whether the current conventional imaging framework and a given velocity model is in any individual case accurate and will suffice. The new imaging framework determines if its services, that is, whether the terms beyond the first term (the first and linear term in ISS imaging corresponds to current linear conventional imaging) are needed and will be called upon, and if it determines a response in the affirmative, then and only then, will it activate the new ISS imaging framework terms and call them into action. That need or

no-need, yes or no ISS imaging decision is made unambiguously and automatically in the first term within the ISS imaging series after the conventional linear image, and a 'no-need' determination not only shuts down the first non-linear term but all subsequent terms in the imaging series at any specific well-located image in the linear conventional migration. How does it know if it's an adequately or an inadequately located image? The guess would be that some criteria is being used by ISS imaging to determine 'wellness' of the image, since we are so oriented to that 'indirect' criteria orientation and religion (e.g., CIG flatness or iterative updating with an objective function and search engine). There is no 'indirect' criteria being employed in any ISS application, rather the directness within the ISS is the driver, and it doesn't provide merely perturbation theory, where some initial estimate is perturbed and updated, but rather purposeful perturbation theory, with 'direct' and 'purposeful' being the key and coupled concepts and the central and essential point. The 'directness' in ISS is what makes each term have a purpose, and identifiable within specific tasks towards inversion, and those terms within the ISS imaging series determine first if their purpose is needed at some location within a conventional migrated image before they act. Direct inversion, provided in the form of a series (perturbation), inexorably leads to purposeful perturbation theory, where each and every term has a unique and specific purpose and role, that can in turn be associated with isolated tasks - within the overall goal of inversion. That's in contrast with indirect methods, e.g., typical iterative linear or other indirect updating and search engine schemes, the latter more often based on mathematics and optimization, on 'all or nothing' thinking, typically settling for the latter. In some circles indirect methods have even defined themselves as the only definition and meaning of inversion as 'datafitting'. The consequences of ignoring the distinction between direct and indirect methods are tremendously significant. From a direct inversion perspective, for determining changes in earth mechanical properties, the so-called 'full wave inversion' methods today are inverting the wrong and fundamentally inadequate P to P data, with wrong algorithms, and with a wrong earth model. Would we today ignore the insights, lessons and the direct solution offered by $x = [-b \pm \sqrt{(b^2 - 4ac)} / 2a]$ for the quadratic equation, $ax^2 + bx + c = 0$ in favor of minimizing and searching various norms of $\| ax^2 + bx + c \|$? The latter is precisely what we are too often pursuing in the field of 'inversion' for changes in Earth mechanical properties. The indirect methods seem based on lack of hope or awareness of direct methods, and depend on big expensive, fast computers - and therefore have the affectation and imprimatur of being modern, computational and 'scientific', but too frequently are merely old ideas dressed up in abstract, rigorous and obfuscating mathematical language (for details and implications see, e.g., Weglein et al., 2009).

All current leading edge migration methods, such as, Beam, Kirchhoff and RTM, are linear. The ISS direct depth imaging without the velocity algorithm is a non-linear relationship between data and the wavefield at depth.

ISS TASK SPECIFIC SUBSERIES FOR MULTIPLE REMOVAL, DEPTH IMAGING AND DIRECT NON-LINEAR AVO

Each and every term and portion of any term within the ISS is computed directly in terms of data. All tasks associated with inversion (e.g., multiple removal, depth imaging, nonlinear direct AVO, and Q compensation) are each contained within the series. Hence, these individual tasks are each achievable directly in terms of data, and without subsurface information. Every seismic processing objective is carried out as an isolated task subseries of the ISS, and operates without subsurface information, by involving distinct non-linear communication of the recorded seismic data. Only the ISS communicates that all seismic objectives can be achieved in basically the same way that free surface multiples are removed. The free surface and internal multiple removal subseries have not only been shown to be viable but have also demonstrated added value and stand alone capability for predicting the amplitude and phase of multiples (see, e.g., Luo et al., 2011; Matson et al., 1999; Weglein and Dragoset, 2005; Fu et al., 2010), in particular, demonstrated under complex marine and on-shore circumstances. In this paper, we examine for the first time the issue of ISS depth imaging viability on field data. All conventional direct depth imaging methods only require knowledge of the velocity model to determine the spatial locations of reflectors. Hence, the ISS direct depth imaging subseries project began by assuming that only the velocity was variable and unknown. While all processing tasks are realizable directly and without subsurface information, all tasks are not equally simple or easy for the inverse series to achieve. For example, for different task specific subseries: one term eliminates each order of free surface multiple, while one term attenuates each order of internal multiple, furthermore, a series can locate reflectors beneath a small difference between actual and reference velocity, and another more inclusive imaging series can deliver the same structure determination effectiveness for larger contrasts in velocity. To-date the evolution and status of ISS imaging algorithms involves greater inclusiveness of ISS imaging terms and types of terms, and capability, but is not close to all of the ISS terms and capability that reside within the ISS. The issue is when a certain degree or state of ISS imaging capture will provide a tool box contribution with differential added-value in comparison to current imaging methods that require a velocity model.

The initial ISS imaging series (Weglein et al., 2002, Shaw et al., 2004, Innanen, 2004) were labeled LOIS for leading order imaging series. That evolved into a higher order cascaded series in closed form developed by Fang Liu (2006) and labeled as HOIS. All of that early development assumed that the only variable and unknown subsurface property was acoustic P wave velocity.

Figs. 1-8 illustrate the ISS imaging results for an earth in which only velocity varies. The algorithms are described in Liu (2006); Liu et al. (2005);

Zhang et al. (2007). The higher order imaging series (HOIS) methods pioneered in Liu and Weglein (2009) developed for velocity only varying media, are multi-dimensional ISS imaging algorithms that address imaging challenges that also exist in a one dimensional subsurface. Fang Liu's HOIS method was extended to HOIS+LE by Wang and Weglein (2011) to incorporate the imaging challenges addressed by HOIS, and in addition to accommodate certain imaging challenges that exclusively arise in a multi-dimensional laterally varying subsurface. The latter higher order imaging series plus laterally exclusive algorithm uses the acronym HOIS+LE. The progression of that velocity only varying subsurface ISS direct depth imaging capability, without the velocity model (HOIS and HOIS+LE) capability is shown in Figs. 1-8, for the fault shadow zone and pre-salt examples. HOIS and HOIS+LE contain higher order imaging terms for large contrasts and duration of those differences, imaging terms extracted from within the ISS. As mentioned above, these algorithms represent increasing capability, but are not containing all orders or all imaging terms for either a one-dimensional or multi-dimensional subsurface. More capability will be included in future algorithms. However, the HOIS and HOIS+LE algorithms are direct, require no velocity model building and updating, are closed form and both are lightning fast. The cost to run the HOIS and HOIS+LE algorithms is roughly 30% more than the single water speed FK Stolt migration. The single water speed migration is the costliest part of the ISS algorithm. It's essentially free, and that's amazing. The imaging results in Figs. 1-8 would be impressive for a conventional method that spent much time and effort to find the velocity from the data with a velocity analysis and then to image through it, that would take

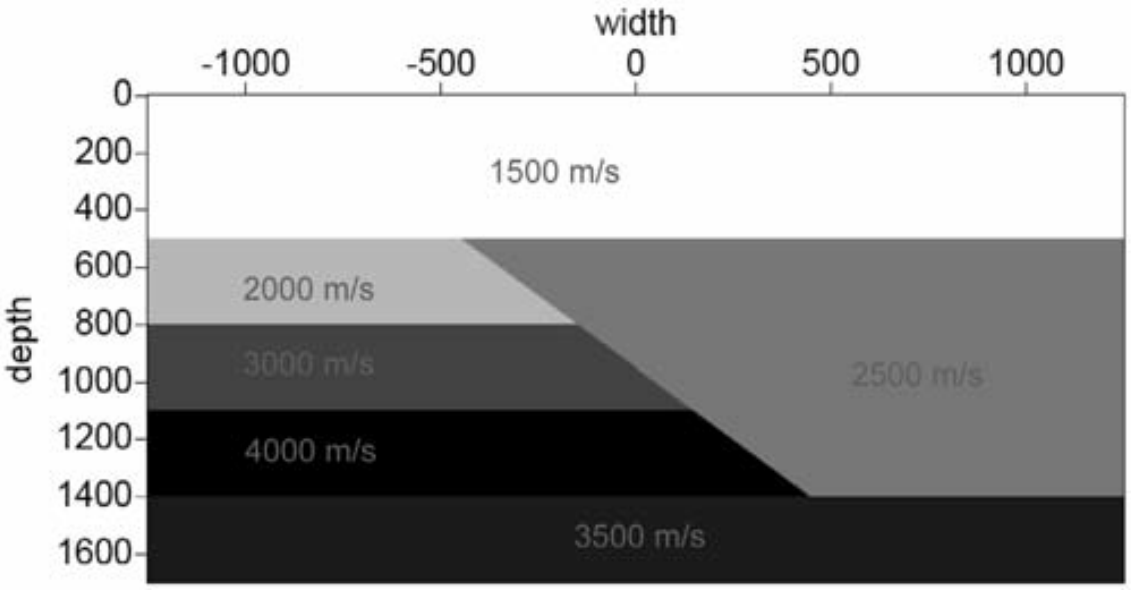

Fig. 1. The fault shadow zone model. Not to scale.

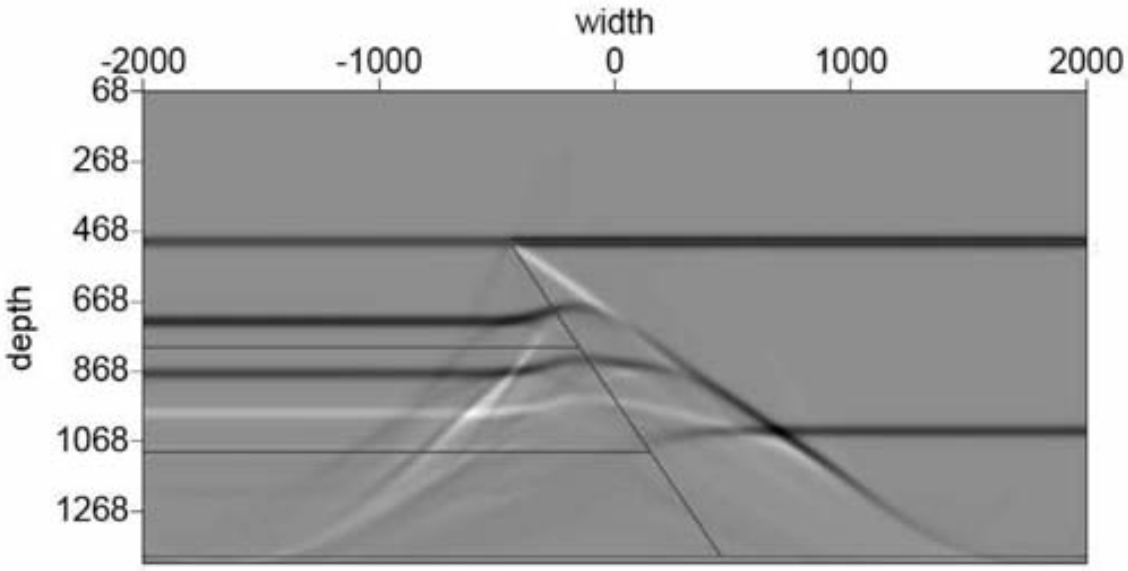

Fig. 2. The water speed pre-stack FK Stolt migration for the data from the fault shadow model (Liu and Weglein, 2009).

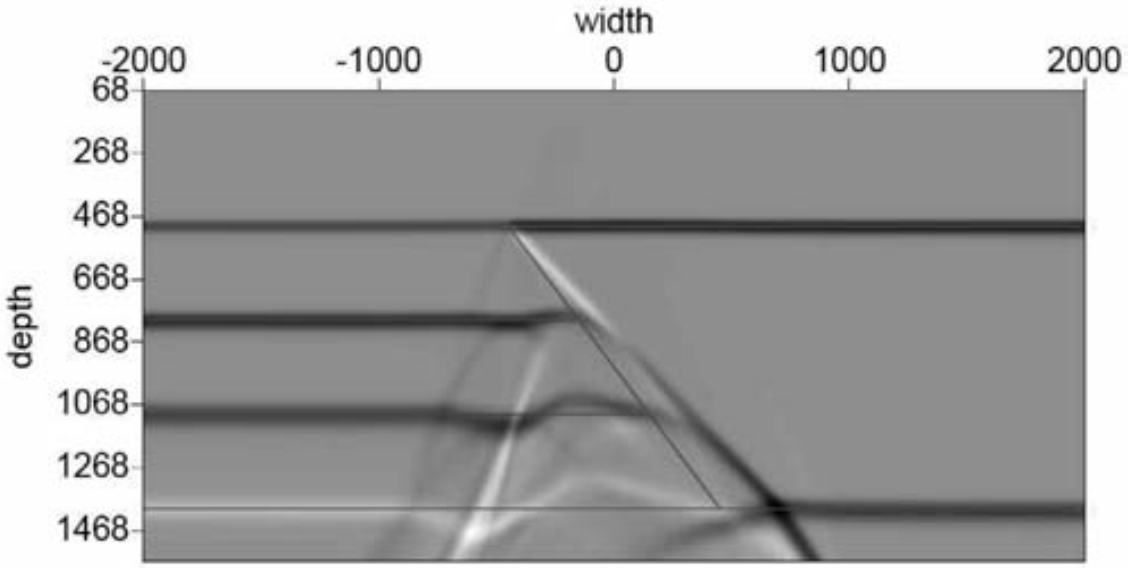

Fig. 3. Fault model - HOIS (Liu and Weglein, 2009).

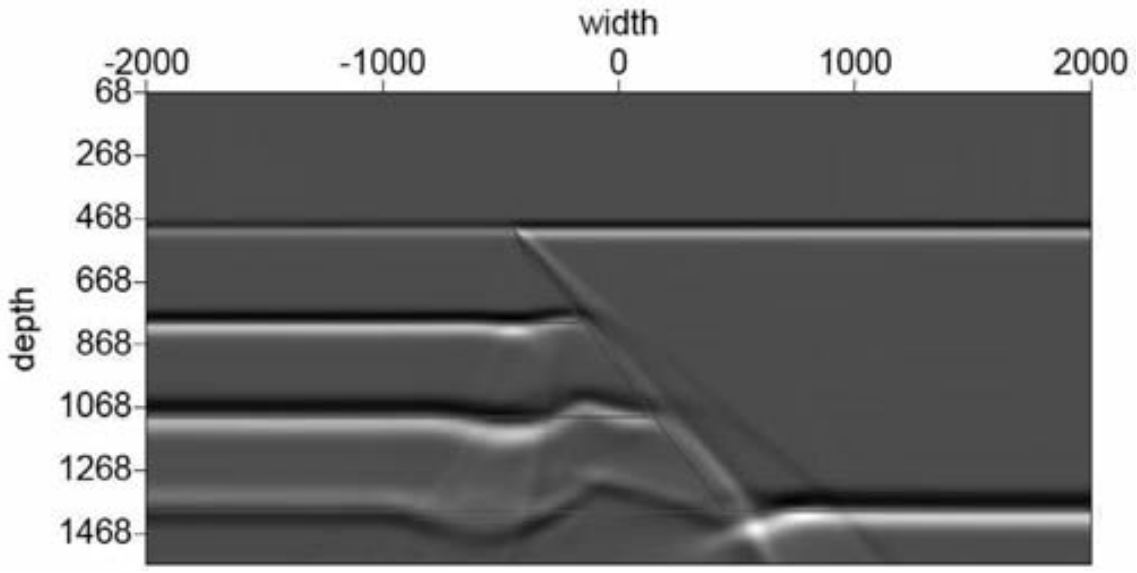

Fig. 4. Fault model HOIS+LE (Wang and Weglein, 2011).

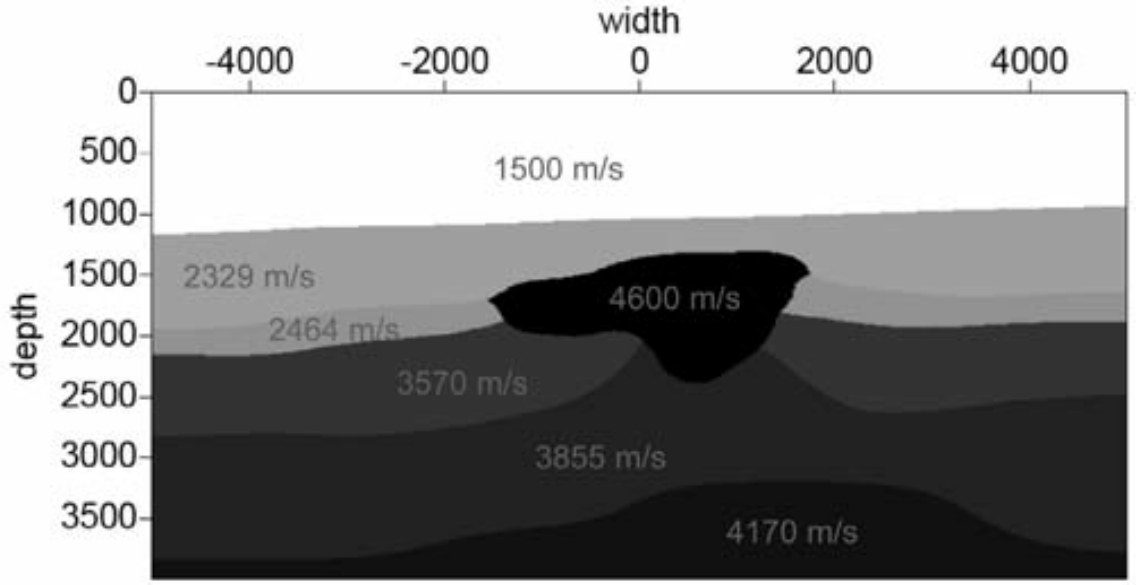

Fig. 5. Salt model.

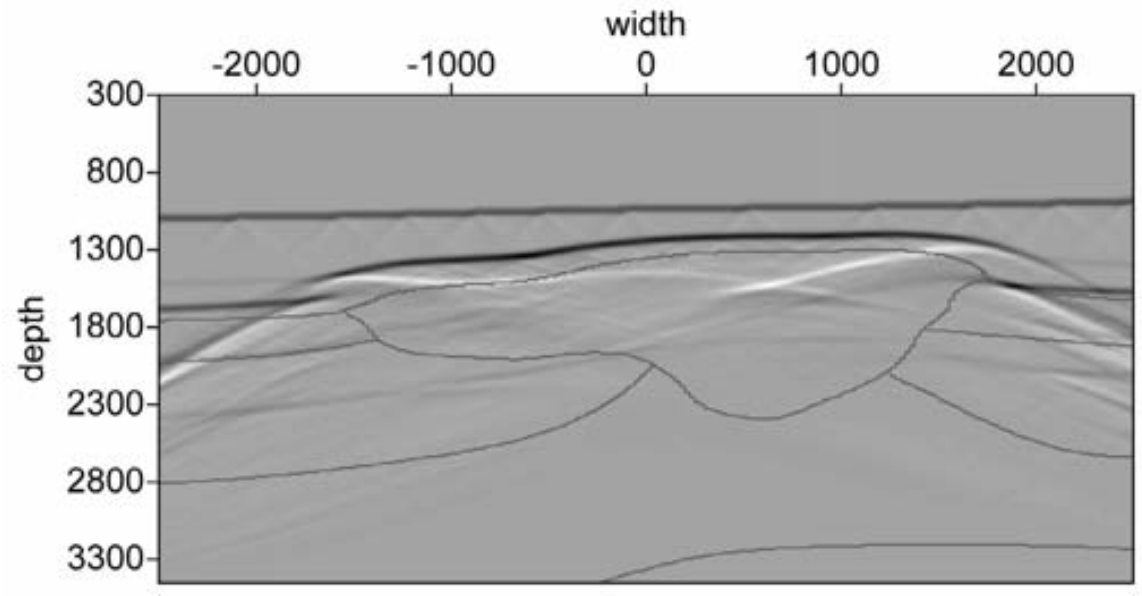

Fig. 6. Salt model water speed migration.

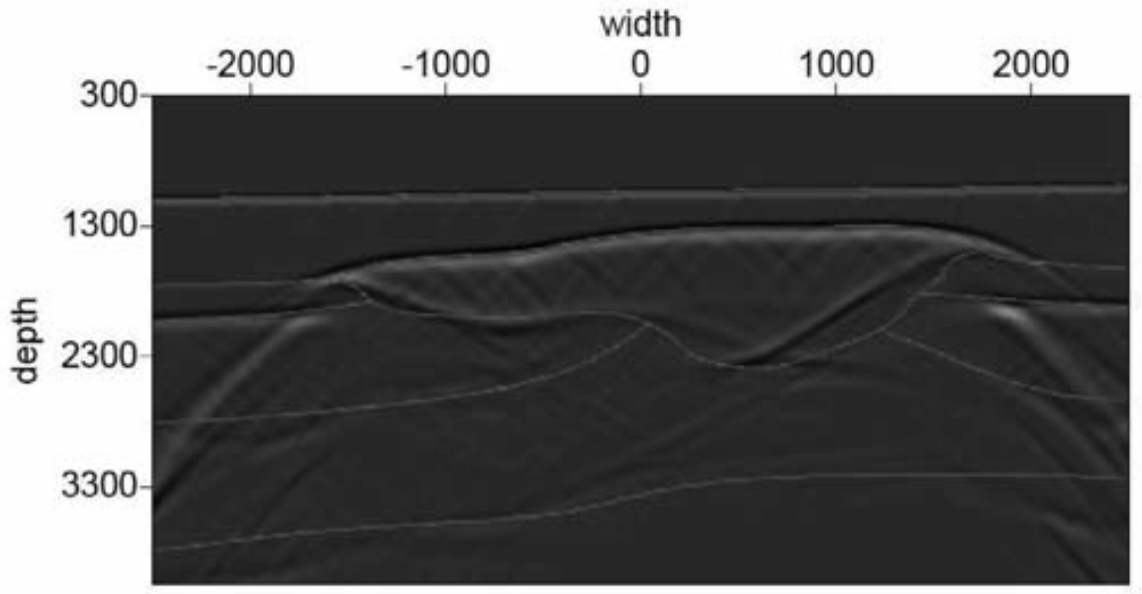

Fig. 7. Salt model - HOIS (Liu, 2006).

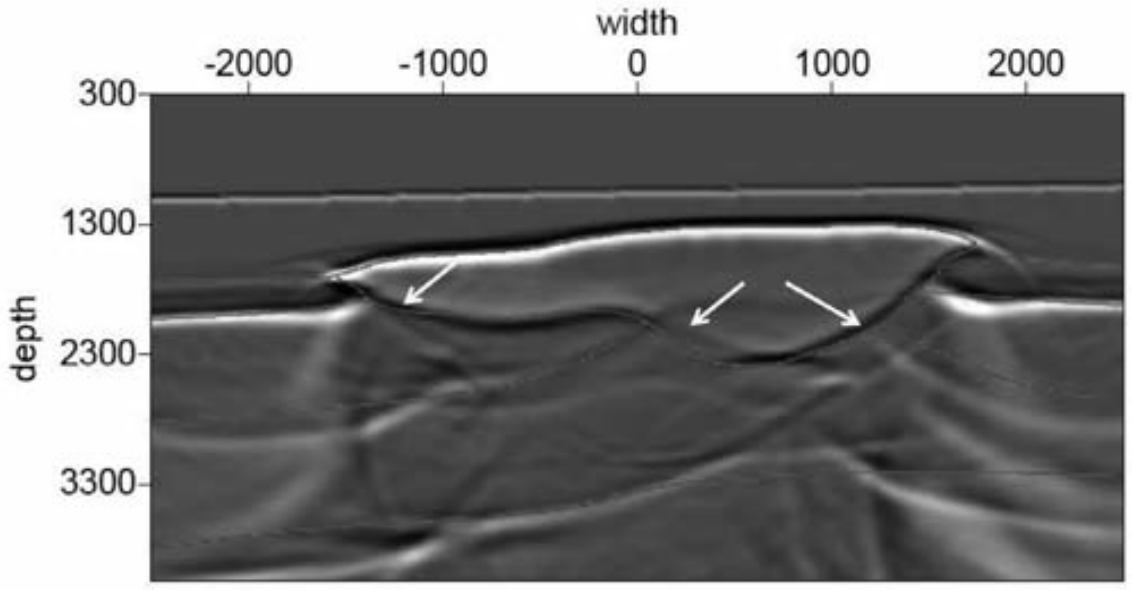

Fig. 8. Salt model - HOIS+LE (Wang and Weglein, 2011).

orders of magnitude longer to approximate the velocity and to migrate and image. These examples and algorithms exemplify the tremendous potential, promise and power that reside within the ISS for direct depth imaging without a velocity model, although these two specific algorithms (HOIS and HOIS+LE) are merely the tip of the iceberg in terms of capturing ISS imaging terms and capability. They represent progress within an important front (assuming that only velocity varies in the subsurface) in the ISS depth imaging campaign.

Imaging methods that require the velocity use only the phase of the data to determine depth. In contrast, all ISS tasks achieve their goals without subsurface information by using both the amplitude and phase of the events in seismic data.

MODEL TYPE AND ISS DEPTH IMAGING

The distinct ISS free surface and internal multiple attenuation subseries are model-type independent (see Weglein et al., 2003). That means those algorithms are completely unchanged if the earth is assumed to be an acoustic, elastic or anelastic medium. The ISS direct depth imaging subseries project has not reached a stage of development where a model-type independent ISS depth imaging algorithm is available. Therefore, at this time, the issue of ISS depth imaging and the assumed earth model-type needs to be considered in developing, evaluating and applying these techniques.

When we assume an acoustic earth model and, furthermore, that mechanical property changes in the medium are only due to velocity changes (and not density changes), then each reflection corresponds to a change in velocity at the reflector. For the latter earth model, if in addition the ISS imaging algorithm assumes (as we assume in this paper) that the reference velocity everywhere is constant and equal to the wave speed above the first and shallowest reflector, then ISS imaging will require (and the ISS depth imaging automatically provides and arranges) that all reflections above every initially mislocated reflector to be included and involved in the ISS depth imaging algorithm's input and action to correctly place the initially misplaced reference velocity imaged reflector.

However, if the medium allows changes in both velocity and density (as can and often does occur in the real earth), then the situation for ISS depth imaging is considerably more complicated both in theory and practice. To understand what gives rise to this new complexity, in a world where we assume that velocity and density can both vary, we will consider a specific example in such a medium, where the velocity is actually constant, and throughout the volume is equal to the constant reference velocity. The reflections in this example are then only caused by density variations. Then the constant reference velocity migration will accurately locate each reflector in this actual velocity equals reference velocity case. There is no need for ISS imaging beyond the first ISS term corresponding to reference velocity migration. Therefore density only reflections do not enter ISS depth imaging algorithms. The latter statement assumes that the objective of depth imaging is simply to locate reflectors and nothing more. Hence, we conclude that for an earth where both density and velocity can vary, that all reflections shallower than a given mislocated reflector are no longer necessarily involved through ISS imaging in aiding a mislocated deeper reflector. If the shallower reflection corresponds to either a velocity change, or to a velocity and density change, then that reflection enters the assistance package to aid the deeper mislocated reflector, but if the shallower reflection corresponds to only a density change, it doesn't enter that ISS depth imaging aid package. That's one of several new issues for a velocity and density varying earth that doesn't exist in a world where velocity is the only parameter that can vary. Further, if an ISS depth imaging algorithm that was derived from the ISS for an earth model where velocity is the only variable that can change, and the data that is input into the algorithm comes from a model where velocity and density can both vary, then initially well-located reflectors can be moved to an incorrect location and erroneously located images will not be corrected. However, there is no need to despair, because the multi-parameter acoustic or elastic ISS imaging, from the moment the multi-parameter ISS is written down, are immediately aware of this new issue that it needs to address, and automatically removes density only reflections from the ISS imaging algorithms, without knowing or determining the velocity and density configuration in the earth. Hence, the consequence of using all of the information in seismic primary

events (amplitude and phase) in ISS depth imaging without the velocity model, ultimately results in the need for ISS depth imaging to preclude density only reflections. The angle dependence of the amplitude of events is used by ISS imaging to preclude density only reflections.

THE EXCLUSION OF DENSITY ONLY REFLECTIONS IS APPROPRIATE FOR ISS MIGRATION FOR STRUCTURE BUT WOULD BE INCLUDED IF MIGRATION-INVERSION IS THE ISS GOAL

The exclusion of density only reflections would be inappropriate if the isolated task was designed to provide both a depth image plus an angle dependent reflection coefficient at those depth images, the latter for the purposes of migration-inversion. The ISS depth imaging in an acoustic earth where the P-wave velocity V_P and density (and for an elastic earth with P-wave velocity V_P, shear wave velocity V_S and density) can all vary and all are initially (and remain, completely) unknown, was formulated in Weglein et al. (2008) to retain the strength of a velocity only earth with a single imaging output, as a generalized reflectivity, while the exclusion of density only reflections is extracted from the strength of the multi-parameter ISS machinery. The results were summarized in Weglein et al. (2010).

THE IMPACT OF DATA LIMITATIONS ON ISS SUBSERIES

Table 1 summarizes the dependence/sensitivity of different ISS subseries on seismic bandwidth. As the latter table indicates, there is an increased dependency as we progress from the ISS free surface multiple case (where the subseries works one frequency at a time, and has absolutely no concern about bandlimited data) to the depth imaging subseries where the absence of low frequency in the data can have a deleterious effect on the ability of the ISS to move from the original linear incorrect depth image to the correct depth.

Table 1. The degree to which each ISS task specific subseries depends on the temporal frequency content of the data.

Specific subseries	Dependence on temporal frequency content of the data
Free surface multiple	None
Internal multiple	Very mild
Depth imaging	Some

THE CONDITIONS/ISSUES/REQUIREMENTS THAT NEED TO BE ADDRESSED FOR ISS DEPTH IMAGING ALGORITHMS TO BE EFFECTIVE ON FIELD DATA AND TO PROVIDE ACCURATE SPATIAL CONFIGURATIONS OF REFLECTORS IN THE SUBSURFACE

There are several absolute conditions, requirements and issues that need to be satisfied or addressed, respectively - in order for the current approach to ISS direct depth imaging without a velocity model to provide an effective and accurate spatial configuration of reflectors and interfaces in the earth. Those issues are: (1) sensitivity to (and interest in) low frequency/low vertical wavenumbers in the data; (2) assuming the appropriate earth model type and number of spatial dimensions in deriving the ISS imaging algorithm; (3) within a given and appropriate earth model type, the inclusion of sufficient imaging terms from the inverse scattering series, to address all shortcomings and problems from using as the first step a single constant velocity migration. Among items the ISS must accommodate, and address are: (I) how different is the actual velocity from the reference value, and the extent, duration, width of the layer, or over what region is that difference occurring; (II) how many parameters are assumed to be unknown in the appropriate model-type - the larger the number of unknown parameters in the model type, the harder the series has to work (that is, more ISS imaging terms have to be included) for the same contrast and duration of differences, in comparison with how hard the imaging series has to work for a single parameter changing model with comparable difference values and duration. The CIG flatness criteria is a necessary and sufficient condition that these conditions (1) and (3) have been satisfied and with an appropriate model type (condition 2) that the direct ISS imaging has produced the correct depth.

In the examples below, we will isolate and separately examine each of these issues. The order that we will follow is: first assume that there is no low frequency issue, and no model type matching issue between the model used to generate the data and the model used for processing the data, that is, the model behind the ISS imaging algorithm. In that first example, we examine the consequence of including or not including sufficient ISS imaging terms, in the ISS imaging algorithm to match and address the contrast in properties between actual and reference, and the duration of those differences. Fig. 9 shows two different ISS imaging results for a layered model. The first is LOIS (Leading Order Imaging Series, see, e.g, Shaw et al., 2004 extended to the multi-parameter case Weglein et al., 2008) and the second is HOIS (Higher Order Imaging Series, see e.g., Liu et al., 2005 also extended to the multi-parameter case Weglein et al., 2008) where LOIS has fewer types of terms and imaging capability in comparison to HOIS. The fact that HOIS is adequate inclusion of imaging terms (and LOIS is not) for this particular example's contrast and duration of differences between reference and actual velocity, is indicated by HOIS predicting the correct depth and having a flat

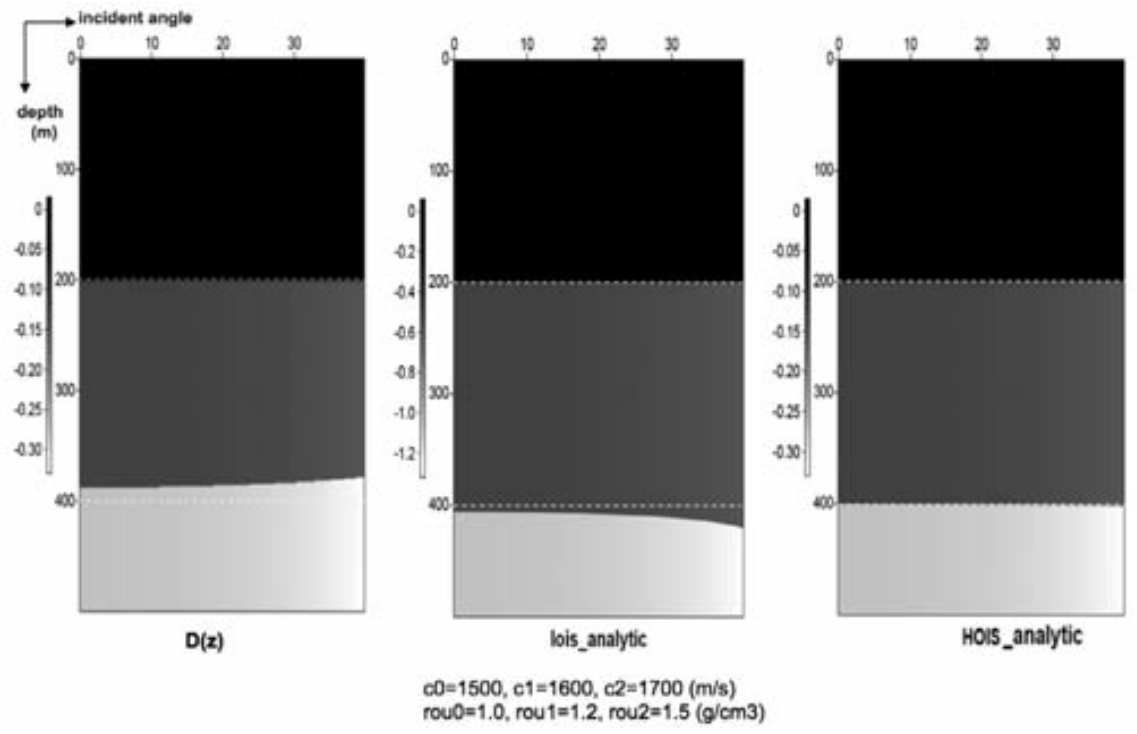

Fig. 9. Left: input FK-migrated data in pseudodepth domain. Center: LOIS result. Right: HOIS result. These figures demonstrate that with more capture, i.e., inclusion of more imaging terms, HOIS imaged the reflectors to their correct depth location, whereas LOIS did not.

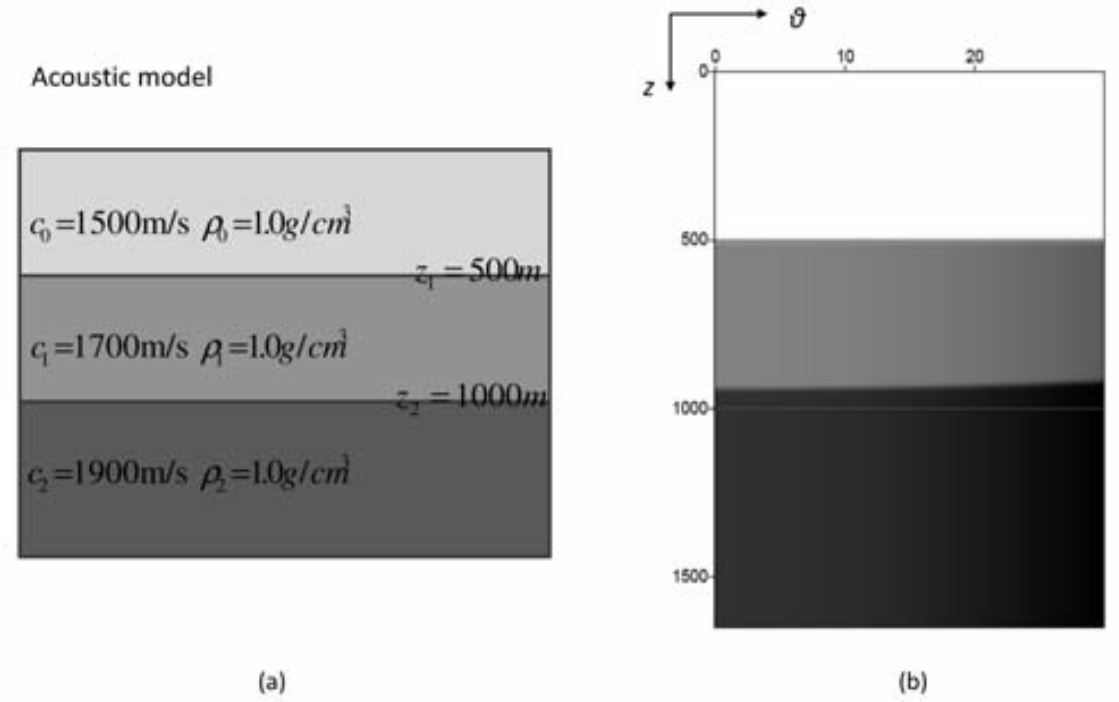

Fig. 10. (a) shows the acoustic model we are testing for evaluating the dependence of ISS on seismic bandwidth. (b) is the water speed FK Stolt migration, the red lines represent the true location of the reflectors.

CIG (Common Image Gather) where the latter only occurs when the correct depth is predicted. Hence, within a given model type and with adequate low frequency (see Figs. 12-14 for the assumed source signature spectrum, with the inclusion of significant low frequency), for ISS imaging to be effective requires adequate inclusion of imaging terms to match the contrasts and durations between actual and reference properties. The LOIS images have a move-out pattern indicating inadequate capture/inclusion of ISS imaging terms. However,the ISS imaging results with HOIS outputs common image gather flatness at the correct depth and indicates that the latter capture of imaging terms matches the contrasts and duration in the data. CIG flatness indicates adequate capture of ISS imaging terms. Hence, within a given model type and adequate low frequency content, the CIG moving and flatness output is a necessary and sufficient condition that this direct ISS depth imaging is working and the spatial configuration of the image is accurate.

All LOIS terms are also within HOIS, plus additional higher order imaging terms to address larger contrasts and duration than LOIS can accommodate. While HOIS is higher order than LOIS, it is not all orders, even for a 1D earth, nor does it accommodate imaging issues and challenges which exclusively exist in a laterally varying earth, for example, like diffractions (see, e.g., Wang and Weglein, 2011).

The second case: assume that the model-type between data generation and processing, that is, the model behind the ISS imaging algorithm, is a match, and that adequate capture is within the ISS imaging algorithm to address and accommodate the contrasts and duration. Now compare the results with adequate (see Fig. 11(a)) and decimated low frequency data, the latter with a sine squared taper (see Fig. 11(b)).

The results are shown in Fig. 11 where the former has adequate low frequency, and the latter has low frequency decimated. With low frequency tapered the result of ISS imaging is severely damaged, becoming equivalent to the original and erroneous water speed FK Stolt migration (see Fig. 10(b)). In Fig. 11(c) a source signature regularization has been applied which first removes the original wavelet and replaces it by a Gaussian. The source regularization of the low frequency tapered data allows the ISS depth imaging to become as effective as when the low frequency content was originally adequate. The ISS imaging results comparing adequate low frequency data, tapered low frequency data, and source signature regularized data are shown in Figs. 11(a), 11(b) and 11(c), respectively. The tapered data is a more severe and daunting test, than often occurs with field data, where some low frequency is present. The absolute shutdown of ISS imaging in the tapered data case, is a bit too severe a conclusion for field data, where some low and zero frequency in the data brings some small ISS effectiveness, where once again it is significantly enhanced by

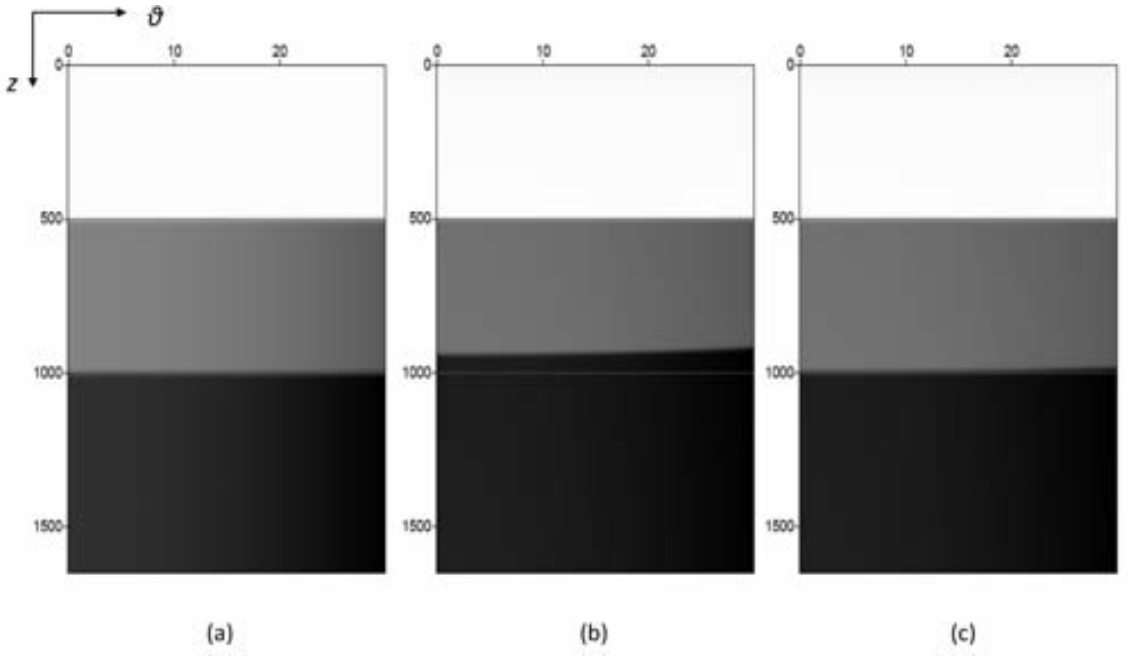

Fig. 11. This figure illustrates the imaging result for a velocity varying only earth model. (a) shows ISS imaging with data which has low frequency information. (b) shows ISS imaging with band-limited data. (c) shows the imaging result with the regularization being applied. This ISS imaging bandwidth issue is documented in Shaw (2005).

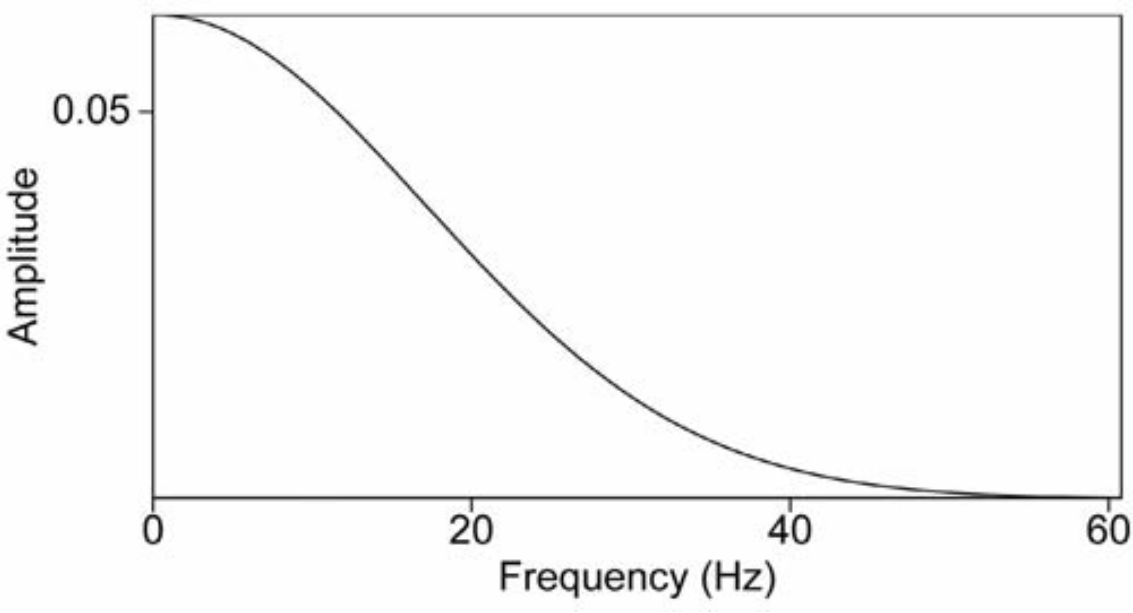

Fig. 12. Spectrum of data with low frequency.

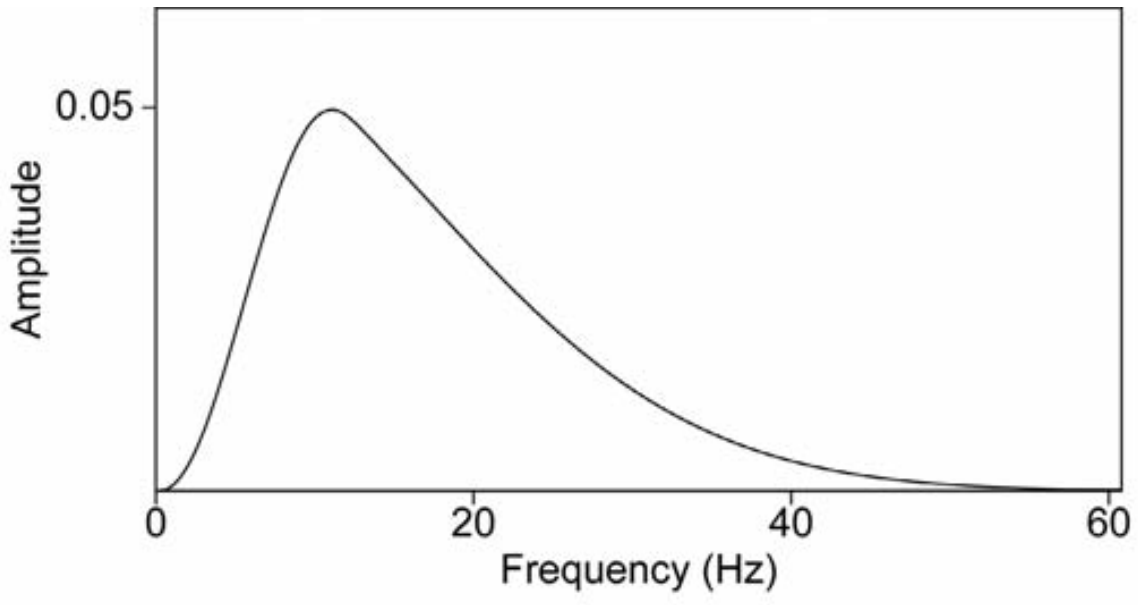

Fig. 13. Spectrum of data with diminished low frequency.

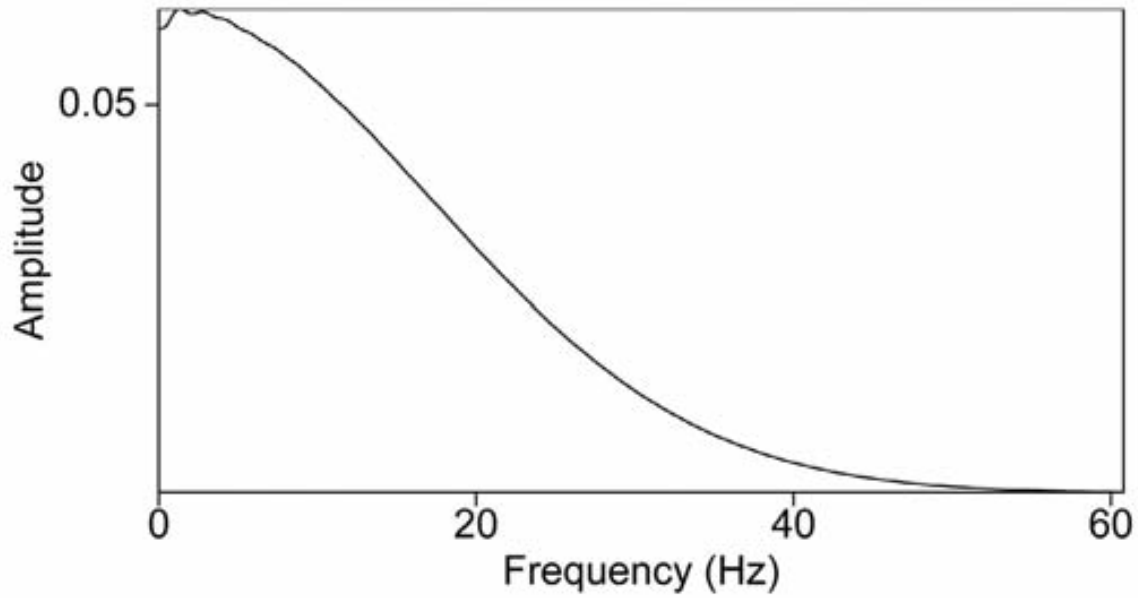

Fig. 14. Spectrum of regularized data.

the regularization. Hence, within a model type match, and adequate imaging term capture, the moved and flat CIG condition is a necessary and sufficient condition that the critical low frequency issue has been addressed. The high bar and demand on the source regularization in this synthetic example is a very positive and encouraging note and message.

Finally, we examine the case where a source signature regularization is needed and has been applied, and while the particular ISS imaging algorithm has adequate capture for a simpler earth model type, it is inadequate for a more

complicated earth model. In that case the data is generated using the more complicated earth model (more 'complicated' means more earth mechanical properties/parameters can vary) but the ISS imaging algorithm corresponds to the simpler model type. We will examine this for the case where the data is generated by a model where velocity and density both vary, but the ISS imaging algorithm assumes that only the velocity varies. That situation is illustrated in Figs. 15 and 16 where: (1) the model, (2) the water speed FK Stolt migration and (3) the velocity only varying ISS imaging algorithm result are shown. The flat CIG result indicates the ISS depth imaging result would produce the accurate depth if the data had come from a velocity only model, and that within the latter model, that effective source regularization and adequate and appropriate capture of ISS imaging terms had taken place. Hence, a flat CIG is a necessary and sufficient condition that source regularization and adequate imaging capability within a model type has been achieved. If the model type is appropriate for the data being imaged then depth will be produced. If the model

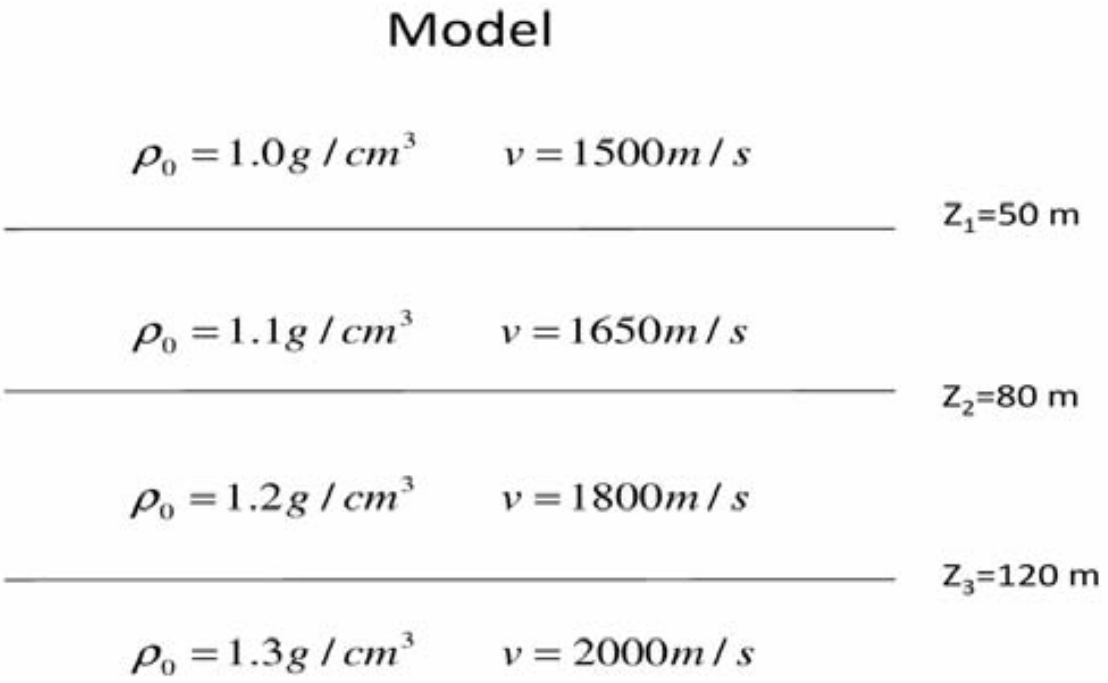

Fig. 15. An acoustic model with both velocity and density variations.

type used in the imaging is not a match with the model of the data, then CIG flatness would indicate that a critical source regularization is effective and that either the depth is being output or depth in a parallel and less complicated world is being accurately predicted. Flat CIG indicates that the critical source signature regularization is working. If you did not adequately source signature regularize and capture imaging terms for a velocity only world, then images would neither move nor flatten from the water speed migration result.

Under the latter circumstances, and as long as the low vertical wave-number sensitivity is addressed then, if: (1) the data comes from an earth where both velocity and density actually vary, (2) the ISS imaging algorithm, that will be used, was derived assuming that only the velocity in the Earth varies, and (3) the ISS imaging algorithm's ISS capture of imaging terms is adequate to correctly locate reflectors in depth if the data had been derived from a velocity only earth model, then the ISS imaging will produce flat common image gathers at the correct depth for a velocity only varying earth but at the incorrect location for an earth model type where velocity and density are both variable. Hence, if you assume a less complete model than is represented by the actual earth, then the ISS imaging output for the less complete model with flat common image gathers indicates it has addressed: (1) the low vertical wave-number issue and (2) adequate capture to produce the correct depth if the

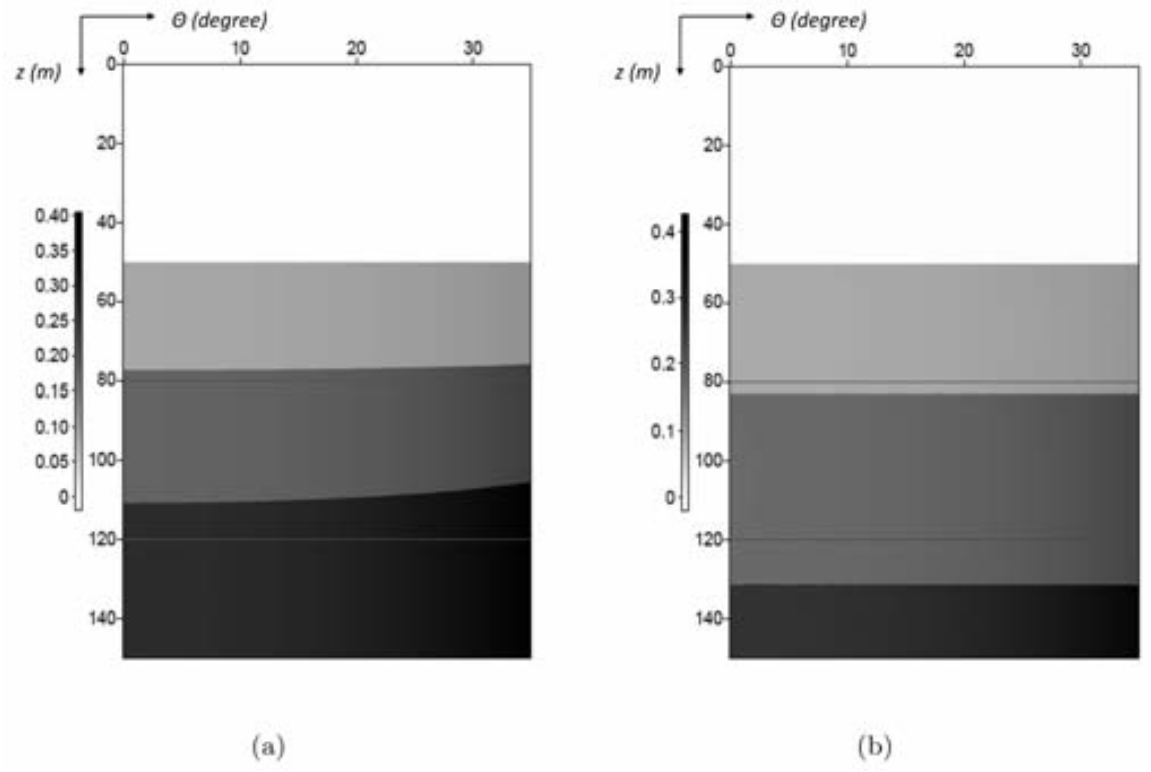

Fig. 16. (a) shows the input data generated from the geological model in Fig. 15. (b) shows ISS imaging results with velocity-only formulism. Red lines indicate the true depth of the reflectors.

lesser model type were adequate. That is behind the base-line ISS depth imaging testing of field data in this paper, and the conclusion that ISS direct depth imaging is viable. Figs. 15-16 demonstrate this idea, by having the actual model correspond to a velocity and density Earth while the ISS imaging assumes that only the velocity is varying. Note the ISS imaging flat CIG in Fig. 16(b).

There are many other issues that need to be taken into consideration in developing practical ISS depth imaging algorithms. Among these issues are: (1) within an appropriate earth model type, whether the necessary number and types of terms from the inverse series have been included to match the imaging challenge due to the difference between the actual and reference velocity, and the duration of that difference; and (2) whether the density only reflections have been excluded from the ISS depth imaging algorithm. All of these issues need to be addressed to have the ISS depth imaging algorithm produce an accurate depth section. When these requirements are met the ISS image moves until it stops, and when it stops it's there. The move-out becomes flat and the imaging series directly produces a flat common image gather (CIG) at the correct depth. In contrast to all current imaging methods where CIG flatness is a necessary but not a sufficient condition for depth imaging accuracy, the CIG flatness is a by-product of ISS imaging, and a necessary and sufficient indication that depth has been found. It's a direct depth finding machine, and when it stops it is done. With ISS imaging CIG flatness is an indication that a direct method is done, not an indirect proxy for velocity used to find the depth, where for the latter conventional use it is necessary but not sufficient for depth location. Within the current ISS imaging formulation, the overriding requirement and number one issue for field data application of ISS depth imaging is being able to address the sensitivity to missing low frequency components in the data (or more accurately, low vertical wave number). If that low frequency sensitivity is not addressed, then gathering or not gathering appropriate and necessary ISS imaging terms or excluding density only reflections will not matter, and will be of no practical consequence. Hence, addressing the bandwidth issue for ISS imaging is the number one priority, the make or break issue for field data application, viability and delivery of its promise of high impact differential added value. A regularization scheme has been developed in Liu et al. (2010) to directly address that low frequency challenge. A key purpose of this paper is to examine whether this regularization method will allow the ISS imaging algorithms to be effective and work on field data. Therefore, with this first field data examination, we relax all of the other requirements for ISS depth imaging and consider the field data as though it were generated by a velocity only varying earth. Within that parallel world where only velocity varies, the ISS depth imaging will need to address the band-limited nature of field data, and also will require having enough ISS imaging terms (within an acoustic velocity only varying subsurface assumption) to be effective for accurately locating reflectors.

The three requirements or conditions of: (1) source signature regularization, (2) adequate algorithmic ISS capture, and (3) appropriate earth model type between data generation and data processing, taken together represent a set of necessary and sufficient conditions that ISS imaging requires to be effective and working. A flat CIG is a necessary and sufficient condition that indicates ISS depth imaging effectiveness within an appropriate earth model type.

KRISTIN FIELD DATA ISS IMAGING

A similar approach is followed for a CMP gather selected from the Kristin data set (Fig. 17, Majdanski et al., 2010). Fig. 20(a) shows a water-speed migration of the data in Fig. 17, while Fig. 20(b) shows the ISS imaging result after regularization. Event 1 is the water bottom primary, event 2 is the sub-water bottom primary, event 3 is the internal multiple between event 1 and 2 and event 4 is the third primary. Event 4, the third primary has a non-flat move-out with a water speed migration. It turns out that event 1, the water-bottom primary, represents a density change but no velocity change. That was deduced by: (1) assuming that the shear velocity was probably close to zero at the water bottom, and hence an acoustic model would be adequate, (2) examining the angle dependence of the data at the water bottom, (3) the angle independence of that water bottom reflection indicates that density changed but not velocity, and (4) that $\alpha_1 - \beta_1$, is the difference between linear estimates of bulk modulus and density (and corresponds to the linear estimate to the change in acoustic velocity), and is zero when the reflection has no velocity change. In acoustics, if the linear estimate of the change in velocity is zero, then the actual change in velocity is zero. Velocity is the only acoustic parameter that exhibits that property. Fig. 21 shows the water bottom has no change in acoustic velocity.

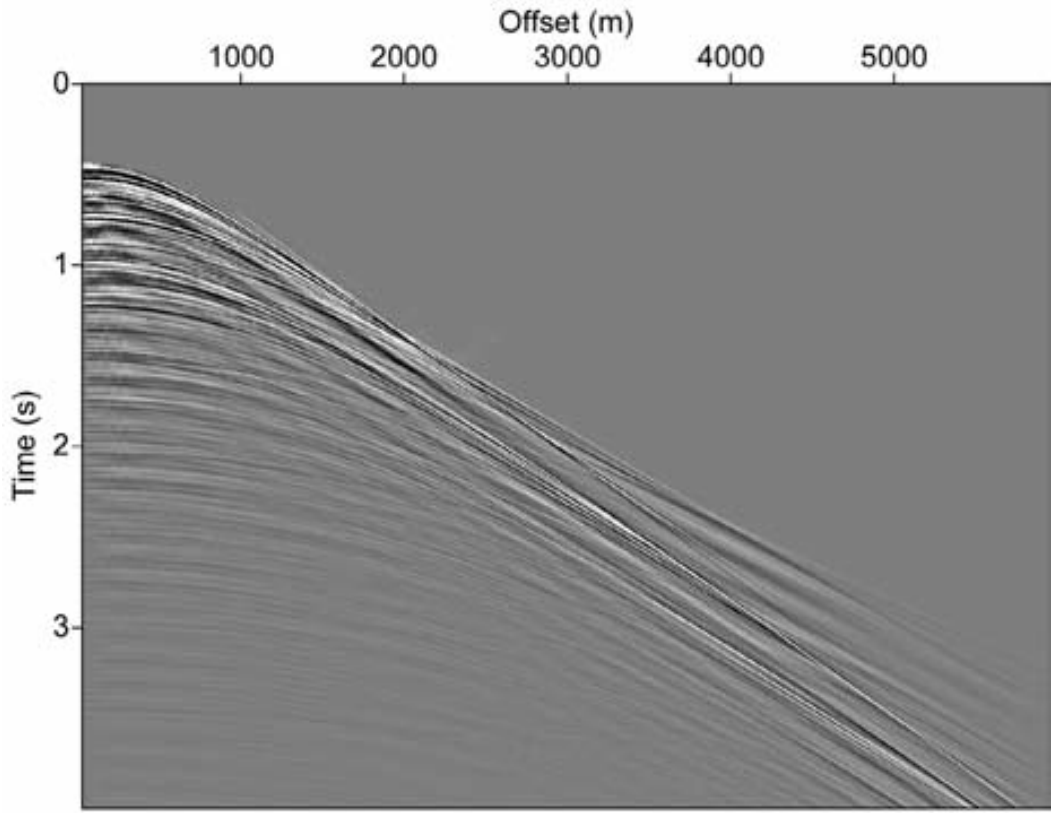

Fig. 17. The CMP gather tested from Kristin data.

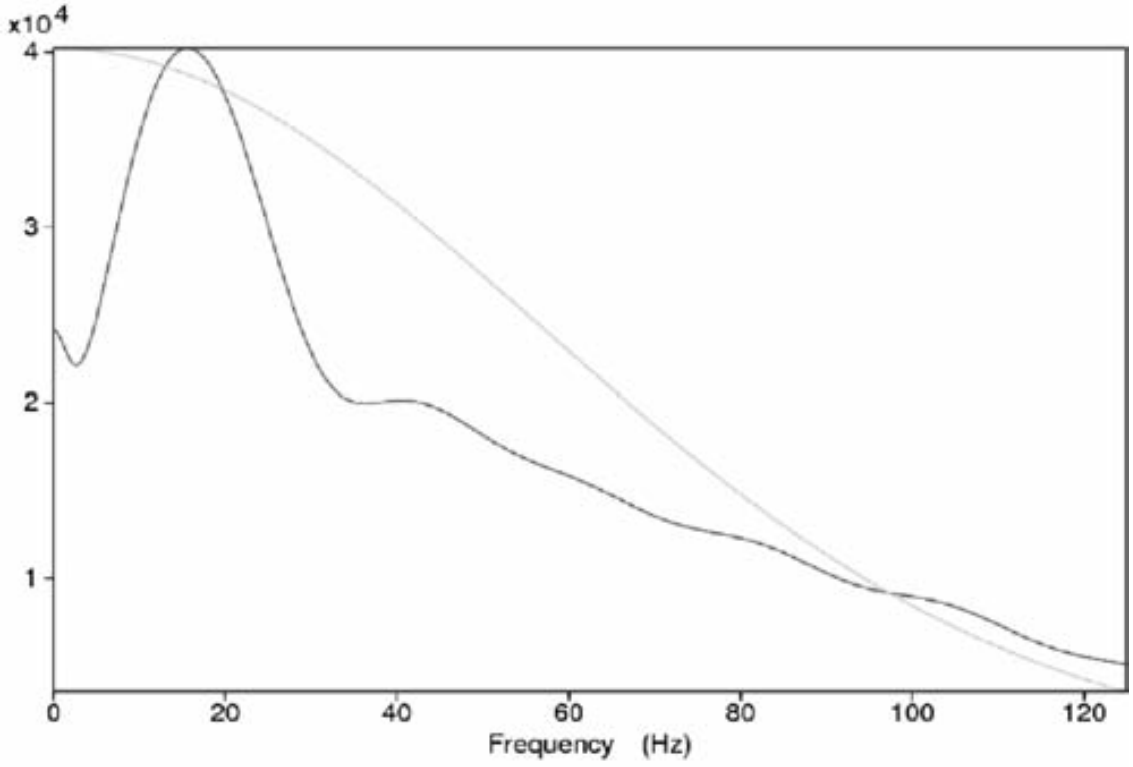

Fig. 18. Source signature regularization analysis. Amplitude spectrum of original wavelet (in red) and the target wavelet we wish to have (in green). We scale the spectrum of the target wavelet [exp $(-\omega^2/a^2)$, where $a = 80\pi$] to be of the same magnitude as that of the original wavelet for easy comparison.

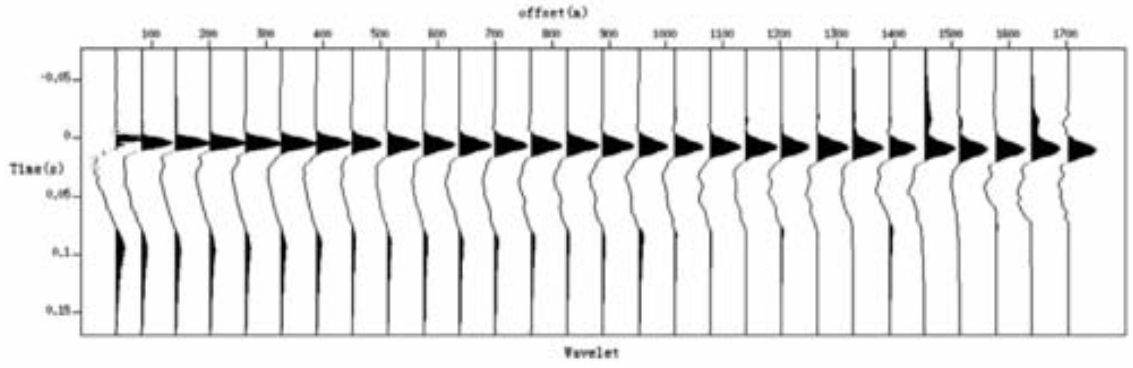

Fig. 19. Wavelet A(t), cable II (source at depth 7 m and receivers at depth 18 m).

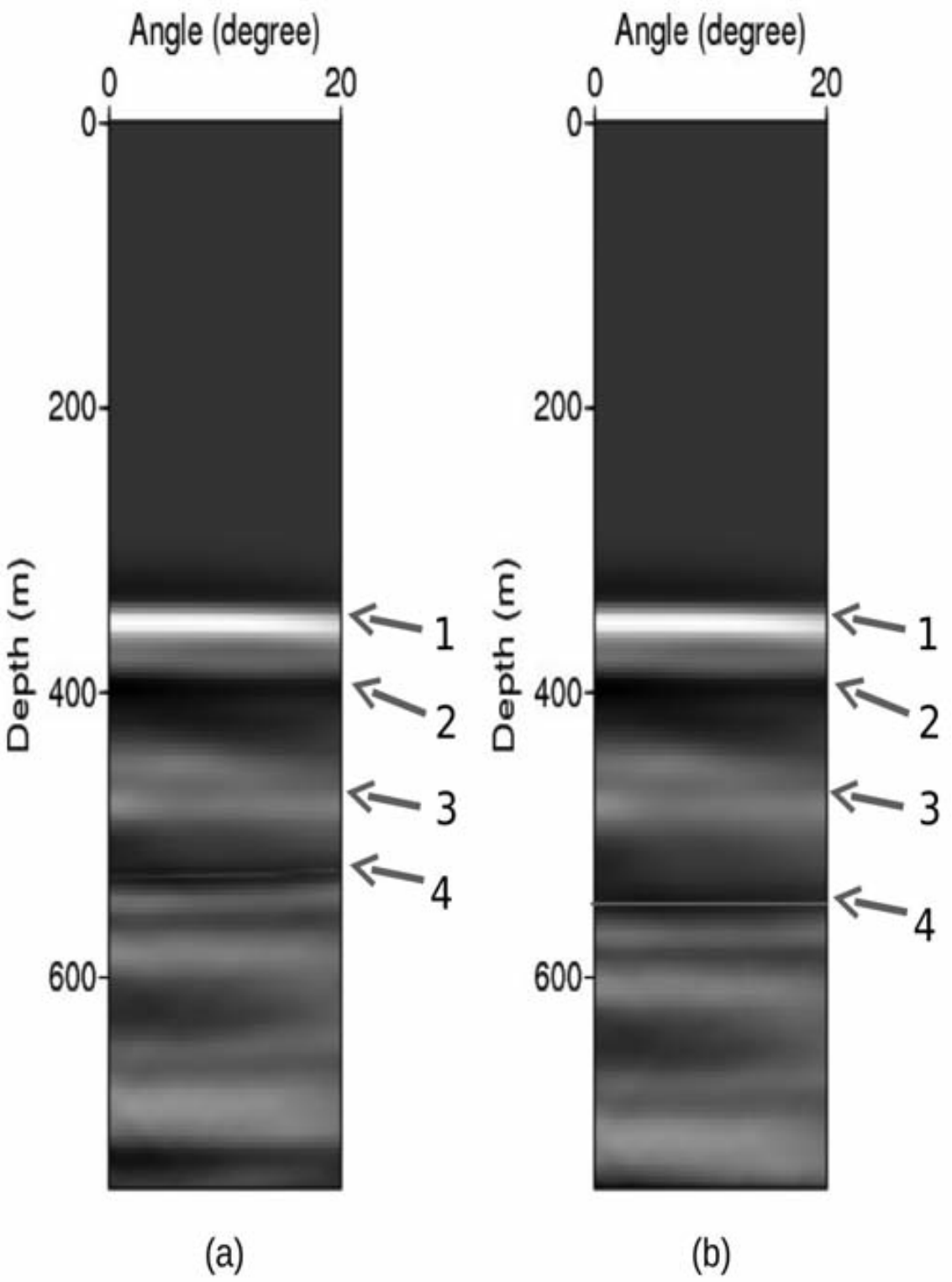

Fig. 20. For the Kristin data test: (a) shows water speed migration. The red line indicates water speed migration image for event 4. (b) shows ISS imaging result. The red line shows ISS image for event 4.

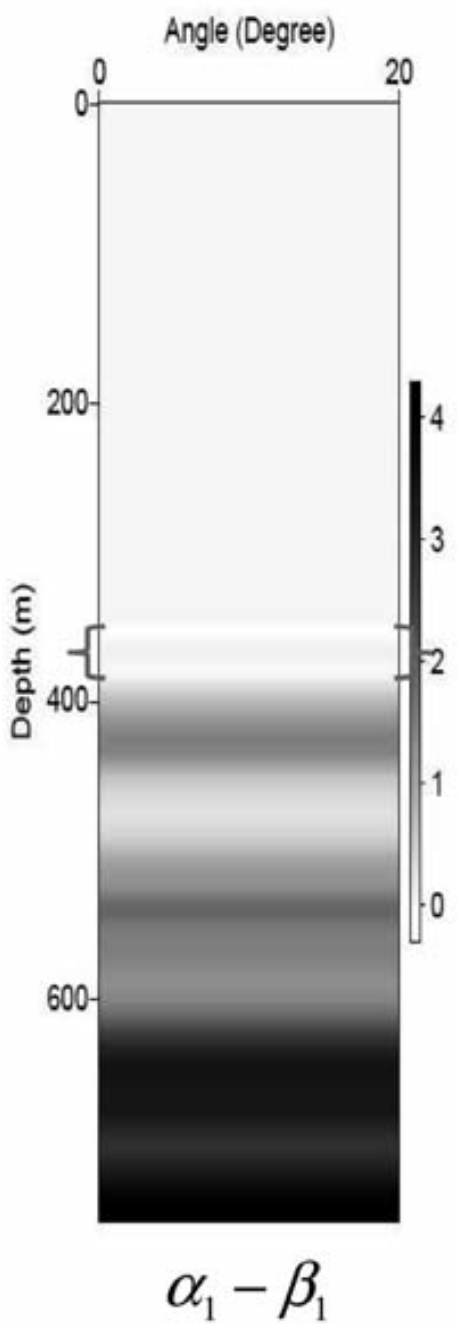

Fig. 21. Kristin data ISS depth imaging result.

Hence, the layer below the water-bottom has the same acoustic velocity as water. Further, the first order internal multiple (event 3) in that first sub-water-bottom layer also has a water-speed move-out. Hence, events 1, 2, and 3 all have flat CIGs with a water-speed FK Stolt migration (Fig. 22). Event 4 has move-out due to a velocity change at the base of the first sub-water-bottom layer. With a regularized ISS depth imaging the result for the image of event 4 is a shifted and flat CIG output. Hence, the ISS depth imaging is working on the very shallow sub-sea-bottom portion of the Kristin data set

within the context of a velocity only varying earth. The shifted ISS image and flat CIG of event 4, the third primary, indicates that bandwidth issues have been addressed, and sufficient capture of ISS imaging terms are within the ISS imaging algorithm. If for this field data set and ISS depth imaging test, either one of these conditions (addressing bandwidth sensitivity and adequate inclusion of ISS imaging terms) were a remaining and outstanding issue, then event 4 would not have moved and produced a flat CIG. The success of this test is thus defined. The next steps are to apply the regularized ISS depth imaging to an acoustic variable velocity and density model for the very shallow and sub-water-bottom reflectors, and a P-wave velocity V_P, shear wave velocity V_S and density varying elastic earth model for the deeper reflectors, to preclude density only reflections, and for outputting actual depth. If the second reflector corresponds to only a velocity change then Fig. 20(b) represents the correct depth of the first, second and third reflectors, the latter corresponding to event 4, directly and without knowing, needing or determining the velocity change across the second reflector.

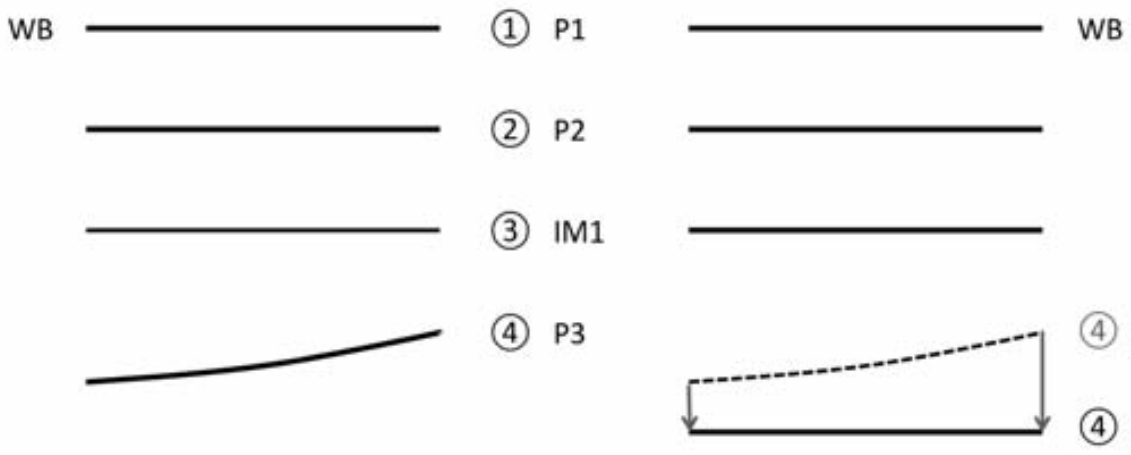

Fig. 22. This figure summarizes the results of the initial ISS depth imaging tests on the very shallow, near ocean bottom section of the Kristin data.

THE PLAN FORWARD

In the entire line of papers and theses within the history of the ISS imaging project, Weglein et al. (2002); Shaw et al. (2004); Liu (2006); Wang and Weglein (2011) there is an assumption (which for a simple two reflector/single layer example, and a chosen constant reference velocity equal

to the actual velocity above the shallower reflector) that the perturbation or difference between the actual and reference properties, and the linear estimate of that perturbation, are both 'box-like' in character. For this simple example, the linear estimate (using the reference velocity to migrate) is a box whose upper surface is at the correct depth and the lower is at the incorrect depth. Within this box-like formulation, defining imaging as locating the edges of the box (reflectors) and hence, structure, the ISS then has to correct the original box into a box whose upper and lower end are both at the correct depth. That change requires the ISS imaging to create a box that takes the mislocated original lower interface and adds a box to bring it to the correct depth. Box construction places a high burden on low vertical wave-numbers. In hindsight, that box-like formulation was not the most strategic, frugal, and well-considered way to correct mislocated images at depth. Constructing boxes when only the location of edges is of interest is paying too high a price for the sought after boundary location output. Staying closer to the data space and away from model space is the key. We plan to recast all ISS imaging methods as we move forward, in terms of moving mislocated data-like 'spikes', and that new formulation will provide a set of theoretical and practical benefits for ISS imaging efficacy that are being formulated and examined at this time. We are also examining reducing the burden of capturing adequate ISS imaging terms in an elastic earth, where the P-wave velocity, shear wave velocity and density are variable and unknown and remain unknown. We are exploring the possibility of reducing the number of independent parameters through either empirical relationships, e.g., using Garner-Garner or Greenburg-Castagna, or effective media (e.g., the optical potential). The combination of: (1) moving spikes (images) rather than boxes, and (2) reducing the elastic parameters to one effective parameter will expedite the promise and delivery of, e.g., Figs. 4 and 8 to field data.

The M-OSRP imaging research team (working in cooperation with our sponsors) is engaged in moving from the current news and report that demonstrates field data viability for ISS imaging to providing added value. The ultimate goal is to have ISS imaging match the efficacy that ISS free surface and internal multiple removal have provided for the removal of coherent noise, i.e., multiples (see, e.g., Weglein et al., 2011a), and to extend that capability for extracting information from signal (the collection of all primaries).

CONCLUSIONS

In this paper, we have shown that the ISS depth imaging algorithm can address the most serious practical limitation/challenge field data will place on ISS depth imaging: that is, limitations in seismic bandwidth. With this accomplished, the further steps to extend these tests to variable density and velocity acoustic and elastic media are achievable, and realizing that is within

the sphere of issues we can influence and make happen. The most significant difference and potential obstacle between synthetic data tests and field data for developing and delivering ISS depth imaging has been addressed.

ACKNOWLEDGMENT

We thank Professor Tadeusz Ulrych for his excellent suggestions and insightful comments in his review of this paper. We thank all the sponsors of M-OSRP for their support and encouragement. We have been partially funded by and are grateful for NSFCMG award DMS-0327778 and DOE Basic Sciences award DE-FG02-05ER15697. M-OSRP would like to thank Statoil ASA, Petoro, ExxonMobil, Eni, Total, and Schlumberger/WesternGeco for granting access to the Kristin data and special thanks to Ed Kragh (Schlumberger Cambridge Research), Joachim Mispel (Statoil ASA), Mariusz Majdanski (Schlumberger Cambridge Research), Mark Thompson, and Einar Otnes for their assistance and cooperation.

REFERENCES

Amundsen, L., Reitan, A., Arntsen, B. and Ursin, B., 2006. Acoustic nonlinear amplitude versus angle inversion and data-driven depth imaging in stratified media derived from inverse scattering approximations. Inverse Problems, 22: 1921.

Amundsen, L., Reitan, A., Arntsen, B. and Ursin, B., 2008. Elastic nonlinear amplitude versus angle inversion and data-driven depth imaging in stratified media derived from inverse scattering approximations. Inverse Problems, 24: 045006.

Amundsen, L., Reitan, A., Helgesen, H.K. and Arntsen, B., 2005. Data-driven inversion/depth imaging derived from approximations to one-dimensional inverse acoustic scattering. Inverse Problems, 21: 1823-1850.

Fu, Q., Luo, Y., Kelamis, P.G., Huo, S., Sindi, G., Hsu, S.-Y. and Weglein, A.B., 2010. The inverse scattering series approach towards the elimination of land internal multiples. Expanded Abstr., 80th Ann. Internat. SEG Mtg., Denver: 3456-3461.

Innanen, K.A., 2004. Methods for the treatment of acoustic and absorptive/dispersive wave field measurements. Ph.D. thesis, University of British Columbia.

Liu, F., 2006. Multi-dimensional depth imaging without an adequate velocity model. Ph.D. thesis, University of Houston.

Liu, F., Li, X. and Weglein, A.B., 2010. Addressing innate data limitations in ISS imaging algorithms: distinct data regularization methods to address different types of data limitations, to facilitate and allow specific ISS imaging steps and goals. 2010 M-OSRP Ann. Rep., 50-81.

Liu, F. and Weglein, A.B., 2009. Inverse scattering series velocity dependent imaging in laterally varying media: analysis of transcendental integrals in the mathematics of multidimensional imaging. 2008 M-OSRP Ann. Mtg.

Liu, F., Weglein, A.B., Nita, B.G. and Innanen, K.A., 2005. Inverse scattering series for vertically and laterally varying media: application to velocity independent depth imaging. M-OSRP Ann. Rep., 4.

Luo, Y., Kelamis, P.G., Fu, Q., Huo, S., Sindi, G., Hsu, S.-Y. and Weglein, A.B., 2011. Elimination of land internal multiples based on the inverse scattering series. The Leading Edge, 30: 884-889.

Majdanski, M., Kostov, C., Kragh, E., Moore, I., Thompson, M. and Mispel, J., 2010. Field data results of elimination of free-surface-related events for marine over/under streamer data. Extended Abstr., EAGE Conf., Barcelona.

Matson, K.H., Corrigan, D.C., Weglein, A.B., Young, C.Y. and Carvalho, P.M., 1999. Inverse scattering internal multiple attenuation: results from complex synthetic and field data examples. Expanded Abstr., 69th Ann. Internat. SEG Mtg., Houston: 1060-1063.

Shaw, S.A., 2005. An Inverse Scattering Series Algorithm for Depth Imaging of Reflection Data from a Layered Acoustic Medium with an Unknown Velocity Model. Ph.D. thesis, University of Houston.

Shaw, S.A., Weglein, A.B., Foster, D.J., Matson, K.H. and Keys, R.G., 2004. Isolation of a leading order depth imaging series and analysis of its convergence properties. J. Seismic Explor., 13: 157-195.

Wang, Z. and Weglein, A.B., 2011. An investigation of ISS imaging algorithms beyond HOIS, to begin to address exclusively laterally varying imaging challenges. M-OSRP 2010 Ann. Mtg., 105-114.

Weglein, A.B., Araújo, F.V., Carvalho, P.M., Stolt, R.H., Matson, K.H., Coates, R.T., Corrigan, D., Foster, D.J., Shaw, S.A. and Zhang, H., 2003. Inverse scattering series and seismic exploration. Inverse Problems, 19: R27-R83.

Weglein, A.B. and Dragoset, W.H., 2005. Multiple Attenuation (Geophysics Reprint No. 24). SEG, Tulsa, OK.

Weglein, A.B., Foster, D.J., Matson, K.H., Shaw, S.A., Carvalho, P.M. and Corrigan, D., 2002. Predicting the correct spatial location of reflectors without knowing or determining the precise medium and wave velocity: initial concept, algorithm and analytic and numerical example. J. Seismic Explor., 10: 367-382.

Weglein, A.B., Hsu, S., Terenghi, P., Li, X. and Stolt, R.H., 2011a. Multiple attenuation: Recent advances and the road ahead (2011). The Leading Edge, 30: 864-875.

Weglein, A.B., Liu, F., Wang, Z., Li, X. and Liang, H., 2010. The inverse scattering series depth imaging algorithms: development, tests and progress towards field data application. Expanded Abstr., 80th Ann. Internat. SEG Mtg., Denver: 4133-4138.

Weglein, A.B., Ramírez, A.C., Innanen, K.A., Liu, F., Lira, J.E. and Jiang, S., 2008. The underlying unity of distinct processing algorithms for: (1) the removal of free surface and internal multiples, (2) Q compensation (without Q), (3) depth imaging, and (4) nonlinear AVO, that derive from the inverse scattering series. Expanded Abstr., 78th Ann. Internat. SEG Mtg., Las Vegas: 2481-2486.

Weglein, A.B., Stolt, R.H. and Mayhan, J.D., 2011b. Reverse-time migration and Green's theorem: Part I - the evolution of concepts, and setting the stage for the new RTM method. J. Seismic Explor., 20: 73-90.

Weglein, A.B., Stolt, R.H. and Mayhan, J.D., 2011c. Reverse time migration and Green's theorem: Part II - a new and consistent theory that progresses and corrects current RTM concepts and methods. J. Seismic Explor., 20: 135-159.

Weglein, A.B., Zhang, H., Ramírez, A.C., Liu, F. and Lira, J.E.M., 2009. Clarifying the underlying and fundamental meaning of the approximate linear inversion of seismic data. Geophysics, 74: WCD1-WCD13.

Zhang, J., Liu, F., Innanen, K. and Weglein, A.B., 2007. Comprehending and analyzing the leading order and higher order imaging closed forms derived from inverse scattering series. 2006 M-OSRP Ann. Rep.: 149-159.

First application of Green's theorem derived source and receiver deghosting on deep water Gulf of Mexico synthetic (SEAM) and field data

James D. Mayhan, Arthur B. Weglein*, and Paolo Terenghi*, M-OSRP/Physics Dept./University of Houston**

Summary

We report the first use of Green's theorem derived source and receiver deghosting on deep water Gulf of Mexico synthetic (SEAM) and field data. Green's theorem derived deghosting has several qualities which separate it from previous deghosting methods: (1) it accommodates a multi-dimensional earth, (2) it doesn't require a Fourier transform over space coordinates, (3) it works in every depth of water, (4) it allows for any shape of measurement surface (e.g., a corrugated water bottom), and (5) it is consistent with wave theory processing methods. The context of Green's theorem deghosting is placed within a single consistent Green's theorem preprocessing and inverse scattering series (ISS) processing chain. Green's theorem derived deghosting theory is presented, and an algorithm implementing the theory is discussed. The algorithm has been tested on field data and several kinds of synthetic data with positive and encouraging results.

Introduction

Deghosting is a long standing problem (see, e.g., Robinson and Treitel, 2008) and is important because (1) removing the downward component of the recorded field (receiver deghosting) enhances seismic resolution with removal of notches and boosts low frequencies, and (2) it is a prerequisite for many processing algorithms including multiple elimination (ISS free surface multiples and internal multiples and SRME) and model matching 'FWI' that benefits from enhanced low frequency data. Hence, deghosting has benefit for both traditional seismic processing as well as playing an important role in all ISS based processing.

Green's theorem derived deghosting (Weglein et al., 2002; Zhang and Weglein, 2005, 2006; Zhang, 2007) has characteristics not shared by previous methods and is consistent with ISS wave theory methods that don't require subsurface information (Weglein et al., 2003). In Mayhan et al. (2011), we reported the first use of Green's theorem derived receiver deghosting on deep water Gulf of Mexico synthetic and field data. In this Expanded Abstract we report the first application of Green's theorem derived source and receiver deghosting on the same data.

While the ISS is independent of subsurface velocity (and in fact of all subsurface properties), it makes certain assumptions about its input data. Weglein et al. (2003) describe how every ISS isolated task subseries requires (1) the removal of the reference wavefield, (2) an estimate of the source signature and radiation pattern, and (3) source and receiver deghosting and how the ISS has a nonlinear dependence on these preprocessing steps. The fact that the ISS is nonlinear places a higher bar on preprocessing requirements. An error in the input to a linear process creates a linear error in its output, but the same error in ISS input creates a combination of linear, quadratic, cubic, etc. errors in its output.

The freedom of choosing a convenient reference medium means Green's theorem offers a flexible framework for deriving a number of useful algorithms. Methods that can be derived from Green's theorem include: wavefield separation (reference and scattered), wavelet estimation, ghost removal, and one way and two way wavefield continuation (RTM). Green's theorem methods are multidimensional, work in the $(\omega, \mathbf{r})$ data space (and hence, are simple to apply to irregularly spaced data), fully consistent with ISS wave equation processing, and make no assumptions about the earth. Therefore, Green's theorem preprocessing methods and ISS isolated task subseries processing are fully consistent. The delivery of the former always benefits the latter.

A brief aside on our terminology. The total wavefield P consists of the reference wavefield P_0 (which for a homogeneous reference medium doesn't experience the earth) and the scattered wavefield P_s (which does experience the earth). Ghosts begin their propagation moving upward from the source (source ghosts) or end their propagation moving downward to the receiver (receiver ghosts) or both (source/receiver ghosts) and have at least one upward reflection from the earth. Primaries and multiples are defined after the reference wavefield and source and receiver ghosts are removed. Primaries have only one upward reflection from the earth. Multiples have more than one upward reflection from the earth. Free surface multiples have at least one downward reflection from the free surface (air-water interface). Internal multiples have all their downward reflections below the free surface.

Theory—Receiver deghosting

Green's theorem derived deghosting establishes an integral relationship between the total wavefield P excited by a source located at $\mathbf{r}_s$ and its ghost free version P'. The relationship is valid within a region of space V (which must include $\mathbf{r}_s$) bounded by a closed surface S (Figure 1). For convenience, the region is chosen such that its lower boundary coincides with the measurement surface defined by the location of the active receivers.

To facilitate solving the problem at hand, a whole space of water is selected as a reference medium (where the

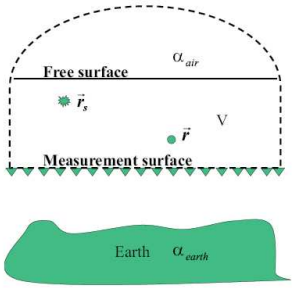

Fig. 1: *Configuration for deghosting using Green's theorem (Zhang, 2007, Fig. 2.10). α_{air} and α_{earth} are perturbations, the differences between the actual medium (air, water, earth) and reference medium (water).*

Green's function is known analytically). A perturbation operator, α, is introduced to characterize the difference between earth and reference properties. For this choice of reference medium, the perturbation may be seen as a quantity describing the capability of the earth to cause scattering (reflections, transmissions, diffractions, etc.) of the reference wave produced by the physical source located in the water column. For our choice of reference medium, the scattering potential is non-zero at and above the free surface and at and below the sea bottom. Therefore, scattering contributions to the wavefield P are expected, which may be interpreted as the product of secondary sources located in the reference medium.

If G_0^d is the Green's function for the reference medium, it can be shown (Weglein and Secrest, 1990) that the integral equation

$$P'_R(\mathbf{r}'_g, \mathbf{r}_s, \omega) = \int_{\text{m.s.}} dS\, \hat{\mathbf{n}}\cdot \tag{1}$$
$$[P(\mathbf{r}, \mathbf{r}_s, \omega)\nabla G_0^+(\mathbf{r}, \mathbf{r}'_g, \omega) - G_0^+(\mathbf{r}, \mathbf{r}'_g, \omega)\nabla P(\mathbf{r}, \mathbf{r}_s, \omega)]$$

(Weglein et al., 2002, equation 5) identifies the contribution to P recorded inside V caused by sources located outside V. Here $\mathbf{r}'_g$ is the prediction point and $\mathbf{r}$ is the measurement point. If the region V is chosen to include water and air, as shown in Figure 1, the only sources are passive scattering sources at and below the water bottom. Hence, evaluating equation 1 with $\mathbf{r}$ in V (above the measurement surface and below the free-surface) provides the portion, P', of P traveling upwards from the subsurface to the receivers.

The implementation of the above theory is done in a straightforward manner. The Green's theorem algorithm computes the surface integral in equation 1. The method requires two wavefields as input, the pressure measurements P and their normal derivatives $\partial P/\partial z'$. The latter requires dual sensor cables or dual streamer cables.

Theory—Source deghosting

The last section has shown how Green's theorem can be applied to select the portion of the seismic wavefield that is up-going at a field position above the cable. The algorithm uses data from a single shot gather and the receiver coordinate as the integration variable. This section shows how the theory can be similarly applied for source deghosting, where the portion of the wavefield that is down-going at the source is sought. An application of reciprocity to the entire set of shot records allows the original receiver ghost removal to become a source ghost removal. Then a second application of Green's theorem over receivers results in source and receiver deghosted data. The direct Greens theorem based method for completely removing source and receiver ghosts requires a collection of single shot experiments where P and dP/dz_g are recorded on the measurement surface (in 2D along a towed streamer). The procedure of receiver deghosting produces the up-going wavefield at $\mathbf{r}$. If $\mathbf{r}$ is chosen shallower than the source ($\mathbf{r}_s$), applying the source-receiver reciprocity principle (i.e., swapping the source and receiver x, y, z coordinates) brings the problem back to the same setup as in receiver deghosting, where the total wavefield and its derivative are known on the receiver side and the up-going portion is sought. The analogous integral is

$$P'_{SR}(\mathbf{r}'_g, \mathbf{r}'_s, \omega) = \int_{\text{sources}} dS\, \hat{\mathbf{n}}\cdot \tag{2}$$
$$[P'_R(\mathbf{r}'_g, \mathbf{r}, \omega)\nabla G_0^+(\mathbf{r}, \mathbf{r}'_s, \omega) - G_0^+(\mathbf{r}, \mathbf{r}'_s, \omega)\nabla P'_R(\mathbf{r}'_g, \mathbf{r}, \omega)].$$

The source and receiver deghosting steps described below essentially follow the method described and exemplified in Zhang, 2007, pp. 33-39. The one difference is that for each shot we input dual measurements of P and dP/dz_g along the towed streamer whereas in J. Zhang the source wavelet and P along the cable are used. The advantage of having the wavefield P and its normal derivative along the towed streamer is to allow deghosting for an arbitrary source distribution without needing to know or to determine the source.

In practice the algorithm in equation 1 is reused via the following steps: (1) Receiver deghosting is performed in the common shot gather (CSG) domain. The Green's theorem algorithm removes down going waves at the receivers, i.e., receiver ghosts and source-receiver ghosts. (2) Source deghosting is performed in the common receiver gather (CRG) domain. We sort the receiver deghosted data from CSGs to CRGs and swap the coordinates of the sources and receivers. The Green's theorem algorithm again removes down going waves at the receivers. Source deghosting assumes reciprocity between sources and receivers. Calculations and numerical tests (Mayhan et al., 2012) support this conclusion. Additional theory and complementary test results are reported in a companion paper by Wang et al. (2012).

Example: Flat layer model

In Figure 2, the upper left panel is the input data from a 1D layer model, designed so that deghosting is easy

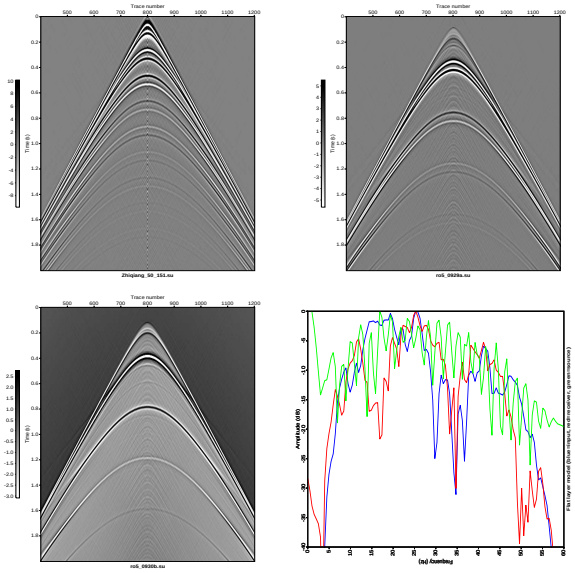

Fig. 2: *Flat layer model (sources at 50m and 52m, cables at 150m and 151m, water bottom at 300m): input data at 151m (upper left), receiver deghosted at 20m (upper right), source and receiver deghosted at 10m (lower left). Frequency spectra (lower right): input data (blue), receiver deghosted (red), source and receiver deghosted (green). The receiver notches (at intervals of 5Hz) and source notches (at intervals of 15Hz) have been filled in.*

to demonstrate. The depth of the receivers is chosen such that primaries and ghosts appear as distinct seismic events. We compute the event times for the data in the upper left panel of Figure 2, upper right panel, and lower left panel. We see that: (1) The events in the upper left panel of Figure 2 are (from the top) the direct wave G_0^d and its free surface (FS) reflection G_0^{FS}, the water bottom (WB) primary and its source ghost, the WB primary's receiver ghost and source/receiver ghost, the first free surface multiple (FSM) and its source ghost, and the first FSM's receiver ghost and source/receiver ghost. (2) In the upper right panel of Figure 2, all events are attenuated except the WB primary and its source ghost and the first FSM and its source ghost. (3) In the lower left panel of Figure 2, all events are attenuated except the WB primary and the first FSM. All source and receiver ghosts are removed.

Example: SEAM application

We applied Green's theorem to the SEAM dataset generated based on a deepwater Gulf of Mexico earth model (The SEG Advanced Modeling Corporation, 2011). We used the special SEAM classic dataset modeled to simulate dual sensor acquisition by recording the pressure wavefield at two different depths, 15 and 17m respectively. This dual sensor data consisted of nine sail lines for an equivalent wide azimuth towed streamer survey. The source interval is 150m by 150m while the receiver interval is 30m in both inline and crossline directions. Given the low frequency of the data (less than 30Hz) and the source and receiver depths of 15m and 17m, the ghost reflections overlap/interfere with non-ghost events in contrast to the previous flat layer model where events and their ghosts were well separated. In this SEAM data test, successful deghosting would correspond to a change in the wavelet shape. The result is shown in Figure 3. In the bottom panel, a window of the first three panels, we see there is no source notch to fill; the first source notch is at 44Hz which lies above the source frequency range (1–30Hz).

Example: Field data

We also applied the deghosting approach to a field survey from the deep water Gulf of Mexico. The data were acquired using dual sensor streamers comprised of hydrophones and vertical geophones. The top panel in Figure 4 shows a zoom in of an input shot record, the second panel displays the same traces after receiver deghosting, and the third panel displays the same traces after source and receiver deghosting. Note the collapsed wavelet in the output images. In the bottom panel note the gradual recovery of the shape of the wavelet: first by receiver deghosting (middle trace) and then by both source and receiver deghosting (right trace).

Conclusions

We have implemented Green's theorem derived source and receiver deghosting for the first time on deep water Gulf of Mexico synthetic and field data. Testing to date has shown the algorithm works with positive and encouraging results. Green's theorem derived deghosting has several qualities which separate it from previous deghosting methods. Green's theorem preprocessing (e.g., source and receiver deghosting and wavefield separation) and ISS processing (e.g., multiple removal and imaging) are a consistent set of methods where the preprocessing works in cooperation with the methods they are meant to serve, do not require a Fourier transform over receivers, and accommodate a not flat measurement surface. The direct Greens theorem based method for completely removing source and receiver ghosts requires a collection of single shot experiments where P and dP/dz_g are recorded on the measurement surface (in 2D along a towed streamer).

ACKNOWLEDGMENTS

We are grateful to the M-OSRP sponsors for their support of this research. The first author is also grateful to ExxonMobil and PGS for internships and Nizar Chemingui for mentoring, sharing his insights, and providing his excellent guidance and encouragement.

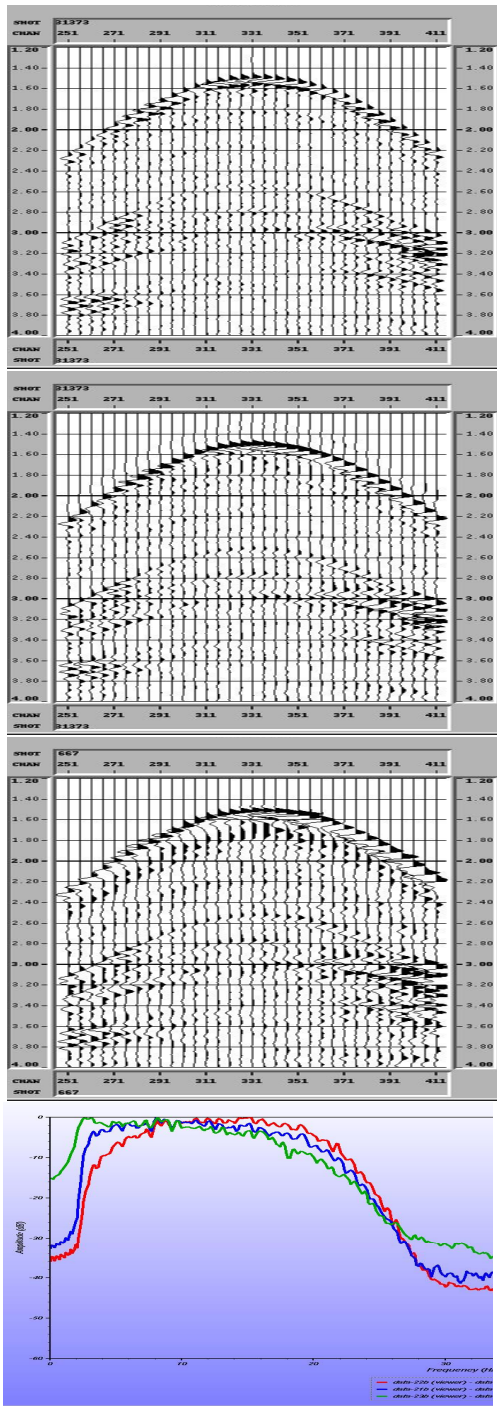

Fig. 3: *SEAM data, shot 131373: recorded data at 17m (top panel), receiver deghosted at 10m (second panel), source and receiver deghosted at 10m (third panel). Note the collapsed wavelets in the second and third panels. Frequency spectra (bottom panel): red=P at 17m, blue=receiver deghosted at 10m, green=source and receiver deghosted at 10m. The first source notch is at 44Hz which lies above the source frequency range (1–30Hz). Note the shift of the spectrum towards lower frequencies (which may be of interest to FWI).*

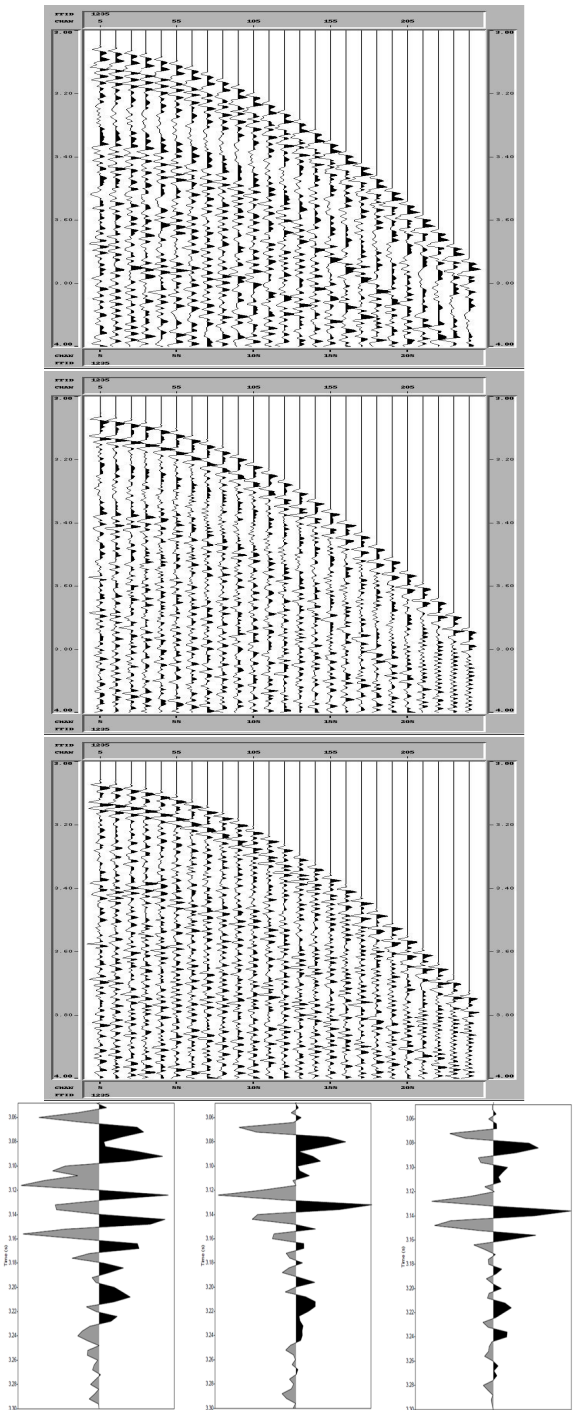

Fig. 4: *Field data: hydrophones at 22–25m (top panel), receiver deghosted at 10.5m (second panel), source and receiver deghosted at 8m (third panel). Note the collapsed wavelets in the second and third panels. Closeup of trace 5 in each of the above panels (bottom panel). Note the gradual recovery of the shape of the wavelet: by receiver deghosting (middle trace) then by both source and receiver deghosting (right trace). Input data courtesy of PGS.*

References

Mayhan, J. D., P. Terenghi, A. B. Weglein, and N. Chemingui, 2011, Green's theorem derived methods for preprocessing seismic data when the pressure P and its normal derivative are measured: 81st Annual International Meeting, SEG, Expanded Abstracts, Society of Exploration Geophysicists, 2722–2726.

Mayhan, J. D., A. B. Weglein, and P. Terenghi, 2012, Preprocessing marine seismic data with Green's theorem: Presented at the M-OSRP 2011 Annual Meeting. (In press).

Robinson, E. A., and S. Treitel, 2008, Digital imaging and deconvolution: The ABCs of seismic exploration and processing: Society of Exploration Geophysicists.

The SEG Advanced Modeling Corporation, 2011, The SEG advanced model: Technical report, Society of Exploration Geophysicists. (`http://www.seg.org/resources/research/seam`).

Wang, Z., A. B. Weglein, J. D. Mayhan, P. Terenghi, and C. Rivera, 2012, Green's theorem derived deghosting: fundamental analysis, numerical test results, and impact on iss free-surface multiple elimination, *in* 82nd Annual International Meeting, SEG, Expanded Abstracts: Society of Exploration Geophysicists. (Submitted).

Weglein, A. B., F. V. Araújo, P. M. Carvalho, R. H. Stolt, K. H. Matson, R. T. Coates, D. Corrigan, D. J. Foster, S. A. Shaw, and H. Zhang, 2003, Inverse scattering series and seismic exploration: Inverse Problems, **19**, R27–R83.

Weglein, A. B., and B. G. Secrest, 1990, Wavelet estimation for a multidimensional acoustic earth model: Geophysics, **55**, 902–913.

Weglein, A. B., S. A. Shaw, K. H. Matson, J. L. Sheiman, R. H. Stolt, T. H. Tan, A. Osen, G. P. Correa, K. A. Innanen, Z. Guo, and J. Zhang, 2002, New approaches to deghosting towed-streamer and ocean-bottom pressure measurements, *in* 72nd Annual International Meeting, SEG, Expanded Abstracts: Society of Exploration Geophysicists, 1016–1019.

Zhang, J., 2007, Wave theory based data preparation for inverse scattering multiple removal, depth imaging and parameter estimation: analysis and numerical tests of Green's theorem deghosting theory: PhD thesis, University of Houston.

Zhang, J., and A. B. Weglein, 2005, Extinction theorem deghosting method using towed streamer pressure data: analysis of the receiver array effect on deghosting and subsequent free surface multiple removal, *in* 75th Annual International Meeting, SEG, Expanded Abstracts: Society of Exploration Geophysicists, **24**, 2095–2098.

———, 2006, Application of extinction theorem deghosting method on ocean bottom data, *in* 76th Annual International Meeting, SEG, Expanded Abstracts: Society of Exploration Geophysicists, **25**, 2674–2678.

Green's theorem derived deghosting: fundamental analysis, numerical test results, and impact on ISS free-surface multiple elimination

Zhiqiang Wang, Arthur B. Weglein*, James D. Mayhan*, Paolo Terenghi*, and Christian Rivera†, M-OSRP/Physics Dept./University of Houston* and TOTAL†*

SUMMARY

Ghosts distort the data spectrum and affect the results of many seismic processing algorithms (e.g., multiple elimination, imaging, and inversion). Green's theorem derived deghosting is a wave theoretic method defined in the frequency-space domain with demonstrated capability, accuracy and flexibility. In this abstract, we present an analytic example and numerical test results of Green's theorem derived receiver and source side deghosting, and its impact on the inverse scattering series (ISS) free-surface multiple elimination.

INTRODUCTION / BACKGROUND

In marine seismic exploration, a source ghost is an event starting its propagation upward from the source, and a receiver ghost ends its propagation moving downward at the receiver. Ghosts have the same frequency content as their primaries and usually arrive shortly after them. The interference of the primaries and their ghosts reduces the low frequency content of the data, lowers the resolution, produces notches in the spectrum, and sometimes generates multiple images of the subsurface. The effective removal of ghosts has been a long standing problem in exploration seismology (Schneider et al., 1964; Amundsen et al., 1995).

The deghosting method derived from Green's theorem (Weglein et al., 2002; Zhang and Weglein, 2005, 2006; Zhang, 2007) is a wave theoretic algorithm defined in the frequency-space domain and can easily accommodate cables of any shape (e.g., slanted or ocean bottom). A complete Green's theorem derived deghosting procedure consists of two steps: receiver side deghosting in common shot domain and source side deghosting in common receiver domain, performed in any order. The receiver side deghosting method was first applied to synthetic datasets in Zhang (2007) and then a field dataset in Mayhan et al. (2011). In this Expanded Abstract, we first provide a brief introduction to the algorithm and then present an analytical example which provides a clear and transparent understanding of the method. Finally, numerical test results for deghosting and its impact on the ISS free-surface multiple elimination algorithm are shown and analysed.

THEORY

The equation for Green's theorem derived receiver side deghosting is

$$P'_R(\mathbf{r'_g},\mathbf{r_s},\omega)=\int_{m.s.}[P(\mathbf{r},\mathbf{r_s},\omega)\nabla G_0^+(\mathbf{r},\mathbf{r'_g},\omega) - G_0^+(\mathbf{r},\mathbf{r'_g},\omega)\nabla P(\mathbf{r},\mathbf{r_s},\omega)]\cdot\hat{\mathbf{n}}\,dS \qquad (1)$$

(Weglein et al., 2002, Equation 5). For all wavefield quantities in this abstract, e.g., $P(\mathbf{r_1},\mathbf{r_2},\omega)$, the leftmost spatial locator $\mathbf{r_1}$ represents the receiver coordinate and the rightmost $\mathbf{r_2}$ the source coordinate. $P(\mathbf{r},\mathbf{r_s},\omega)$ and $\nabla P(\mathbf{r},\mathbf{r_s},\omega)$ are the hydrophone measurement and its derivative, $P'_R(\mathbf{r'_g},\mathbf{r_s},\omega)$ is the receiver side deghosted wavefield, $G_0^+(\mathbf{r},\mathbf{r'_g},\omega)$ is the causal Green's function of the reference medium (chosen as water), and $\int_{m.s.} dS$ is an integration over the measurement surface. Note that the use of $\nabla P(\mathbf{r},\mathbf{r_s},\omega)\cdot\hat{\mathbf{n}}$ requires the availability of the field and its normal derivative on the measurement surface, which can be acquired from measurements using dual sensor cable or over/under cables, or derivation using the source wavelet and P on the measurement surface (Zhang, 2007, pp. 33-39). The former method allows deghosting for an arbitrary source distribution without needing to know the source and is the one we will use for the numerical tests in this abstract. The expression does not contain an integration along the source coordinates of the measured field. Hence, the Green's theorem receiver side deghosting only requires the data from a single shot experiment and can be applied independently to each shot gather.

Using arguments based on the reciprocity principle, a similar algorithm can be derived to address source side deghosting

$$P'_{SR}(\mathbf{r'_g},\mathbf{r'_s},\omega)=\int_{sources}[P'_R(\mathbf{r'_g},\mathbf{r},\omega)\nabla G_0^+(\mathbf{r},\mathbf{r'_s},\omega) - G_0^+(\mathbf{r},\mathbf{r'_s},\omega)\nabla P'_R(\mathbf{r'_g},\mathbf{r},\omega)]\cdot\hat{\mathbf{n}}\,dS. \qquad (2)$$

Here $\int_{sources} dS$ is an integration over the sources, P'_R is the receiver side deghosted data, and $\nabla P'_R\cdot\hat{\mathbf{n}}$ is its normal derivative over the sources. Our numerical testing uses over/under sources. However, this does not imply a need for two sources because following Zhang (2007) the second source line can be predicted using Green's theorem.

Further details behind the theory can be found in the companion paper by Mayhan et al. (2012).

1D ANALYTIC EXAMPLE

A simple 1D normal incidence analytic example can provide useful insights into the Green's theorem derived deghosting algorithm.

The causal whole space Green's function in the reference medium has the form

$$G_0(z,z'_g,\omega)=\frac{e^{ik|z-z'_g|}}{2ik}, \qquad (3)$$

and

$$P(z_g,z_s,\omega) = R\left[\frac{e^{ik(2z_{wb}-z_g-z_s)} - e^{ik(2z_{wb}-z_g+z_s)}}{2ik} + \frac{-e^{ik(2z_{wb}+z_g-z_s)} + e^{ik(2z_{wb}+z_g+z_s)}}{2ik}\right]. \quad (4)$$

represents the water-bottom reflected primary and its source, receiver, and source and receiver ghosts respectively. Here $k = \omega/c_0$ is the wave number, R is the water-bottom reflection coefficient, z_g is the receiver depth, z_s is the source depth, z_{wb} is the water-bottom depth, and we suppose the free surface is at depth 0 and the sources and receivers are placed between free surface and water bottom ($0 < z_s < z_g < z_{wb}$).

Substitute the Green's function G_0 and the wavefield P into Equation 1 to perform receiver side deghosting,

$$\begin{aligned} &P^{deghosted}_{receiver}(z'_g,z_s,\omega) \\ &= [P(z,z_s,\omega)\frac{dG_0^+(z,z'_g,\omega)}{dz} - G_0^+(z,z'_g,\omega)\frac{dP(z,z_s,\omega)}{dz}]|_{z=z_g} \\ &= R\left[\frac{e^{ik(2z_{wb}-z'_g-z_s)} - e^{ik(2z_{wb}-z'_g+z_s)}}{2ik}\right]. \end{aligned} \quad (5)$$

Here we assume $z'_g < z_g$, which means the predicted cable is shallower than the actual cable. The receiver side ghosts are removed and only the primary and its source side ghost remain in Equation 5. Further, we feed the receiver side deghosted data into Equation 2 for source side deghosting,

$$\begin{aligned} &P^{deghosted}(z'_g,z'_s,\omega) \\ &= [P^{deghosted}_{receiver}(z'_g,z,\omega)\frac{dG_0^+(z,z'_s,\omega)}{dz} \\ &\quad - G_0^+(z,z'_s,\omega)\frac{dP^{deghosted}_{receiver}(z'_g,z,\omega)}{dz}]|_{z=z_s} \\ &= \frac{Re^{ik(2z_w-z'_g-z'_s)}}{2ik}. \end{aligned} \quad (6)$$

Again we assume $z'_s < z_s$ (e.g., the predicted source is shallower than the actual source). The result of equation 6 is the water bottom reflected primary, without source, receiver, or source and receiver ghosts.

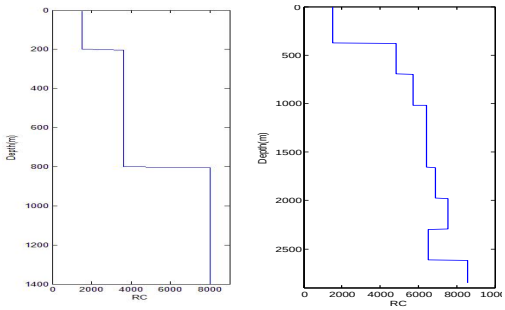

(a) Model one (b) Model two

Figure 1: Models for testing.

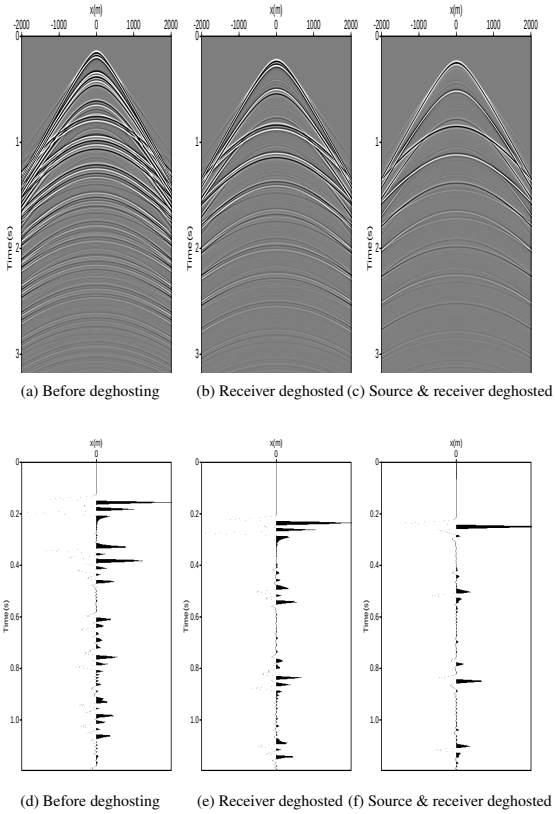

(a) Before deghosting (b) Receiver deghosted (c) Source & receiver deghosted

(d) Before deghosting (e) Receiver deghosted (f) Source & receiver deghosted

Figure 2: Deghosting for model one.

NUMERICAL TESTING

The code used to compute the results in this abstract is the receiver side deghosting code written by J. Mayhan and released in 2011 to the M-OSRP consortium. Changes were made to accommodate both receiver and source side deghosting. As mentioned above, we will use data with over/under sources and over/under receiver cables.

The first tested case (Figure 1a) is a three layer model with sources at 30m and 32m and receivers at 140m and 142m, such that the ghosts are not overlapping either with the corresponding primaries or among themselves. Figure 2b is the result after receiver side deghosting and Figure 2c is source and receiver side deghosting. Figures 2d, 2e, and 2f are the wiggle plots of the zero-offset traces. We can see the ghosts are mainly removed and the algorithm works with good accuracy.

The second tested case (Figure 1b) has 9 layers and is extracted from a velocity model provided by TOTAL. In this case, we choose the sources at 5m and 7m and receivers at 10m and 15m, so the events and their ghosts are overlapping. The data, its receiver side deghosted result, and both source and receiver side deghosted result are in Figures 3a, 3b, and 3c, respectively. Figures 3d, 3e, and 3f represent the wiggle plots of the zero-offset traces and Figures 3g, 3h and 3i are the spectrum plots of their wavelets. The notch at $c_0/(2d) = 1500/(2*12)hz = 62.5hz$ is removed after receiver side deghosting and

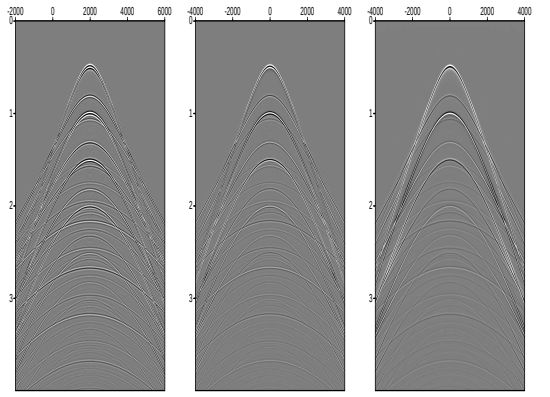

(a) Before deghosting (b) Receiver deghosted (c) Source & receiver deghosted

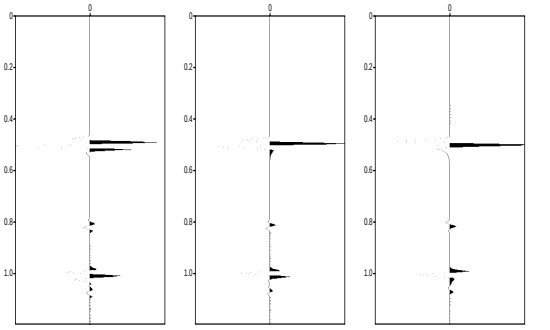

(d) Before deghosting (e) Receiver deghosted (f) Source & receiver deghosted

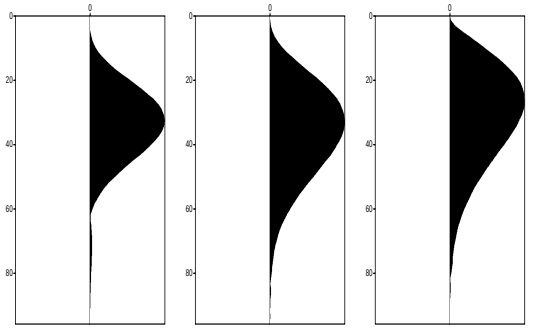

(g) Before deghosting (h) Receiver deghosted (i) Source & receiver deghosted

Figure 3: Deghosting for model two.

both receiver side deghosting and source side deghosting recover more low frequency information.

Results are positive and encouraging for both receiver side deghosting and source side deghosting when the data with dual sources and dual receiver cables are provided. Below we examine the consequences of two issues associated with the input data:

1. One issue is that in common practice, the derivative of the field (either through direct measurement or through dual cables) may not be available, especially on the source side. The industry trend has data with over/under streamers available today, and sometimes over/under sources, as well. However, Zhang (2007) uses Green's theorem to develop and exemplify a method that completely removes receiver and source ghosts with over/under streamers/receivers or with a single streamer and a source signature. The method does not require over/under sources. Another method that can be applied is based on the notion that the pressure field on the free surface D_{fs} is zero. This information can be used as another cable. Figure 4 shows the result when this property is used for model two. Comparing with the result using dual sources (Figures 3), the source ghosts are satisfactorily removed, although some high frequency information has been damaged. For low-frequency, this could be satisfactory.

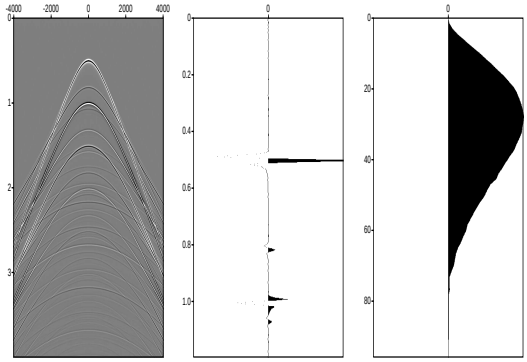

(a) Shot plot (b) Wiggle plot (c) Spectrum plot

Figure 4: Source deghosting using $D_{fs} = 0$ for model two.

2. Another issue is the sensitivity to how accurate the depth of the cable is known due to a division if over/under cables are used. The Green's theorem method is robust to depth sensitivity (Zhang, 2007). Figure 5 compares the results when different depth intervals are used for receiver deghosting. The ghosts are well removed and not visible after deghosting when the cable intervals are 2 meters, 5 meters, or 10 meters. When the interval gets to 20 meters, the ghosts are still largely attenuated (comparing with Figures 2a and 2d).

IMPACT ON FREE-SURFACE MULTIPLE ELIMINATION

ISS free-surface multiple elimination method has the theoretical capability of predicting the exact phase and amplitude of multiples if its pre-requisites (source and receiver deghosting in particular) are satisfied. Figure 6 shows the result of applying the deghosted data into ISS free-surface multiple elimination algorithm. The right half is generated by directly subtracting the prediction from the input without any adaptive subtraction tool. We can see that all free-surface multiples are well attenuated and primaries are not touched.

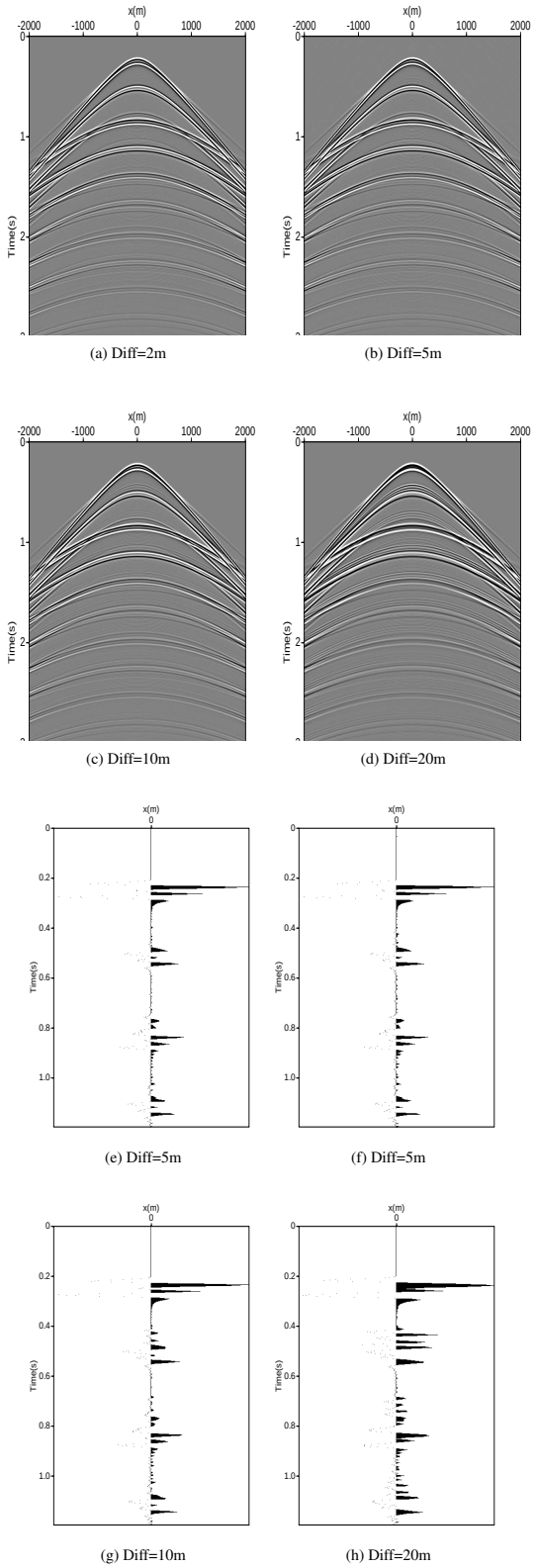

(a) Diff=2m (b) Diff=5m

(c) Diff=10m (d) Diff=20m

(e) Diff=5m (f) Diff=5m

(g) Diff=10m (h) Diff=20m

Figure 5: Compare different intervals between cables.

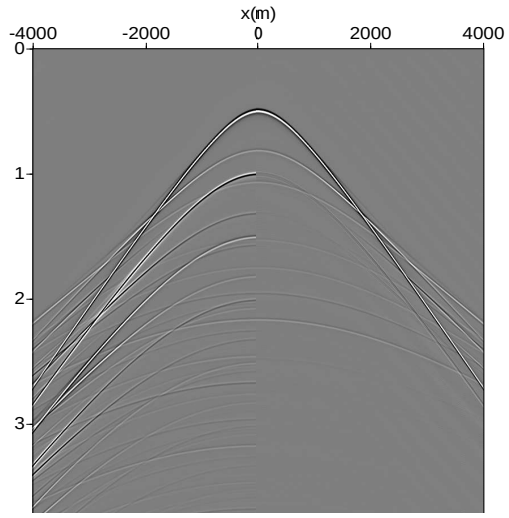

(a) (b)

Figure 6: ISS free-surface multiple elimination using deghosted data without adaptive subtraction for model two. (a) and (b) are the input (deghosted) and the output of the free-surface multiple elimination algorithm, respectively.

CONCLUSIONS

We tested Green's theorem derived source and receiver side deghosting algorithm using a 1D analytic example and two different sets of multi-offset 1D-earth synthetics with different source and receiver depth configurations. The complete source and receiver Green's theorem deghosting method (Zhang, 2007) exemplified in this paper requires either (1) a collection of shot records with over/under receivers or (2) a collection of shot records and the source signature. Over/under source lines are not needed. The companion paper Mayhan et al. (2012) complements the analysis and examples in this paper. Tests indicate that for most practical cases (less than 20 meters), the distance between over/under receiver cables would not be an issue. Green's theorem can predict the over/under source experiment required in Equation 2, without acquiring over/under source data. Alternatively, using the free surface can be a useful approach when the source depth is known. Tests of ISS free-surface multiple removal using the deghosted data confirms the good quality of the deghosted data. The results are positive and encouraging.

ACKNOWLEDGEMENTS

We thank the M-OSRP sponsors, NSFCMG award DMS-0327778 and DOE Basic Energy Sciences award DE-FG02-05ER15697 for their encouragement and support. The first author is grateful to: (1) Arthur B. Weglein, Christian Rivera, Jim Mayhan, Paolo Terenghi, Henri Houllevigue, and Wafik Beydoun for their mentoring, and (2) TOTAL for the internship opportunity and the permission to publish the results.

REFERENCES

Amundsen, L., B. G. Secrest, and B. Amtsen, 1995, Extraction of the normal component of the particle velocity from marine pressure data: Journal of Seismic Exploration, **14**, 51–62.

Mayhan, J. D., P. Terenghi, A. B. Weglein, and N. Chemingui, 2011, Greens theorem derived methods for preprocessing seismic data when the pressure p and its normal derivative are measured: 81st Annual International Meeting, SEG, Expanded Abstracts.

———, 2012, First use of greens theorem derived source side deghosting on deep water gulf of mexico synthetic and field data: 82st Annual International Meeting, SEG, Expanded Abstracts.

Schneider, W. A., K. L. Larner, J. P. Burg, and M. M.Backus, 1964, A new data processing technique for the elimination of ghost arrivals on reflection seismograms: Geophysics, **29**, 783805.

Weglein, A. B., S. A. Shaw, K. H. Matson, J. L. Sheiman, R. H. Solt, T. H. Tan, A. Osen, G. P. Correa, K. A. Innanen, Z. Guo, and J. Zhang, 2002, New approaches to deghosting towed-streamer and ocean-bottem pressure measurements: 72nd Annual International Meeting, SEG, Expanded Abstracts, 1016–1019.

Zhang, J., 2007, Wave theory based data preparation for inverse scattering multiple removal, depth imaging and parameter estimation: analysis and numerical tests of green's theorem deghosting theory: PhD thesis, University of Houston, Houston.

Zhang, J., and A. B. Weglein, 2005, Extinction theorem deghosting method using towed streamer pressure data: Analysis of the receiver array effect on deghosting and subsequent free surface multiple removal, *in* 75th Annual International Meeting, SEG, Expanded Abstracts: Society of Exploration Geophysicists, **24**, 2095–2100.

———, 2006, Application of extinction theorem deghosting method on ocean bottom data, *in* 76th Annual International Meeting, SEG, Expanded Abstracts: Society of Exploration Geophysicists, **25**, 2674–2678.

A new higher order Inverse Scattering Series (ISS) internal multiple attenuation algorithm addresses a limitation in the current leading order algorithm: derivation for a three-reflector model and a test with analytic data

Chao Ma, Hong Liang* and Arthur B. Weglein*, M-OSRP/Physics Dept./University of Houston**

SUMMARY

The Inverse Scattering Series (ISS) is a comprehensive framework for achieving seismic data processing goals without requiring subsurface information. Distinct isolated task-specific subseries can accomplish free surface multiple removal, internal multiple removal, depth imaging and inversion of primaries. The ISS can predict and eliminate internal multiples without a priori information. Although the leading order ISS internal multiple attenuation algorithm for the first order internal multiples has shown unmatched capability on complex synthetic and onshore data compared with other methods (e.g., Fu et al. (2010); Luo et al. (2011)), there are open issues to be addressed (e.g., Weglein et al. (2011)). For example, spurious events can be predicted from the first order attenuator (leading order prediction of the first order internal multiples) when there are both primaries and internal multiples in the input data. This paper and the companion and complementary paper (Liang et al., 2012) propose a new algorithm to directly respond to this issue. The new algorithm maintains the strength of the current algorithm and, in addition, can accommodate data consisting of both primaries and internal multiples.

INTRODUCTION

In seismic exploration, primaries are events that have experienced only one upward reflection while multiples are events that have experienced multiple upward reflections. Multiples are classified by the location of the downward reflection. Multiples that have at least one downward reflection at the free surface (air-water or air-land) are free surface multiples. Multiples that have experienced all their downward reflections below the free surface are internal multiples. The order of an internal multiple depends on the number of downward reflections it has experienced. For example, first order internal multiples have only one downward reflection (dashed line in Figure 1). The primaries-only assumption in seismic data analysis requires multiple removal. The methods for multiple removal are classified as separation and wavefield prediction (e.g.,Weglein (1999)). The separation methods sought a characteristic to distinguish primaries from multiples, while the early wavefield prediction methods first modeled and then subtracted multiples. Each of these approaches have earned their place in the seismic toolbox. However, as seismic exploration moves toward more complex areas, these methods have limitations due to their assumptions and the requirements for subsurface information. The ISS free surface multiple removal algorithm (Carvalho, 1992; Weglein et al., 1997) and internal multiple attenuation algorithm (Araújo, 1994; Weglein et al., 1997) start by avoiding the assumptions of the earlier methods, e.g., they are completely multi-D and have no requirements for subsurface information. There are both separation and wavefield prediction ingredients in the ISS multiple removal methods and they can be viewed as a next step in the development of separation and wavefield prediction methods (Weglein et al., 2011). For example, the ISS free surface multiple separation distinguishes the free surface multiples from other events by the downward reflection at the free surface. In contrast, the ISS internal multiple separation is realized without any a priori information by understanding the difference in the construction of primaries and internal multiples in the forward series. As an example, the leading order ISS prediction for the removal of the first order internal multiple calls upon a "lower-higher-lower"relationship in the pseudo-depth domain. It assumes only primaries as subevents to predict the first order internal multiples from all reflectors, at all depths at once, and without any subsurface information.

The leading order ISS internal multiple attenuation algorithm predicts the first order internal multiples combining primaries in the input data. However, the input data consists of primaries and internal multiples. Using the leading order algorithm with primaries and internal multiples as input data can lead to spurious prediction under circumstances where there are three or more reflectors generating significant internal multiples. While we recognize the shortcomings of the current leading order ISS internal multiple attenuation algorithm, we also recognize that addressing them resides in the ISS (Weglein et al., 2011). In this paper, we show how higher order ISS terms address and eliminate that shortcoming while retaining the strength of the leading order algorithm. Each term in the subseries achieves what the order of that term enables it to achieve. For example, it requires an infinite series (in a closed form) to completely eliminate all first order internal multiples generated at the shallowest reflector when the properties at and above that reflector are unknown (Ramírez and Weglein, 2005). Similarly, the internal multiple attenuation task is more difficult when the input data contains internal multiples as well as primaries, so the leading order ISS internal multiple attenuation algorithm needs to combine with higher order terms to address spurious prediction. In this paper, we provide an understanding of the leading order prediction of the first order internal multiples when the input data consists of both primaries and internal multiples. We also provide a new ISS internal multiple attenuation algorithm to address a particular type of spurious event that is predicted when the middle subevent in the first order attenuator is an internal multiple.

A new higher order ISS internal multiple attenuation algorithm

AN OVERVIEW OF THE ISS LEADING ORDER INTERNAL MULTIPLE ATTENUATION ALGORITHM

The leading order contribution to constructing a class of multiples in the forward series suggests the leading order contribution for their removal in the inverse series (Weglein et al., 2003). A subseries that focuses on internal multiple removal can be isolated from the inverse series. The ISS internal multiple attenuation algorithm starts with the input data, $D(k_g,k_s,\omega)$, which is the Fourier transform of the deghosted prestack data, with the wavelet deconvolved and the free surface multiples removed. The leading order prediction of the first order internal multiples makes the leading term contribution to their removal. In a $2D$ earth, the leading order contribution is,

$$b_3(k_g,k_s,\omega) = \frac{1}{(2\pi)^2}\int_{-\infty}^{\infty} dk_1 \int_{-\infty}^{\infty} dk_2 e^{-iq_1(z_g-z_s)} e^{iq_2(z_g-z_s)} \times \int_{-\infty}^{\infty} dz_1 b_1(k_g,k_1,z_1) e^{i(q_g+q_1)z_1} \times \int_{-\infty}^{z_1-\varepsilon} dz_2 b_1(k_1,k_2,z_2) e^{-i(q_1+q_2)z_2} \times \int_{z_2+\varepsilon}^{\infty} dz_3 b_1(k_2,k_s,z_3) e^{i(q_2+q_s)z_3}, \quad (1)$$

where ω is temporal frequency, k_s and k_g are the horizontal wavenumbers for the source and receiver coordinates, respectively; q_g and q_s are the vertical source and receiver wavenumbers defined by $q_i = sgn(\omega)\sqrt{\frac{\omega^2}{c_0^2}-k_i^2}$ for $i = (g,s)$; z_s and z_g are source and receiver depths; and z_j $(j = 1,2,3)$ represents the pseudo-depth using reference velocity migration. The quantity $b_1(k_g,k_s,z)$ corresponds to an uncollapsed migration (Weglein et al., 1997) of effective plane-wave incident data, and $b_1(k_g,k_s,q_g+q_s) = -2iq_sD(k_g,k_s,\omega)$.

With the input data and the leading order prediction of the first order internal multiples, we can obtain the data with the first order internal multiples attenuated, given by

$$D(k_g,k_s,\omega) + D_3(k_g,k_s,\omega), \quad (2)$$

where $D_3(k_g,k_s,\omega) = (-2iq_s)^{-1}b_3(k_g,k_s,q_g+q_s)$.

For a $1D$ earth and a normal incident plane wave, equation 1 reduces to

$$b_3(k) = \int_{-\infty}^{\infty} dz_1 e^{ikz_1} b_1(z_1) \int_{-\infty}^{z_1-\varepsilon} dz_2 e^{-ikz_2} b_1(z_2) \times \int_{z_2+\varepsilon}^{\infty} dz_3 e^{ikz_3} b_1(z_3). \quad (3)$$

The leading order ISS internal multiple attenuation algorithm for the first order internal multiples of a $1D$ earth and an impulsive incident plane wave is

$$b_1 + b_3. \quad (4)$$

Note that the $(-2iq_s)$ factor is not needed here. However, for an incident Green's function, the output of the ISS leading order removal of the first order internal multiples needs the $(-2iq_s)$ factor to take b to D as in equation 2.

The portion of the third term of the ISS that predicts the first order internal multiple attenuation is isolated by requiring the "lower(A)-higher(B)-lower(C)"relationship in pseudo-depth domain as shown in Figure 1. The assumption behind the first order internal multiple prediction in Figure 1 is that all subevents have to be primaries for the prediction to be an internal multiple. There are circumtances, shown in the next section, where the "lower-higher-lower"template would produce spurious events when one of the subevents is an internal multiple. However, these spurious events are fully anticipated and attenuated by other higher order terms in the inverse series.

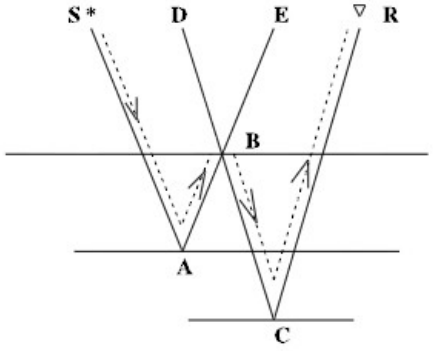

Figure 1: Combination of subevents for the first order internal multiple (dashed line), $(SABE)_{time} + (DBCR)_{time} - (DBE)_{time} = (SABCR)_{time}$, figure adapted from Weglein et al. (2003). The capitalized letters stand for a primary or an internal multiple.

A NEW ISS INTERNAL MULTIPLE ATTENUATION ALGORITHM TO ATTENUATE THE SPURIOUS EVENTS ARISING IN A THREE-REFLECTOR MODEL

We examine the prediction of the first order internal multiple attenuator using input data that consist of three primaries and an internal multiple associated with the first two reflectors in a three reflector model (see Figure 2).

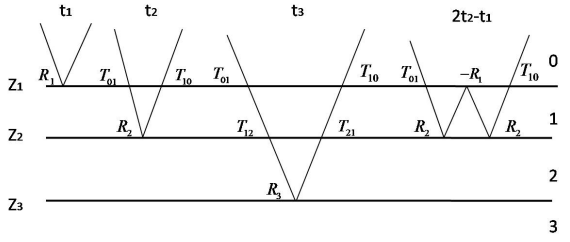

Figure 2: Three primaries and one internal multiple in a three-reflector model.

A new higher order ISS internal multiple attenuation algorithm

For an impulsive incident wave $\delta(t-\frac{z}{c})$ the data is

$$D(t)=R_1\delta(t-t_1)+R_2'\delta(t-t_2)+R_3'\delta(t-t_3)+R_4'\delta(t-(2t_2-t_1)), \tag{5}$$

where $R_2'=T_{01}R_2T_{10}$, $R_3'=T_{01}T_{12}R_3T_{21}T_{10}$, $R_4'=T_{01}R_2(-R_1)R_2T_{10}$, and t_i, R_i are two way times and reflection coefficients from the ith reflector, respectively. T_{ij} is the transmission coefficient between the ith and jth reflector.

Given this data, we find from equation 3 that

$$\begin{aligned}
&b_3(t)= \\
&R_1(R_2')^2\delta(t-(2t_2-t_1))+2R_1R_2'R_3'\delta(t-(t_2+t_3-t_1)) \\
&+R_1(R_3')^2\delta(t-(2t_3-t_1))+R_2(R_3')^2\delta(t-(2t_3-t_2)) \\
&+2R_1R_2'R_4'\delta(t-(3t_3-2t_1))+R_2'(R_4')^2\delta(t-(3t_3-2t_2)) \\
&+2R_1R_3'R_4'\delta(t-(t_3+2t_2-2t_1))+R_1(R_4')^2\delta(t-(4t_2-3t_1)) \\
&+2R_2'R_3'R_4'\delta(t-(t_3+t_2-t_1))+(R_3')^2R_4'\delta(t-(2t_3-(2t_2-t_1))).
\end{aligned} \tag{6}$$

We have assumed $t_3>2t_2-t_1$ in deriving equation 6. In addition to the four first order internal multiples (first two rows in equation 6), the first order attenuator, b_3, predicts some additional events due to the internal multiple in the input. Analysis of the traveltimes of these additional events shows that each of them corresponds to an internal multiple of higher order with the exception of the last event $(R_3')^2R_4'\delta(t-(2t_3-(2t_2-t_1)))$, which is a spurious event prediction.

Properties of the first order attenuator when both primaries and internal multiples are input and act as subevents

When there are internal multiples in the data, there will be many other possible subevent combinations in the first order internal multiple attenuator, b_3. When

$$b_1=P+I,$$

it follows from equation 3 that

$$\begin{aligned}
b_3&=b_1*b_1*b_1 \\
&=(P+I)(P+I)(P+I) \\
&=PPP+PPI+PIP+IPP+PII+IPI+IIP+III.
\end{aligned}$$

where $*$ stands for the nonlinear interaction between the data. P stands for primaries, and I stands for internal multiples. In addition to the primary only subevent combination, that is PPP, there are subevent combinations involved with the internal multiple that produce the spurious event. A more detailed analysis shows that the spurious event, $(R_3')^2R_4'\delta(t-(2t_3-(2t_2-t_1)))$, in equation 6 results from PIP as shown in Figure 3 .

We use a diagram to illustrate the generation of the spurious event by PIP subevent combination. The diagram for the PIP subevent is shown in the left side in Figure 4 which satisfies the "lower-higher-lower"relationship, as required by the algorithm. Following the logic of predicting internal multiples by the "lower-higher-lower"pattern of three primary subevents, the PIP diagram will split into a "lower-higher-much higher-lower-much lower"configuration

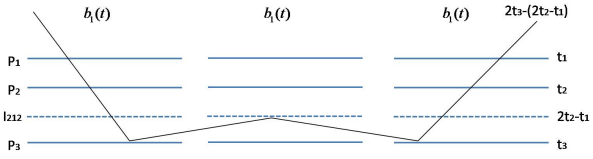

Figure 3: An analogous *W-like* configuration to produce the spurious event using the internal multiple as a subevent.

on the right side of Figure 4. The resulting configuration does not agree with the double *W-like* configuration which constructs second order internal multiples using five primary subevents. The pseudo-depth of the two outermost P should

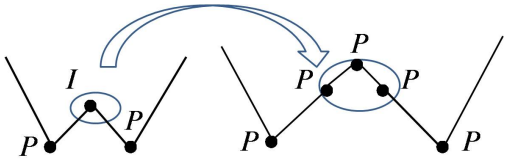

Figure 4: Separation for PIP into *W-like*

be deeper than the effective pseudo-depth of the middle I to allow the PIP spurious events to happen, see Figure 3. In other words, the PIP spurious events can exist in a medium which has three or more reflectors. That explains the fact that there are no spurious events produced in a two-reflector example in Zhang and Shaw (2010) even though an internal multiple is included in their data.

When the internal multiple in PPI or IPP is separated into three "lower-higher-lower"primary subevents, it leads to a double *W-like* configuration which will predict the second order internal multiple as shown in Figure 5. This also explains the additional higher order internal multiple predictions in b_3 from our analytic example. It can be shown that there are circumstances where PPI produces spurious events in a medium which has more than three reflectors (Liang et al., 2012).

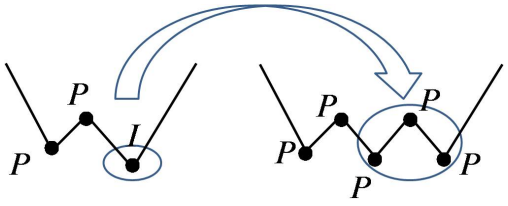

Figure 5: One possible separation for PPI into double *W-like*

Terms like IIP or III may also produce spurious events. However, when compared with PIP, these terms can often be ignored in practice. Removal of the latter spurious events also resides in the higher order ISS terms, and beyond those considered and included in this paper.

A new ISS contribution to attenuate the *PIP* spurious event

To remove the spurious events produced by the first order attenuator when using an internal multiple as a subevent in the middle integral, a new and higher order ISS term, which has that capability, is combined with the current leading order algorithm.

Figure 4 shows the geometric relationship used to locate the ISS contribution towards the attenuation of the first order internal multiples that also accommodates an internal multiple in the second integral. In this paper, we examine a term, $G_0V_1G_0V_3G_0V_1G_0$, that fits that geometry and performs that function. That term in $1D$ is

$$b_5^{PIP} = \int_{-\infty}^{\infty} dz_1 e^{ikz_1} b_1(z_1) \int_{-\infty}^{z_1-\varepsilon} dz_2 e^{-ikz_2} b_3(z_2) \times \int_{z_2+\varepsilon}^{\infty} dz_3 e^{ikz_3} b_1(z_3), \quad (7)$$

where $b_1(z)$ is an uncollapsed migration and $b_3(z)$ is the first order attenuator. Compared with equation 3, this equation also requires the "lower-higher-lower"relationship, but the middle b_1 becomes b_3 to obtain a prediction of the spurious event and accommodating the internal multiple subevent.

Equation 7 and equation 3 together provide a new ISS intenral multiple attenuation algorithm for a $1D$ earth,

$$\begin{aligned} & b_1 + b_3^{PPP} + b_5^{PIP} \\ =& b_1 + \int_{-\infty}^{\infty} dz_1 e^{ikz_1} b_1(z_1) \int_{-\infty}^{z_1-\varepsilon} dz_2 e^{-ikz_2} (b_1(z_2) + b_3(z_2)) \\ & \times \int_{z_2+\varepsilon}^{\infty} dz_3 e^{ikz_3} b_1(z_3), \end{aligned} \quad (8)$$

where $b_3^{PPP} = b_3$. The superscript indicates the subevent combination that the algorithm can accommodate. Compared with the original algorithm (equation 4), the new algorithm includes a portion of higher order term (b_5^{PIP}) to attenuate the *PIP* spurious events predicted by b_3^{PPP} when internal multiples are in the data.

We use the same analytic example to test the new algorithm. Substituting $D(t)$ in equation 5 and b_3 in equation 6 into equation 7 produces

$$\begin{aligned} b_5^{PIP} =& R_1(R_2')^2(R_3')^2\delta(t-(2t_3-(2t_2-t_1))) \\ & + (2R_1R_2'R_4'(R_3')^2 + R_2'(R_4')^2(R_3')^2)\delta(t-(2t_3-(3t_2-2t_1))) \\ & + R_1(R_4')^2(R_3')^2\delta(t-(2t_3-(4t_2-3t_1))). \end{aligned} \quad (9)$$

The first term is the prediction of the spurious event. Substitution of $R_2' = T_{01}R_2T_{10}$ leads to

$$(T_{01}T_{10})^2R_1(R_2)^2(R_3')^2\delta(t-(2t_3-(2t_2-t_1))).$$

The last term $(R_3')^2R_4'\delta(t-(2t_3-(2t_2-t_1)))$ in equation 6 is the spurious event. Substitution of $R_4' = T_{01}R_2(-R_1)R_2T_{10}$ leads to

$$(-T_{01}T_{10})R_1(R_2)^2(R_3')^2\delta(t-(2t_3-(2t_2-t_1))).$$

When added to b_3, the first term in equation 9 will effectively attenuate the spurious event.

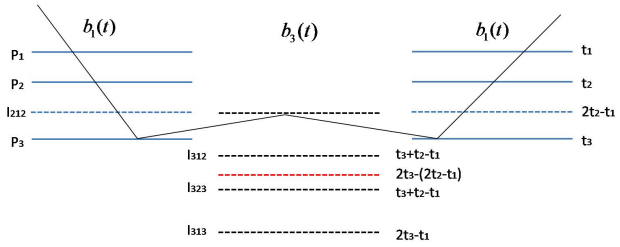

Figure 6: Illustration of the spurious event prediction in b_5^{PIP}. Notice the middle b_3 produces predicted internal multiples which have the opposite sign of the actual internal multiples. Only the first order predicted internal multiples (black dashed line) and spurious event (red dashed line) are shown.

It is the geometric similarity (single *W-like*) between b_5^{PIP} and b_3 that enables b_5^{PIP} to contribute to removing the spurious events produced in b_3 (see Figure 4). We note that each term in the inverse series does what the order of that term is capable of performing. Different portions of a given order term in the ISS can contribute to different tasks. For example, in our case, although both the leading order prediction of the second order internal multiples b_5 (right side in Figure 5) and b_5^{PIP} (right side in Figure 4) come from the fifth order term in the inverse series, they have different tasks determined by their different geometries. b_5^{PIP} has a single *W-like* geometry that is capable of attenuating the spurious events from b_3 while b_5 has a double *W-like* geometry which is capable of predicting second order internal multiples using primaries. Both are contained in the fifth order term in the ISS.

DISCUSSION AND CONCLUSION

In this paper, we provide both: (1) an algorithm to address certain significant spurious events observed in Fu et al. (2010) and Luo et al. (2011) and (2) a template for locating ISS terms addressing the more general spurious events that can arise from using a leading order internal multiple attenuation algorithm on a complex media and complex data. The ISS can remove all internal multiples without subsurface information and also remove spurious events that arise from using a complex data in a leading order algorithm. We exemplify that capability in this and the companion and complementary paper by Liang et al. (2012). To conclude, the new algorithm in this paper retains the strength of the original leading order algorithm while addressing a limitation in the latter and provides an initial extention to accommodate data consisting of both primaries and internal multiples.

ACKNOWLEDGMENTS

We thank M-OSRP sponsors for their support of this research. The authors would like to thank Wilberth Herrera, Jim Mayhan, and Paolo Terenghi for useful discussions.

REFERENCES

Araújo, F. V., 1994, Linear and non-linear methods derived from scattering theory: backscattered tomography and internal multiple attenuation: PhD thesis, Universidade Federal da Bahia.

Carvalho, P. M., 1992, Free-surface multiple reflection elimination method based on nonlinear inversion of seismic data: PhD thesis, Universidade Federal da Bahia.

Fu, Q., Y. Luo, P. Kelamix, S. Huo, G. Sindi, S.-Y. Hsu, and A. B. Weglein, 2010, The inverse scattering series approach towards the elimination of land internal multiples: SEG Expanded Abstracts, 3456–3461.

Liang, H., C. Ma, and A. Weglein, 2012, A new iss internal multiple attenuation algorithm addressing a shortcoming of the current leading-order iss algorithm for removing first order internal multiples: derivation and testing of the algorithm for arbitrary number of reflectors: To be submitted to the SEG Expanded Abstracts.

Luo, Y., P. G. Kelamis, Q. Fu, S. Huo, G. Sindi, S.-Y. Hsu, and A. B. Weglein, 2011, Elimination of land internal multiples based on the inverse scattering series: The Leading Edge, 884–889.

Ramírez, A. C., and A. Weglein, 2005, An inverse scattering internal multiple elimination method: Beyond attenuation, a new algorithm and initial tests: SEG Expanded Abstracts., 2115–2118.

Weglein, A. B., 1999, Multiple attenuation: an overview of recent advances and the road ahead (1999): The Leading Edge, 40–44.

Weglein, A. B., F. V. Araújo, P. M. Carvalho, R. H. Stolt, K. H. Matson, R. T. Coates, D. Corrigan, D. J. Foster, S. A. Shaw, and H. Zhang, 2003, Inverse scattering series and seismic exploration: Inverse Problems, R27–R83.

Weglein, A. B., F. A. Gasparotto, P. M. Carvalho, and R. H. Stolt, 1997, An inverse-scattering series method for attenuating multiples in seismic reflection data: Geophysics, **62**, 1975–1989.

Weglein, A. B., S.-Y. Hsu, P. Terenghi, X. Li, and R. H. Stolt, 2011, Multiple attenuation: Recent advances and the road ahead (2011): The Leading Edge, 864–875.

Zhang, H., and S. Shaw, 2010, analytic analysis of higher order internal multiples predicted via the inverse scattering series based algorithe: SEG Expanded Abstracts, **29**, 3493–3498.

A new ISS internal multiple attenuation algorithm addressing a shortcoming of the current leading-order ISS algorithm for removing first order internal multiples: derivation and testing of the algorithm for arbitrary number of reflectors

Hong Liang, Chao Ma and Arthur B. Weglein, M-OSRP/Physics Dept./University of Houston*

SUMMARY

Multiple removal is a prerequisite for depth imaging and target identification. The inverse scattering series (ISS) predicts and removes internal multiples directly and without any subsurface information. This is achieved through a task-specific subseries within the overall ISS. The ISS leading order attenuator is the leading order term of the subseries contributing to the removal of first order internal multiples. The idea behind the leading order attenuator is that the time of the first order internal multiples can be predicted from primaries in the data that act as subevents of the first order internal multiples. However, the entire data consisting of primaries and internal multiples enters the algorithm. When internal multiples in the data themselves act as subevents, the leading order attenuator produces not only first order internal multiples, but also higher order internal multiples and at times spurious events which have been observed in the tests of Fu et al. (2010) and Luo et al. (2011). Weglein et al. (2011) has also pointed this out and suggested that the resolution of the problem would reside in other terms of the ISS. Within the framework of ISS, each term of a task-specific subseries only performs a certain specific task. The ISS leading order attenuator has shown stand-alone capabilities for removing internal multiples. This paper shows that the removal of the spurious events arising from the leading order attenuation algorithm is performed by other higher order terms. Hence, a shortcoming of the current leading order internal multiple algorithm is anticipated and addressed in later terms in the ISS. The resulting new ISS internal multiple algorithm presented in this abstract retains the strengths of the current algorithm while avoiding a serious shortcoming.

INTRODUCTION

The inverse scattering series can achieve all processing objectives directly and without subsurface information. Compared to the ISS free-surface multiple removal methods where the location and the properties of the free surface responsible for free-surface multiples are well-defined, the ISS internal multiple method does not require information concerning the properties of the Earth where internal multiples have experienced a shallowest downward reflection. It is data-driven and predicts internal multiples at all depths at once.

The ISS internal multiple attenuation algorithm was first proposed by Araújo et al. (1994) and Weglein et al. (1997). This algorithm does not depend on the earth model type (Weglein et al., 2003) and is applicable for towed-streamer field data, land data, and ocean bottom data (Matson and Weglein, 1996; Matson, 1997) and can accommodate internal multiples with converted wave phases (Coates and Weglein, 1996). Ramírez and Weglein (2005) extended the attenuation algorithm towards an elimination method. The ISS internal multiple algorithm has shown encouraging results and differential added value when compared to all other internal multiple methods (Fu et al., 2010; Hsu et al., 2011; Terenghi et al., 2011; Weglein et al., 2011; Luo et al., 2011).

The ISS internal multiple method operates without a priori information and its tasks are more complex than the ISS free-surface multiple method. Early analysis of the ISS leading order attenuator focused on using only primary subevents to predict internal multiples. However, the input data contains both primaries and internal multiples and all events in the data will be treated as subevents. Under some circumstances treating internal multiples as subevents in the first order internal multiple algorithm can lead to spurious events. We define the conditions when that can occur and how terms further in the ISS address and remove those spurious events. Following the suggestion of Weglein et al. (2011) the companion paper Ma et al. (2012) derives the new ISS internal multiple algorithm addressing the shortcomings arising from the second of the three integrals of the ISS leading order attenuator in a three-reflector medium. This paper evaluates that algorithm using numerical examples, and also extends the algorithm to a medium with an arbitrary number of reflectors.

THE LEADING-ORDER ISS INTERNAL MULTIPLE ATTENUATION ALGORITHM

The ISS internal multiple attenuation algorithm is a subseries of the inverse scattering series. The first term in the algorithm is the deghosted input data D with the reference wavefield and free-surface multiples removed. The second term in the algorithm is the leading order attenuator which attenuates first order internal multiples (the order of an internal multiple is defined by the total number of downward reflections). The leading order attenuator in a 2D earth is given by Araújo et al. (1994) and Weglein et al. (1997) (see equation 37). For a 1D earth and a normal incidence wave the equation reduces to

$$b_3^{PPP}(k) = b_3(k) = \int_{-\infty}^{\infty} dz_1 e^{ikz_1} b_1(z_1) \int_{-\infty}^{z_1-\varepsilon} dz_2 e^{-ikz_2} b_1(z_2) \int_{z_2+\varepsilon}^{\infty} dz_3 e^{ikz_3} b_1(z_3), \quad (1)$$

where the deghosted data , $D(t)$, for an incident spike wave, satisfies $D(\omega) = b_1(2\omega/c_0)$, $b_1(z) = \int_{-\infty}^{\infty} e^{-ikz} b(k) dk$, $k = 2\omega/c_0$ is the vertical wavenumber, c_0 is a reference velocity, and $b_1(z)$ corresponds to an uncollapsed FK migration of an incident plane-wave data. For non-spike data, there is an obliquity factor in the relations between the data D and b_1 in the frequency domain (see Page R64 and R65 in Weglein

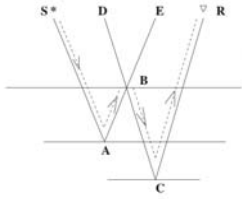

Figure 1: An internal multiple (dashed line) constructed by the "lower-higher-lower" pattern of three primary subevents (solid line). Figure adapted from Weglein et al. (2003).

et al. (2003)) Here, we introduce a new notation b_3^{PPP} where the superscript ("p" represents primary) indicates which events in the data input in each of the three integrals that the algorithm can accommodate towards the overall purpose of removing first order internal multiples. The data with first order internal multiples attenuated is

$$D(t)+D_3(t), \tag{2}$$

where $D_3(t)$ is the inverse Fourier transform of $D_3(\omega)$ and $D_3(\omega)=b_3(k)$ for an incident spike wave. Weglein and Matson (1998) showed that this algorithm can be interpreted using the subevent concept (see Figure 1).

THE GENERAL OUTPUT OF THE LEADING ORDER ATTENUATOR WHEN AN INTERNAL MULTIPLE IS TREATED AS A SUBEVENT

Early analysis focused exclusively on predicting the internal multiples using primaries as subevents. However, seismic data contains not only primary events but also internal multiples. Zhang and Shaw (2010) have shown that higher order internal multiples can be predicted by the leading order attenuator using internal multiples as subevents in a two-interface example. However, the situation is considerably more complicated when the data from three or more reflectors are considered. In the latter case, spurious events can be predicted whose traveltimes do not correspond to an event in the data. In this section, we illustrate the specific conditions under which the spurious events are produced by the leading order attenuator using one internal multiple subevent in a 1D earth.

An internal multiple subevent in the second integral

In the companion paper (Ma et al., 2012) it is shown that in a medium with three reflectors, and when an internal multiple acts as a subevent in the second of the three integrals (see equation 1) a spurious event can be produced. In this section, we interpret this diagrammatically using Figure 2 (pseudo-depth is determined by the water speed image, $b_1(z)$). An internal multiple has each of its downward reflections between two upward reflections. Then, in the diagrammatic representation of an internal multiple (Figure 2(a)) a higher red circle with a "-" sign should have lower blue circles with "+" signs on both side. However, in Figure 2(c) each of the two red circles has only one lower blue circle on one side, and one higher blue circle on the other side. Thus, this predicted event is neither an internal multiple, nor a primary.

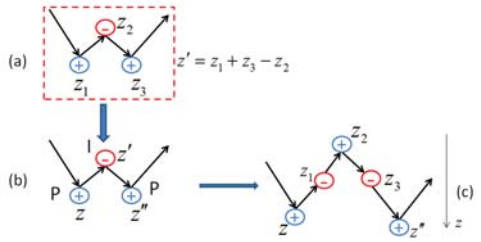

Figure 2: Diagrammatic illustration of the generation of a spurious event. (a) The diagram of a first order internal multiple. The sign "+" ("-") means upward (downward) reflection or the pseudo-depth is added (subtracted). (b) Three subevents used by the leading order attenuator: a primary ("P") with pseudo-depth z, an internal multiple ("I") with pseudo-depth z', and a primary with pseudo-depth z'', with $z' < z, z''$. (c) The generated spurious event with pseudo-depth $(z+z''-(z_1+z_3-z_2))$.

The spurious event described here is generated by the leading order attenuator using an internal multiple subevent in the second integral. The way it is generated suggests the way it can be removed. For the removal of this type of spurious events, substituting b_3 for the second b_1 in equation 1 leads to equation 3. The subevent combination of "primary–predicted internal multiple–primary" in equation 3 can be used to attenuate the spurious event. In this paper, we examine one of the fifth order terms ($G_0V_1G_0V_3G_0V_1G_0$) that satisfies the required Figure 2(c) geometry . The derivation and analytical examples are shown in Ma et al. (2012).

$$b_5^{PIP}(k)=\int_{-\infty}^{\infty}dz_1e^{ikz_1}b_1(z_1)\int_{-\infty}^{z_1-\varepsilon}dz_2e^{-ikz_2}b_3(z_2)\int_{z_2+\varepsilon}^{\infty}dz_3e^{ikz_3}b_1(z_3) \tag{3}$$

The output of the new ISS internal multiple algorithm for this three reflectors case is

$$D(t)+D_3(t)+D_5^{PIP}(t), \tag{4}$$

where $D_5^{PIP}(t)$ is the inverse Fourier transform of $D_5^{PIP}(\omega)$ and $D_5^{PIP}(\omega)=b_5^{PIP}(k)$ for spike data. The original algorithm (see equation 2) attenuates the first order internal multiples and preserve primaries but can also output spurious events. The new algorithm in equation 4 provides the benefit of the original algorithm while addressing issues due to spurious events.

An internal multiple subevent in either of the outer integrals

The problem is yet more complicated when a first order internal multiple subevent is in either of the outer integrals. As shown in the left panel of Figure 3, when an internal multiple with pseudo-depth z'' is in the rightmost integral ($z, z'' > z'$),

and since $z'' = (z_1 + z_3 - z_2) > z'$, there are several possible relations between z_1, z_2, z_3 and z', which are as follows:

- As shown by the first arrow in Figure 3, when $z_1 > z', z_2 \neq z$ and $z_3 \neq z'$, the predicted event has the same pseudo-depth as a second order internal multiple. Its subevent construction is shown in Figure 4(a), and this occurs in a medium with number of reflectors $N \geq 2$.
- The second arrow in Figure 3 shows that when $z_1 = z'$, the predicted event has the same pseudo-depth as a first order internal multiple. Figure 4(b) describes its subevent construction, which only happens in a medium with $N \geq 3$.
- The third arrow in Figure 3 shows that a spurious event is produced with $z_1 < z'$ and $z_3 < z'$ (the red circle at z' has only one lower blue circle on one side). Its subevent construction is illustrated by Figure 4(c). This type of spurious event can only be generated in a medium with $N \geq 4$.

Using the same logic and analysis as the previous section, we propose another method to address this type of spurious events by replacing the third b_1 in equation 1 with b_3, and the new term is shown in equation 5. Since this type of spurious event could be produced by the leading order attenuator using a first order internal multiple subevent in either of the outer integrals (these two cases are equivalent), there is a leading coefficient 2 in the equation 5. This term is also identified from a portion of the fifth order term in the ISS (from the term $G_0V_1G_0V_1G_0V_3G_0$).

$$b_5^{PPI}(k) = 2\int_{-\infty}^{\infty} dz_1 e^{ikz_1} b_1(z_1) \int_{-\infty}^{z_1-\varepsilon} dz_2 e^{-ikz_2} b_1(z_2) \int_{z_2+\varepsilon}^{\infty} dz_3 e^{ikz_3} b_3(z_3) \quad (5)$$

The new ISS internal multiple algorithm for this case with more than three reflectors is

$$D_1(t) + D_3(t) + D_5^{PIP}(t) + D_5^{PPI}(t). \quad (6)$$

where $D_5^{PPI}(t)$ is the Fourier transform of $D_5^{PPI}(\omega)$ and $D_5^{PPI}(\omega) = b_5^{PIP}(k)$ for an incident spike wave. This new general algorithm in equation 6 retains the strengths of the original algorithm while addressing issues due to spurious events.

NUMERICAL EXAMPLES

In this section, we will compute and analyze the new terms for one dimensional, three reflector models. The spurious event would be produced when the internal multiple subevent is in the second of the three integrals. Thus, only the term in equation 3 will be tested in this section.

Numerical tests using analytic data

For a 1D three-interface model the reflection data due to an impulsive incident wave $\delta(t - \frac{z}{c})$ is

$$D(t) = R_1\delta(t-t_1) + T_{01}R_2T_{10}\delta(t-t_2) + T_{01}T_{12}R_3T_{21}T_{10}\delta(t-t_3) - T_{01}R_2^2R_1T_{10}\delta(t-(2t_2-t_1))\ldots, \quad (7)$$

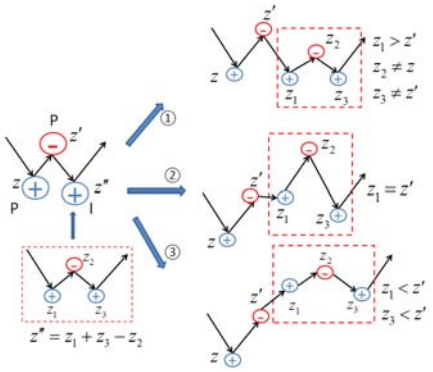

Figure 3: Diagrammatic illustration of predicted events when an internal multiple subevent is in either of the outer integrals.

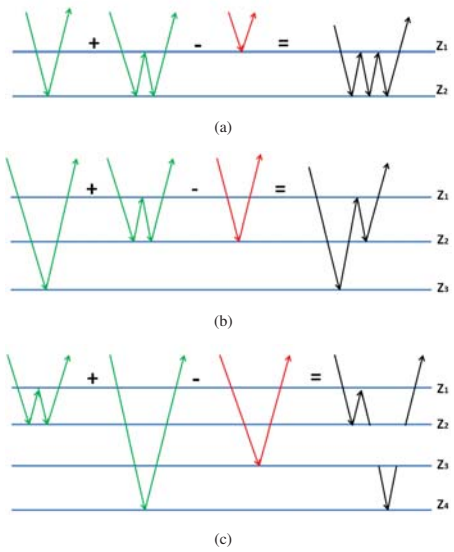

Figure 4: Events generated by the leading order attenuator using an internal multiple subevent in either of the outer integrals: (a) a second order internal multiple, (b) a first order internal multiple, and (c) a spurious event, $2z_2 - z_1 > z_3$.

where $t_1 = 0.4s$, $t_2 = 0.5s$, and $t_3 = 1.0s$ are two way times. The velocities in each layer are $c_0 = 1500m/s$, $c_1 = 2500m/s$, $c_2 = 4000m/s$, and $c_3 = 6000m/s$. Densities are constant. R_i and T_{ij} are reflection and transmission coefficients, respectively. We choose the data so that it contains only primaries and first order internal multiples. The data is first transformed to the frequency domain $D(\omega)$ (Weglein et al., 2003) and then we can get

$$b_1(k) = D(\omega) = R_1e^{ikz_1} + T_{01}R_2T_{10}e^{ikz_2} + T_{01}T_{12}R_3T_{21}T_{10}e^{ikz_3} - T_{01}R_2^2R_1T_{10}e^{ik(2z_2-z_1)}\ldots, \quad (8)$$

where the pseudo-depth z_i is defined as $z_i = c_0t_i/2$. From equation 8 we can calculate $b_1(z)$, which is then inputted to equation 1 to calculate b_3. Both b_1 and b_3 are used by equation 3 to calculate b_5^{PIP}.

Figure 5(a) shows the data consisting of primaries (P_i) and first

order internal multiples (I_{ijk}). Figure 5(b) shows the events predicted by b_3, where the spurious event is at time $1.4s$ and has negative polarity. The spurious event is produced by the subevents combination of "P_3–I_{212}–P_3". Figure 5(c) shows the events predicted by b_5^{PIP}, where the predicted spurious event is produced by the subevents combination of "P_3–predicted I_{212}–P_3" and has positive amplitude. If we add the the result in Figure 5(c) to that in Figure 5(b), the amplitude of the remaining spurious event would be significantly attenuated.

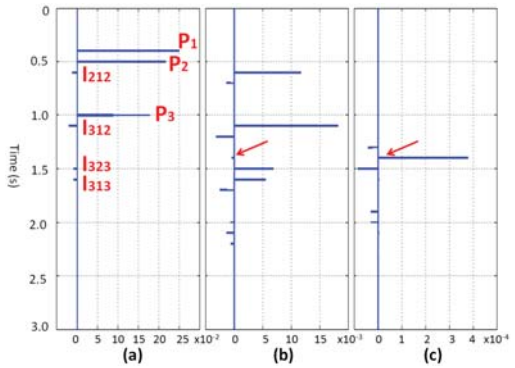

Figure 5: (a) Input data. (b) Events predicted by b_3 including predicted internal multiples and the spurious event (pointed by the red arrow and amplitude is -3.9331×10^{-4}). (c) Events predicted by b_5^{PIP} where the predicted spurious event is pointed by the red arrow and its amplitude is 3.7832×10^{-4}).

It should be noted that in Figure 5(b) the internal multiple I_{323} predicted by b_3 is composed of three subevent combinations: "P_3–P_2–P_3", "P_3–I_{212}–I_{312}" and "I_{312}–I_{212}–P_3". From Figure 5(c) we can see that the term b_5^{PIP} can also predict internal multiples since all the events in b_1 are used as subevents in equation 3. For example, the event at 1.5s in Figure 5(c) has the same traveltime as I_{323} and negative polarity, and it can be generated by the following subevent combination: I_{312} from b_1 (negative), predicted I_{212} from b_3 (positive) and P_3 from b_1 (positive). The new algorithm represents progress in the attenuation of first order internal multiples. Research is ongoing to provide further insight and capability.

Numerical tests using synthetic data

In this section, a 1D two-parameter (with both velocity and density variation) model with three interfaces is used to generate the synthetic data by the finite difference modeling method. The chosen parameters for the model are: $c_0 = 1500m/s, c_1 = 2500m/s, c_2 = 3500m/s, c_3 = 4500m/s$; $\rho_0 = 1.0g/cm^3, \rho_1 = 2.0g/cm^3, \rho_2 = 3.0g/cm^3, \rho_3 = 4.0g/cm^3$; $z_1 = 500m, z_2 = 500m, z_3 = 2500m$, where c_i and ρ_i represent the velocity and density in each layer, respectively, and z_i is the depth of each interface. Figure 6(a) shows the zero-offset data. The output of the leading order attenuator is shown in Figure 6(b), where the red arrow points to the produced spurious event. In Figure 7(b) each event produced by b_3^{IM} is labeled, e.g., "2-1-2" means the first order internal multiple generated between the first two reflectors. Figure 7(a) shows the events generated by b_5^{PIP}.

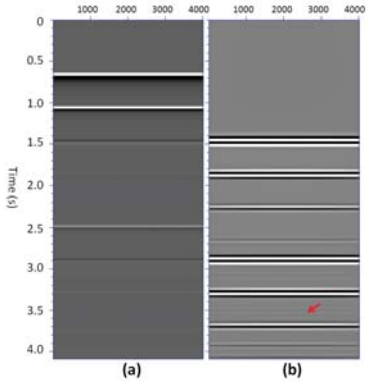

Figure 6: (a) Zero-offset data, where three primaries are at $0.667s$, $1.067s$ and $2.495s$, respectively. (b) Events predicted by b_3, with red arrow pointing to the spurious event (at $3.524s$).

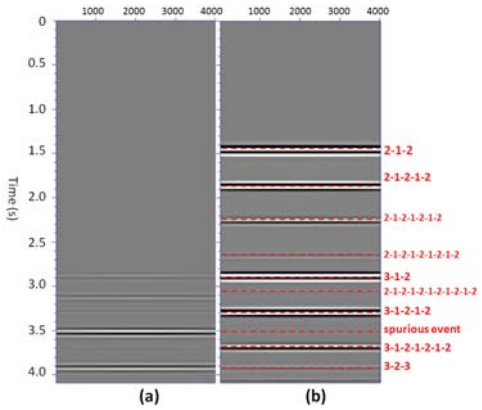

Figure 7: (a) Events predicted by b_5^{PIP} where the negative of the spurious event is at $3.524s$. (b) Events produced by b_3 with labels.

CONCLUSIONS

While the ISS leading order attenuator has demonstrated its capability for internal multiple removal, it has strengths and limitations as implied by "leading order" and "attenuator".The algorithm presented in this paper and the companion paper, Ma et al. (2012) addresses a shortcoming of the current leading order ISS internal multiple attenuation algorithm that are observed in the examples of Fu et al. (2010) and Luo et al. (2011). The new ISS internal multiple attenuation algorithm retains the benefit of the original algorithm while addressing one of its shortcomings. It now accommodates both primaries and internal multiples in the input data.

ACKNOWLEDGMENTS

We are grateful to all M-OSRP sponsors for their support of this research. Special thanks to Paolo Terenghi for assistance, Jim Mayhan for reviewing, and Adriana Ramírez for useful comments.

REFERENCES

Araújo, F. V., A. B. Weglein, P. M. Carvalho, and R. H. Stolt, 1994, Inverse scattering series for multiple attenuation: An example with surface and internal multiples: SEG Technical Program Expanded Abstracts, 1039–1041.

Coates, R. T., and A. B. Weglein, 1996, Internal multiple attenuation using inverse scattering: Results from prestack 1 & 2D acoustic and elastic synthetics: SEG Technical Program Expanded Abstracts, 1522–1525.

Fu, Q., Y. Luo, G. K. Panos, S. Huo, G. Sindi, S. Hsu, and A. B. Weglein, 2010, The inverse scattering series approach towards the elimination of land internal multiples: SEG Technical Program Expanded Abstracts, 3456–3461.

Hsu, S., P. Terenghi, and A. B. Weglein, 2011, The properties of the inverse scattering series internal multiple attenuation algorithm: Analysis and evaluation on synthetic data with lateral variations, choosing reference velocity and examining its sensitivity to near surface properties: Mission-Oriented Seismic Research Program (M-OSRP), Annual Report, 16–28.

Luo, Y., P. G. Kelamis, Q. Fu, S. Huo, G. Sindi, S. Hsu, and A. B. Weglein, 2011, Elimination of land internal multiples based on the inverse scattering series: The Leading Edge, 884–889.

Ma, C., H. Liang, and A. B. Weglein, 2012, A new Inverse Scattering Series (ISS) internal multiple attenuation algorithm responds to a limitation in the current algorithm: derivation for a three-reflector model and a test with analytic data: to be submitted to the SEG Technical Program Expanded Abstracts.

Matson, K. H., 1997, An inverse-scattering series method for attenuating elastic multiples from multi-component land and ocean bottom seismic data: PhD thesis, University of British Columbia.

Matson, K. H., and A. B. Weglein, 1996, Removal of elastic interface multiples from land and ocean bottom data using inverse scattering: SEG Technical Program Expanded Abstract, 1526–1530.

Ramírez, A. C., and A. B. Weglein, 2005, An inverse scattering internal multiple elimination method: beyond attenuation, a new algorithm and initial test: SEG Technical Program Expanded Abstracts, 2115–2118.

Terenghi, P., S. Hsu, A. B. Weglein, and X. Li, 2011, Exemplifying the specific properties of the inverse scattering series internal-multiple attenuation method that reside behind its capability for complex onshore and marine multiples: The Leading Edge, 876–882.

Weglein, A. B., F. V. Araújo, P. M. Carvalho, R. H. Stolt, K. H. Matson, R. T. Coates, D. Corrigan, D. J. Foster, S. A. Shaw, and H. Zhang, 2003, Inverse scattering series and seismic exploration: Inverse Problems, R27–R83.

Weglein, A. B., F. A. Gasparotto, P. M. Carvalho, and R. H. Stolt, 1997, An inverse-scattering series method for attenuating multiples in seismic reflection data: Geophysics, 1975–1989.

Weglein, A. B., S. Hsu, P. Terenghi, X. Li, and R. Stolt, 2011, Multiple attenuation: Recent advances and the road ahead 2011: The Leading Edge, 864–875.

Weglein, A. B., and K. H. Matson, 1998, Inverse scattering internal multiple attenuation: an analytic example and subevent interpretation: Mathematical Methods in Geophysical Imaging V, 108–117.

Zhang, H., and S. Shaw, 2010, 1-D analytical analysis of higher order internal multiples predicted via the inverse scattering series based algorithm: SEG Technical Program Expanded Abstracts, 3493–3498.

First field data examples of inverse scattering series direct depth imaging without the velocity model

Arthur B. Weglein[*], Fang Liu[*], Xu Li[*], Paolo Terenghi[*], Ed Kragh[†], James D. Mayhan[*], Zhiqiang Wang[*], Joachim Mispel[‡], Lasse Amundsen[‡], Hong Liang[*], Lin Tang[*], and Shih-Ying Hsu[*], M-OSRP/Physics Dept./UH[*], SCR/Schlumberger[†], and Statoil ASA[‡]

Summary

In Weglein et al. (2010) an update and status report were provided on the progress on the inverse scattering series (ISS) direct depth imaging without the velocity model.

In that report, results on synthetics with sufficient realism indicated that field data tests were warranted. This paper documents those first field data tests. These first early tests are encouraging and indicate that ISS direct depth imaging on field data is possible. The next steps on the road between viable and providing relevant and differential added value to the seismic tool-box are described and discussed.

Introduction / Background

All currently applied direct depth imaging methods and indirect imaging concepts firmly believe that depth and velocity are inextricably linked. That cornerstone of all current imaging means that any direct imaging method requires an accurate velocity model to produce an accurate image in depth.

It is essential to understand the significance of the term 'direct' in 'direct depth imaging'. Given an accurate velocity model, all current leading-edge imaging methods (e.g., Kirchhoff, FK, Beam and RTM) are able to directly output the depth (the actual spatial configuration) of reflectors.

Indirect imaging methods (e.g., flat common image gathers, differential moveout, CFP, CRS and 'path integral' approaches) seek to satisfy a property or condition that an image with an accurate velocity would satisfy. Those properties are necessary conditions, but not sufficient, and hence satisfying the indirect proxy for an adequate velocity model is not equivalent to knowing the velocity and direct depth imaging. Hence, satisfying these indirect criteria is no guarantee, and can lead to the correct depth or to any one of a set of incorrect depths. The latter truth is rarely (if ever) spoken and even rarer to find mentioned in print. Most importantly, these indirect approaches fervently believe that a direct depth imaging method would require and demand a velocity model, and that there is absolutely no way around it, and that depth and velocity are inextricably connected. That thinking is clear, and 100% correct within the framework of current imaging concepts and methods.

However, that thinking is superseded by the new broader framework for imaging provided by the ISS.

Amundsen et al. 2005, 2006, 2008 have developed direct inversion methods for 1D acoustic and elastic media. The ISS is the only direct inversion for both a 1D and a multi-D acoustic, elastic and anelastic earth.

In addition to being direct and applicable and applied for a multi-D earth, the ISS (Weglein et al. (2003)) allows for all processing objectives (including multiple removal and depth imaging) to be achieved directly and without subsurface information.

In the same 'direct' sense, that current imaging methods can directly output the spatial configuration of reflectors with a velocity model, ISS imaging algorithms can directly output the correct spatial configuration without the velocity model. It is the only method with that capability.

The ISS subseries for direct depth imaging communicates that depth and velocity are not inextricably linked.

The ISS provides a new superseding theory that views the current velocity-depth relationship and framework as a special limiting case, as quantum mechanics and relativity view classical physics as a limiting and special case, within a new comprehensive and broader platform and framework.

The new broader framework for imaging reduces to current imaging algorithms when the velocity model is adequate, and most amazingly it determines on its own for any particular data set, or portion of a data set, whether the new framework is needed, or whether the current conventional imaging framework will suffice. The new imaging framework determines if its services are called upon, and then and only then, will it activate the new ISS imaging framework terms and call them into action.

All current leading edge migration methods, such as, beam, Kirchhoff and RTM, are linear. In contrast, the ISS direct depth imaging without the velocity algorithm is a non-linear relationship between data and the wavefield at depth.

ISS task specific subseries for multiple removal, depth imaging and direct non-linear AVO

Each and every term and portion of any term within the ISS is computed directly in terms of data. All tasks associated with inversion (e.g., multiple removal, depth imaging, non-linear direct AVO, and Q compensation) are each contained within the series. Hence, these individual tasks are each achievable directly in terms of data, without subsurface information. Every seismic processing objective is carried out as a subseries of

the ISS, and operates without subsurface information, by involving distinct non-linear communication of the recorded seismic data. Only the ISS communicates that all seismic objectives can be achieved in basically the same way that free surface multiples are removed.

The free surface and internal multiple removal subseries have not only been shown to be viable but have also demonstrated added value and stand alone capability for predicting the amplitude and phase of multiples (See, e.g., Luo et al. 2011; Weglein and Dragoset 2005; Fu et al. 2010), in particular, demonstrated under complex marine and on-shore circumstances. In this paper, we examine for the first time the issue of ISS depth imaging viability on field data.

All conventional imaging methods require knowledge of the velocity model to determine the spatial locations of reflectors. Hence, the ISS series project began by assuming that only the velocity was variable and unknown. Figures 1-3 illustrate the ISS imaging results for an earth in which only velocity varies. The algorithms are described in Liu (2006); Liu et al. (2005); Zhang et al. (2007).

Imaging methods that require the velocity use only the phase of the data to determine depth. In contrast, all ISS tasks achieve their goals without subsurface information by using both the amplitude and phase of seismic data. The latter difference requires the exclusion of events from imaging subseries that do not relate to or contribute towards the task of depth imaging. Reflections that correspond to density only changes must be precluded from exclusively depth imaging tasks. The ISS depth imaging in an acoustic earth where V_p and density (and for an elastic earth with V_p, V_s and density), can all vary and all are initially (and remain, completely) unknown was formulated and the results were summarized in Weglein et al. (2010).

The impact of data limitations on ISS subseries

Table 1 summarizes the dependence/sensitivity of different ISS subseries on seismic bandwidth. As the latter table indicates, there is an increased dependency as we progress from the ISS free surface multiple case to the depth imaging subseries where (in the current "box-moving" formulation) the absence of low frequency in the data can have a deleterious effect on the ability of the ISS to move from the original linear incorrect depth image to the correct depth.

There are many other issues that need to be taken into consideration in developing practical ISS depth imaging algorithms. Among these issues are: (1) have the appropriate number and types of terms from the inverse series been included to match the imaging challenge due to the difference between the actual and reference velocity, and the duration of that difference; and (2) have the density only reflections been excluded from the ISS depth imaging algorithm. All of these issues need to be addressed to have the ISS depth imaging algorithm produce an accurate depth section. The moveout becomes flat and the imaging series directly produces a flat common image gather (CIG) at the correct depth.

In contrast to all current imaging methods where CIG flatness is a necessary but not a sufficient condition for depth imaging accuracy, the CIG flatness is a by-product of ISS imaging, and a necessary and sufficient indication that depth has been found. It's a direct depth finding machine, and when it stops it is done. With ISS imaging CIG flatness is an indication that a direct method is done, not an in-direct proxy for velocity used to find the depth, where for the latter conventional use it is necessary but not sufficient for depth location.

The overriding requirement and number one issue for field data application of ISS depth imaging is being able to address the sensitivity to missing low frequency components in the data (or low vertical wave number). If that low frequency sensitivity is not addressed, then gathering or not gathering appropriate and necessary ISS imaging terms or excluding density only reflections will not matter, and will be of no practical consequence. Hence, addressing the bandwidth issue for ISS imaging is the number one priority, the make or break issue for field data application, viability and delivery of its promise of high impact differential added value. A regularization scheme has been developed in Liu and Weglein (2009) to directly address that low frequency challenge. The purpose of this paper is to examine whether this regularization method will allow the ISS imaging algorithms to be effective and work on field data. Therefore, with this first field data examination, we relax all of the other requirements for ISS depth imaging and consider the field data as though it were generated by a velocity only varying earth. Within that parallel world where only velocity varies, the ISS depth imaging will need to address the band-limited nature of field data, and also will require having enough ISS imaging terms (within an acoustic velocity only varying subsurface assumption) to be effective for accurately locating reflectors.

In Figure 4, we present an acoustic model with no density variations and the water speed migration for the data from that model. Figure 5 (a) shows the inverse scattering imaging series ideal result, with full band-width data. In (b), the data has been altered by a sine squared taper up to $10Hz$ which damped the low frequency information and the ISS imaging without regularization is ineffective. In (c), with the regularization applied, the ISS depth imaging successfully corrects the data move-out and reveals the correct depth.

A similar approach is followed for a CMP gather selected from the Kristin data-set (Figure 7, Majdanski et al. (2010)). Figure 8 (a) shows a water-speed migration of the data in Figure 7, while Figure 8 (b) shows the ISS imaging result after regularization.

Event 1 is the water bottom primary, event 2 is the subwater bottom primary, event 3 is the internal multiple between event 1 and 2 and event 4 is a third primary. Event 4, the third primary has a moveout with a water

speed migration.

It turns out that event 1, the water-bottom primary, represents a density change but no velocity change. Hence, the layer below the water-bottom has the same acoustic velocity as water. Further, the first order internal multiple (event 3) in that first sub-water-bottom layer also has a water-speed move out. Hence, events 1, 2, and 3 all have flat CIGs with a water-speed FK Stolt migration (Figure 6). Event 4 has move-out due to a velocity change at the base of the first sub-water-bottom reflector.

With a regularized ISS depth imaging the result for the image of event 4 is a shifted and CIG flat output. Hence, the ISS depth imaging is working on the very shallow subsea-bottom portion of the Kristin data set within the context of a velocity only varying earth. The shifted ISS image and flat CIG of event 4, the third primary, indicates that bandwidth issues have been addressed, and sufficient capture of ISS imaging terms are within the ISS imaging algorithm. If for this field data set and ISS depth imaging test, either one of these conditions (addressing bandwidth sensitivity and adequate inclusion of ISS imaging terms) were a remaining and outstanding issue, then event 4 would not have moved and produced a flat CIG. The success of this test is thus defined. A more detailed and comprehensive analysis behind the logic and conclusions of this paper will appear in Weglein et al. (2012). The next steps are to apply the regularized ISS depth imaging to an acoustic variable velocity and density model for the very shallow and sub-water-bottom reflectors, and a Vp, Vs and density varying elastic earth model for the deeper reflectors, to preclude density only reflections, and for outputting actual depth. The M-OSRP imaging research team is engaged in moving from the current news and report that demonstrates field data viability for ISS imaging to providing added value. The ultimate goal is to have ISS imaging match the efficacy that ISS free surface and internal multiple removal have provided for the removal of coherent noise, and to extend that capability for extracting information from signal (the collection of all primaries).

Conclusions

In this paper, we have shown that the ISS depth imaging algorithm can address the most serious practical limitation/challenge field data will place on ISS depth imaging: that is, limitations in seismic bandwidth. With this accomplished, the further steps to extend these tests to variable density and velocity acoustic and elastic media are achievable, and realizing that is within the sphere of issues we can influence and make happen. The most significant difference between synthetic data and field data for ISS depth imaging has been examined and addressed.

Acknowledgment

We thank all the sponsors of M-OSRP for their support and encouragement. We have been partially funded by and are grateful for NSFCMG award DMS-0327778 and DOE Basic Sciences award DE-FG02-05ER15697. The M-OSRP group would like to thank Statoil ASA and Schlumberger/WesternGeco for granting access to the Kristin data and Mark Thompson, Mariusz Majdanski and Einar Otnes for their assistance and cooperation.

Figures

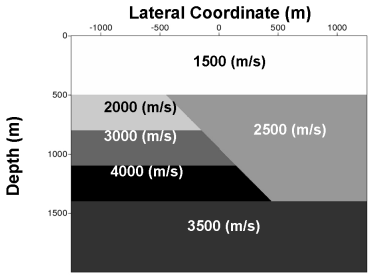

Fig. 1: The fault shadow zone model.

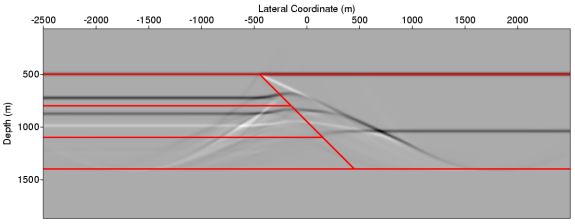

Fig. 2: The water speed pre-stack FK Stolt migration for the data from the fault shadow model.

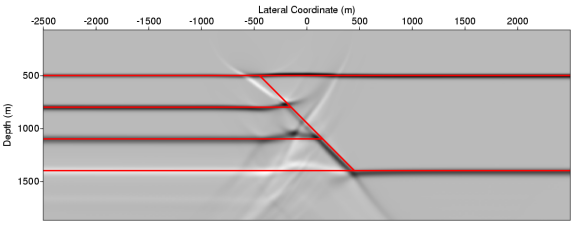

Fig. 3: The inverse scattering series image (with partial capture of ISS imaging capability) for the fault shadow model.

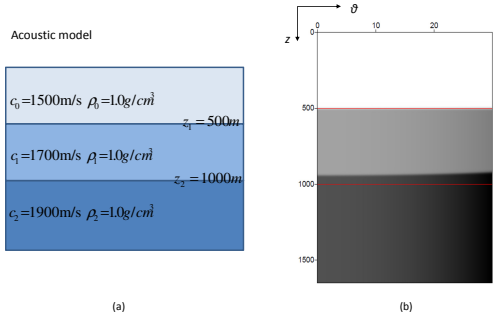

Fig. 4: Figure (a) shows the acoustic model we are testing for evaluating the dependence of ISS on seismic bandwidth. Figure (b) is the water speed FK Stolt migration, the red lines represent the true location of the reflectors.

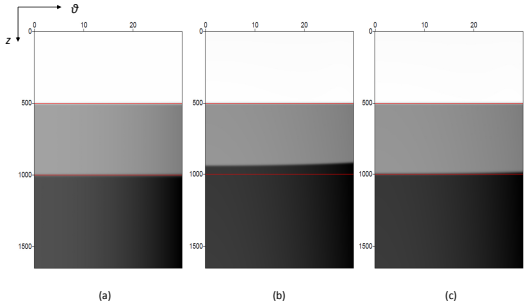

Fig. 5: This figure illustrates the imaging result for a velocity varying only earth model. Figure (a) shows ISS imaging with data which has low frequency information. Figure (b) shows ISS imaging with band-limited data. Figure (c) shows the imaging result with the regularization being applied. This ISS imaging bandwidth issue is documented in Shaw (2005).

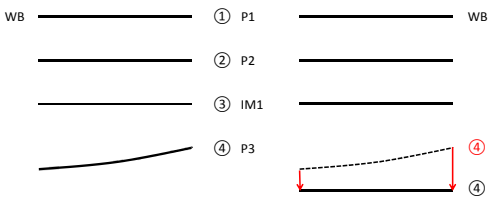

Fig. 6: This figure summarizes the results of the initial ISS depth imaging tests on the very shallow, near ocean bottom section of the Kristin data.

Dependence on temporal frequency content of the data	Specific subseries
None	Free surface multiple
Very mild	Internal mulitple
Some	Depth imaging

Table 1: This table shows the dependence of ISS specific subseries on temporal frequency content of the data.

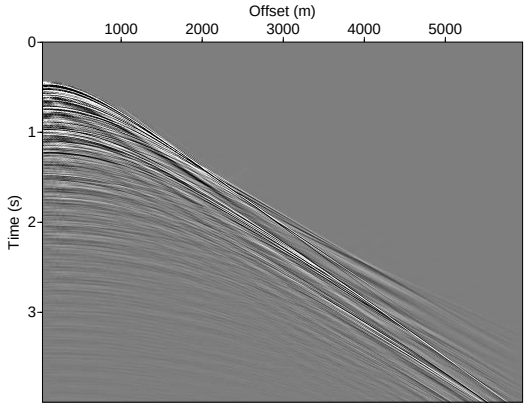

Fig. 7: The CMP gather we tested from Kristin data.

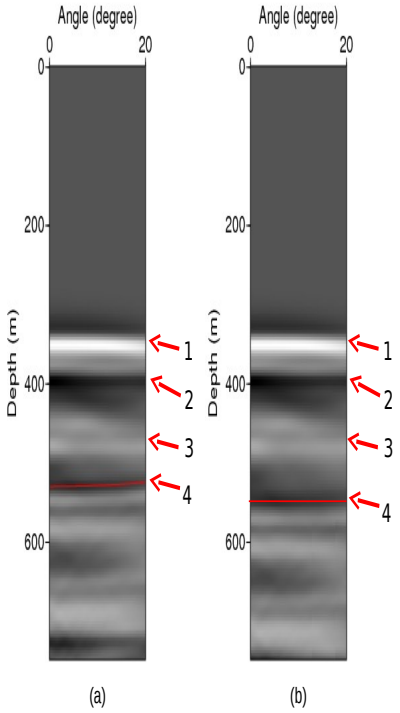

Fig. 8: For the Kristin data test: Figure (a) shows water speed migration. The red line indicate water speed migration image for event 4. Figure (b) shows ISS imaging result. The red line shows ISS image for event 4.

References

Amundsen, L., A. Reitan, B. Arntsen, and B. Ursin, 2006, Acoustic nonlinear amplitude versus angle inversion and data-driven depth imaging in stratified media derived from inverse scattering approximations: Inverse Problems, **22**, 1921.

———, 2008, Elastic nonlinear amplitude versus angle inversion and data-driven depth imaging in stratified media derived from inverse scattering approximations: Inverse Problems, **24**, 045006.

Amundsen, L., A. Reitan, H. K. Helgesen, and B. Arntsen, 2005, Data-driven inversion/depth imaging derived from approximations to one-dimensional inverse acoustic scattering: Inverse Problems, **21**, 1823–1850.

Fu, Q., Y. Luo, P. G. Kelamis, S. Huo, G. Sindi, S.-Y. Hsu, and A. B. Weglein, 2010, The inverse scattering series approach towards the elimination of land internal multiples: SEG Technical Program Expanded Abstracts, **29**, 3456–3461.

Liu, F., 2006, Multi-dimensional depth imaging without an adequte velocity model: PhD thesis, University of Houston.

Liu, F., and A. B. Weglein, 2009, Addressing the bandlimited nature of seismic source and rapid lateral variations of the earth: source regularization and cascaded imaging operator: 2009 M-OSRP Annual Report, 72–117.

Liu, F., A. B. Weglein, B. G. Nita, and K. A. Innanen, 2005, Inverse scattering series for vertically and laterally varying media: application to velocity independent depth imaging: M-OSRP Annual Report, **4**.

Luo, Y., P. G. Kelamis, Q. Fu, S. Huo, G. Sindi, S.-Y. Hsu, and A. B. Weglein, 2011, Elimination of land internal multiples based on the inverse scattering series: The Leading Edge, **30**, 884–889.

Majdanski, M., C. Kostov, E. Kragh, I. Moore, M. Thompson, and J. Mispel, 2010, Field data results of elimination of free-surface-related events for marine over/under streamer data: EAGE, Expanded Abstracts.

Shaw, S. A., 2005, An inverse scattering series algorithm for depth imaging of reflection data from a layered acoustic medium with an unknown velocity model: PhD thesis, University of Houston.

Weglein, A. B., F. V. Araújo, P. M. Carvalho, R. H. Stolt, K. H. Matson, R. T. Coates, D. Corrigan, D. J. Foster, S. A. Shaw, and H. Zhang, 2003, Inverse scattering series and seismic exploration: Inverse Problems, **19**, R27–R83.

Weglein, A. B., and W. H. Dragoset, 2005, Multiple attenuation (geophysics reprint no. 24): Soc. Expl. Geophys.

Weglein, A. B., F. Liu, X. Li, P. Terenghi, E. Kragh, J. D. Mayhan, Z. Wang, J. Mispel, L. Amundsen, H. Liang, L. Tang, and S.-Y. Hsu, 2012, Inverse scattering series direct depth imaging without the velocity model: First field data examples: Journal of Seismic Exploration. (Submitted).

Weglein, A. B., F. Liu, X. L. Z. Wang, and H. Liang, 2010, The inverse scattering series depth imaging algorithms: development, tests and progress towards field data application, *in* 80th Annual Internat. Mtg., Soc. Expl. Geophys., Expanded Abstracts: Soc. Expl. Geophys., 4133–4138.

Zhang, J., F. Liu, K. Innanen, and A. B. Weglein, 2007, Comprehending and analyzing the leading order and higher order imaging closed forms derived from inverse scattering series: 2006 M-OSRP Annual Report, 149–159.

Unraveling internal multiples via the reflector spectrum concept

Yi Luo[*1], *Hong Liang*[2], *Panos G. Kelamis*[1], *Arthur B. Weglein*[2]
[1]*EXPEC Advanced Research Center, Saudi Aramco*
[2]*University of Houston*

SUMMARY

When suppressing multiples in seismic data, it is important to identify which reflectors the multiples, especially the internal multiples, originated from. In this abstract, we present a method to relate all seismic arrivals, including primaries and multiples, to their originating reflectors. The method makes use of the reflectivity forward modeling method to isolate reflectors and determine the contribution of an individual reflector to an arrival in a seismic trace. Repeating this process for all reflectors produces a *reflector spectrum*, which shows quantitatively the relative contribution of each reflector to all arrivals in a trace. We use the reflector spectrum with a velocity model constructed from field sonic logs to demonstrate that internal multiples originate from many reflectors distributed throughout the model, rather than from a few major ones.

INTRODUCTION

When interpreting seismic data, we often use synthetic traces generated from 1D velocity models obtained from sonic logs to associate surface seismic events with well information and to distinguishing primary reflections from multiples. However, it is important to address and identify the reflectors that an arrival in a synthetic trace originated from. Relating seismic arrivals to their reflectors can help interpreters link seismic events to the corresponding geological formations, and can also provide insight into where multiples, especially internal multiples, originated.

Others (Foster and Yin, 1995; Resnick, et al., 1986) have proposed methods to determine how seismic reflections are generated and propagate in finely laminated thin layers. One method for identifying reflectors that generate internal multiples follows a trial and error approach. The method first sets impedance contrasts to zero at selected depths in a velocity model, and then the resulting wavefield is observed. If internal multiples disappear after an impedance contrast is removed, then it is concluded that the removed impedance contrast generated the multiples. The disadvantage of this method is that altering the velocity model affects not only the impedance contrasts of reflectors, but also the traveltimes of seismic waves.

In this paper, we propose a method for analyzing individual reflectors and the arrivals they generate, without changing the velocity model. This *reflector spectrum* method allows us to quantify the contribution of a single reflector to all arrivals in a seismic trace, or conversely, to identify all contributing reflectors for a single arrival.

METHOD

The reflector spectrum method uses the reflectivity forward modeling (Kennett, 2003) method. For a given velocity function $v(z_i)$, where z_i is depth of the i^{th} reflector and i is the layer index which takes values from 1 to N, the reflection coefficients due to the velocity contrast between two adjacent layers $v(z_i)$ and $v(z_{i+1})$ are

$$r_d(z_i) = \frac{v(z_{i+1}) - v(z_i)}{v(z_{i+1}) + v(z_i)}, \quad (1)$$

and

$$r_u(z_i) = \frac{v(z_i) - v(z_{i+1})}{v(z_{i+1}) + v(z_i)}, \quad (2)$$

where $r_d(z_i)$ and $r_u(z_i)$ are down and up reflection coefficients, respectively. For simplicity, we are neglecting the density in this description, although density does affect the reflection coefficients. Besides defining the reflectivity coefficients, the velocity $v(z_i)$ also determines the traveltimes for waves traveling in between interfaces.

Because the reflectivity method separates the roles of reflectivity and travel time, it allows us to change a single reflection coefficient while keeping the remaining reflection coefficients as well as the traveltime unchanged. As a result, we can simply set one of the reflection coefficients to zero without changing the velocity function itself. In this way, the effect of the corresponding reflector is isolated.

Figure 1 shows a simple example to illustrate this concept. The velocity function is shown in Figure 1a, and the calculated reflection coefficients are shown in Figure 1b. Using the velocity, reflectivity, and a wavelet, we compute the synthetic trace shown in Figure 1c. Zeroing the reflection coefficient corresponding to the first interface (Figure 1d) produces a new trace (Figure 1e), which we subtract from the original trace shown in Figure 1a to obtain the difference trace shown in Figure 1f. The events seen in the difference trace originate from the reflector located at the first interface, and include the primary

reflection at top of the layer (at 400 ms) and a first order internal multiple (at 1000 ms).

Similarly, we can zero the reflection coefficient for the bottom reflector, and the second primary and the associated multiple (the same one at 1000 ms in Figure 1f) will disappear. Note that muting either the top or bottom reflector will eliminate the same multiple at 1000 ms. In this example, we muted both the up and down reflection coefficients simultaneously for each interface. If only one type of coefficient, e.g., $r_d(z_i)$, is muted, then the internal multiple will appear only once in the spectrum. We will revisit this idea later.

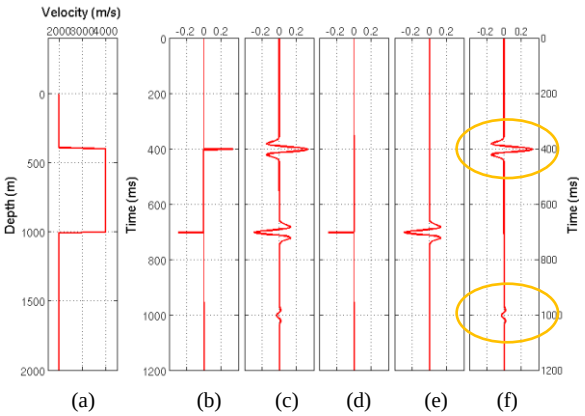

Figure 1: A synthetic example showing (a) the velocity function, (b) reflection coefficients, (c) synthetic trace computed from (b), (d) zeroing of the reflection coefficient of the first interface, (e) synthetic trace computed from (d), and (f) difference between (c) and (e).

Figure 1 shows that muting a reflection coefficient produces a difference trace that contains reflections originating from the muted reflector. Next, by individually zeroing reflection coefficients for interfaces 1 to $N-1$, we obtain $N-1$ difference traces. These $N-1$ traces are displayed as the image shown in Figure 2, in which each column contains the difference trace corresponding to the reflection coefficient directly above in the velocity function. The trace shown in the left panel in Figure 2 is the full synthetic trace. For this example, we only model primary reflections, so the reflector spectrum in Figure 2 indicates where the primaries originated. This method for identifying reflectors corresponding to primary reflections can also be used to identify other types of reflections such as surface multiples or internal multiples.

The reflector spectrum allows us to easily relate arrivals in a seismic trace to their corresponding reflectors in the velocity function. For any event in the reflector spectrum, the vertical coordinate indicates the arrival time of the reflection, while the horizontal coordinate indicates the depth of the corresponding reflector.

Values in the reflector spectrum have units of seismic amplitude, and the value at a point (t,z) in the spectrum is the seismic amplitude contributed by the reflector at depth z to the seismic arrival at time t. Thus, a vertical trace in a reflector spectrum at depth z shows all seismic arrivals generated by the reflector at that depth. Muting a single reflector will mute an entire trace in a reflector spectrum. Moreover, a horizontal trace at time t identifies all reflectors that contribute to the arrival at time t in the seismic trace.

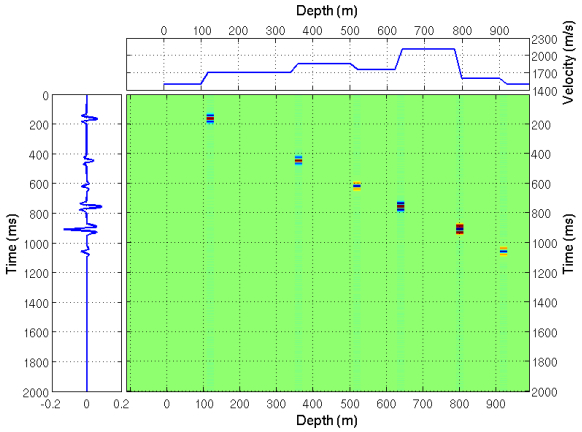

Figure 2: Reflector spectrum for primaries only. The top panel shows the velocity function, while the left panel shows the trace containing all primary reflections.

In a first glance of Figure 2, we might think that the reflector spectrum looks like displaying of VSP data which also has the two coordinates of time and depth. However, they are very different. Each traces at depth z in VSP is a record of the wave field at that depth, however, as we mentioned before, a vertical trace in a reflector spectrum at depth z shows all seismic arrivals generated by the reflector at that depth.

The reflector spectrum can be viewed as a well-known mathematical operator—the Fréchet derivative, i.e., the derivative of the calculated trace with respect to each individual reflection coefficient. Further investigation of this property could lead to an inversion scheme for primary reflections only, for example.

REFLECTOR SPECTRUM

Figure 3 shows the reflector spectrum for a more complex velocity function, which we derived from a sonic log. Using the same velocity function shown in Figure 3, a reflector spectrum for internal multiples only is produced and shown in Figure 4. Figure 5 shows two vertical traces extracted from Figures 3 and 4 at the locations indicated by the blue arrows. From Figure 5, we see that the reflector at depth 400 m generates one primary reflection (Figure 5a) and many internal multiples (Figure 5b).

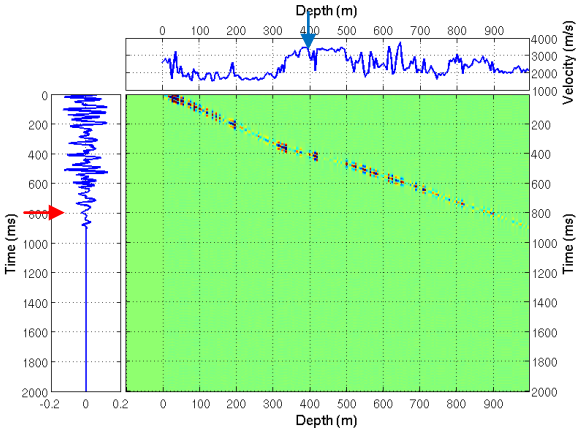

Figure 3: Reflector spectrum for primaries only. The top panel shows the velocity function, while the left panel shows the trace containing all primary reflections.

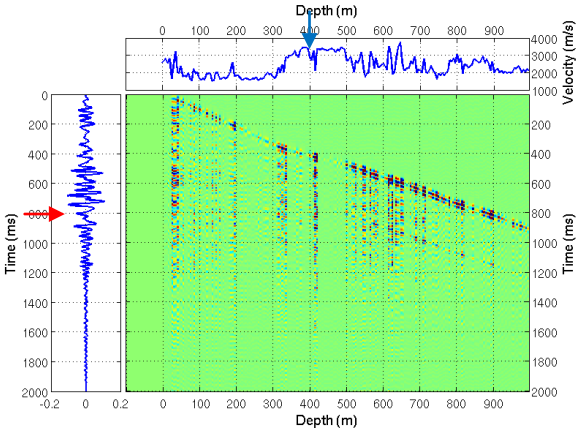

Figure 4: Reflector spectrum for internal multiples only. The top panel shows the velocity function, while the left panel shows the trace containing all internal multiples.

Figure 6 shows two horizontal traces extracted from Figures 3 and 4 at the locations indicated by the red arrows. Not surprisingly, we see that the primary reflections originate from reflectors confined to a small region in depth, while the internal multiples originate from many reflectors over a wide range of depths ranging from shallow to deep. Note that the primaries (near 900 m in Figure 6a) and the internal multiples (near 900 m in Figure 6b) will be mixed in a synthetic trace including all kinds of reflections (O'doherty and Anstey, 1971; Foster and Yin, 1995).

The traces in Figure 6, along with the reflector spectrum in Figure 4, suggest that an internal multiple is related to many reflectors. This is to be expected, since an internal multiple involves at least two reflectors (or reflecting at least three times). Although the reflector spectrum relates an internal multiple to all contributing reflectors, the fact that each multiple can appear numerous times may be undesirable, and summing the reflector spectrum over

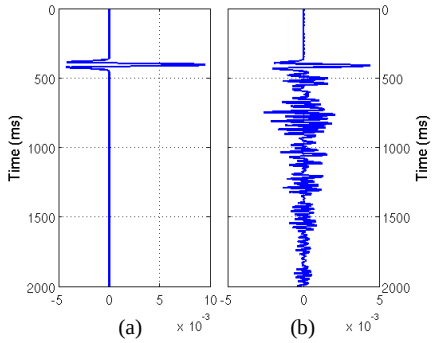

Figure 5: Primaries (a) and internal multiples (b) originating from the reflector at depth 400 m.

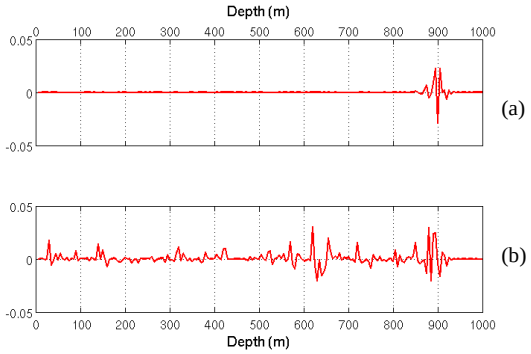

Figure 6: The contributions from all reflectors at all depths to the primaries (a) and internal multiples (b) at time 800 ms.

depth will not produce the synthetic trace shown on the left. Therefore, we propose to modify the reflector spectrum so that each multiple appears only once.

SHALLOW-REFLECTOR SPECTRUM

Here we introduce the shallow-reflector spectrum, which is a modified reflector spectrum that provides a simplified view of how multiples are generated. In a shallow-reflector spectrum, multiples are related only to the shallowest corresponding reflectors. This is typical in land seismic datasets (Luo et al., 2011; Kelamis et al., 2008). As a result, each multiple will appear only once in this spectrum, unlike the reflector spectrum for internal multiples shown, for example, in Figure 4, in which each multiple can appear more than once. Because each multiple appears only once, stacking a shallow-reflector spectrum over horizontal axis will reproduce the original seismic trace.

Figures 7 and 8 show, respectively, the reflector spectrum and the shallow-reflector spectrum for surface-related multiples only. Figure 7 reflects the true physics and indicates where all surface-related multiples originated. In comparison, Figure 8 indicates only the shallowest reflector for each surface-related multiple.

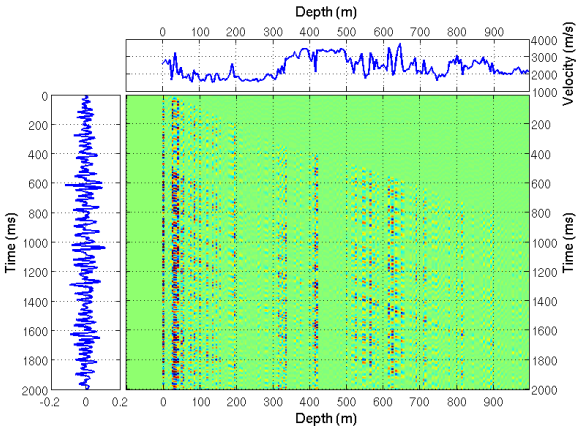

Figure 7: Reflector spectrum for surface-related multiples only. This spectrum indicates that not only the free surface, but also many deeper reflectors, contribute to the surface-related multiples.

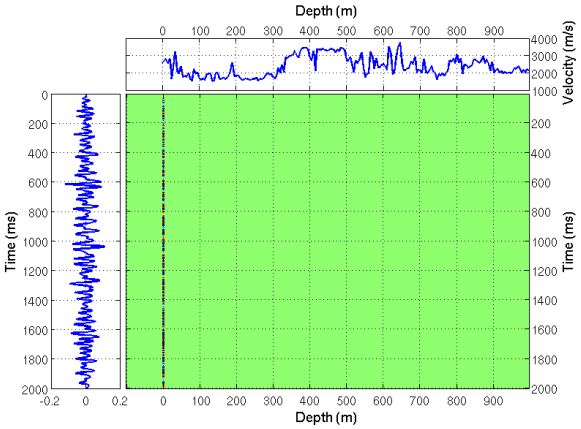

Figure 8: Shallow-reflector spectrum for surface-related multiples only. Because all surface-related multiple can be attributed to the surface, all surface-related multiples can be eliminated by removing the free surface reflector.

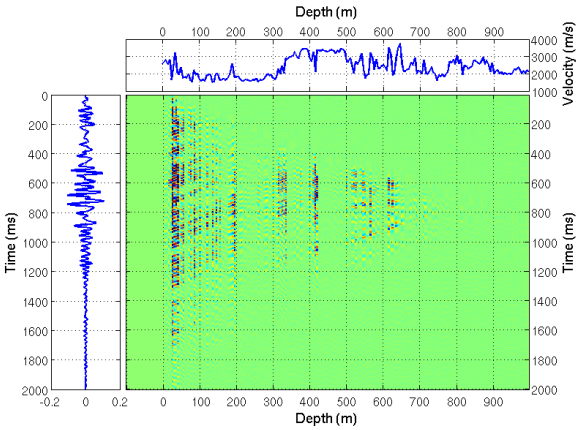

Figure 9: Shallow-reflector spectrum for internal multiples only. Internal multiples cannot be attributed to a single reflector, as was the case for the surface-related multiples shown in Figure 8.

Figure 8 suggests that all surface-related multiples can be eliminated if the surface reflector is somehow removed. In fact, others (Verschuur and Berkhout, 1997; Weglein et al., 1997; Moore and Dragoset, 2008; Tsai, 1985) have proposed methods to do exactly this. The success of these surface-related multiple elimination techniques is perhaps due in part to the simplicity of the shallow-reflector spectrum for surface-related multiples (e.g., Figure 8), which indicates that *all* surface-related multiples can be removed simply by removing the surface reflector.

Figure 9 shows the shallow-reflector spectrum for internal multiples only. For comparison, the reflector spectrum is shown in Figure 4. Note that because each internal multiple appears only once in a shallow-reflector spectrum, we can conclude from Figure 9 that the internal multiples originate from many reflectors. Not surprisingly, we cannot hope to eliminate all internal multiples by simply removing a single reflector, as was the case for surface-related multiples. Perhaps the most attractive feature of the shallow-reflector spectrum is that summation of, for example, the spectrum shown in Figure 9 over horizontal axis will produce the trace shown in the left panel in Figure 9. This property could prove useful when developing internal multiple elimination techniques.

The shallow-reflector spectrum provides an indication of the fewest number of reflectors responsible for multiples, or, in other words, the fewest number of reflectors we would need to remove in order to eliminate the multiples. For surface-related multiples, the shallow-reflector spectrum confirms that only one reflector, i.e., the free surface, is responsible for the multiples. For internal multiples, however, the shallow-reflector spectrum shows that many reflectors are responsible for the multiples. Thus, we cannot eliminate all internal multiples by removing any single reflector or even a few of the strongest reflectors.

CONCLUSION

We have presented a new method for generating a reflector spectrum, which relates seismic arrivals or events to all reflectors from which they originated. We have also proposed a shallow-reflector spectrum, which relates seismic arrivals to only the shallowest corresponding reflector. Our study confirms that internal multiples originate from many reflectors. Thus, internal multiples cannot be eliminated by removing any single reflector or even a few major reflectors.

ACKNOWLEDGMENTS

The authors thank the Saudi Arabian Oil Company (Saudi Aramco) for support and permission to present this research.